LA-UR-00-1531

Approved for public release;
distribution is unlimited.

REVIEWS OF MODELS FOR ADSORPTION OF SINGLE VAPORS, MIXTURES OF VAPORS, AND VAPORS AT HIGH HUMIDITIES ON ACTIVATED CARBON FOR APPLICATIONS INCLUDING PREDICTING SERVICE LIVES OF ORGANIC VAPOR RESPIRATOR CARTRIDGES.

prepared by

Gerry O. Wood

Industrial Hygiene & Safety Group
Environment, Safety, and Health Division
Los Alamos National Laboratory

for

Organization Resources Counselors, Inc.
Respiratory Cartridge Testing Task Force
Washington, D.C.

Funds-in-Agreement No. FIA-98-045-A001

March 2000

Los Alamos
NATIONAL LABORATORY

REVIEWS OF MODELS FOR ADSORPTION OF SINGLE VAPORS, MIXTURES OF VAPORS, AND VAPORS AT HIGH HUMIDITIES ON ACTIVATED CARBON FOR APPLICATIONS INCLUDING PREDICTING SERVICE LIVES OF ORGANIC VAPOR RESPIRATOR CARTRIDGES.

Abstract

Theories, equations, and models of adsorption and supporting data on adsorption of organic vapors on activated carbon have been accumulated and analyzed. The target application is the prediction of service lives of organic vapor air-purifying respirator cartridges. The extensive information on single vapors at dry conditions needs to be extended to mixtures of vapors and high humidity situations.

First, breakthrough curve models, adsorption equilibrium (isotherm) models, and adsorption rate (kinetic) models for single vapors were examined. The Dubinin/Radushkevich equation seems to have the best applicability for predicting adsorption capacities. An expanded database of affinity coefficients was used to develop improved correlations with molecular parameters. Most of the adsorption rate models studied did not predict the trend with vapor type. Only the Lodewyckx and Wood/Stampfer equations were successful in doing this. Of the existing predictive complete breakthrough models studied, the Wood semi-empirical model was the most successful.

Second, twelve models for adsorption capacities and data for adsorption rates of mixtures of organic vapor on activated carbon were studied. The Grant-Manes (Polanyi) and Ideal Adsorbed Solution Theory equations showed the most promise for predicting equilibrium capacities of components of mixtures. However, it is uncertain how much one vapor affects the adsorption *rate* of the other. A generic procedure for calculating complete breakthrough curves for components of mixtures and including rollover effects was developed.

Third, tabulated, empirical, and correlation models for high relative humidity effects on breakthrough times were examined. Adsorption capacity models for organic vapor in the presence of water vapor were compared with data for coadsorption. A Doong-Yang Model gave good predictions

and has some desirable characteristics for equilibrium effects of water vapor. However, the likelihood of not being at water equilibrium for a respirator cartridge application must be considered.

Finally, recommendations for putting together predictive models from current knowledge and for developing improved models are presented.

CONTENTS

I. Introduction…….1

II. Models for Adsorption of a Single Organic Vapor

A. Fundamentals…….….3
B. Breakthrough Curve Models……...5
C. Adsorption Capacity Models……...….9
D. Affinity Coefficient Models……..16
E. Adsorption Rate Models……18
F. Effects of Temperature on Rate Coefficients……26
G. Breakthrough Time Models …….27
Table I. Predictive Models Used to Estimate Breakthrough Times (Service Lives)
Table II. Correlative Models Used to Estimate Breakthrough Times (Service Lives)
H. Review of Single Vapor Breakthrough Time Databases……30
Table III. Candidate Single-Vapor Breakthrough Time Databases for Evaluations of Service Life Models
I. Comparisons of Complete Predictive Models……30
Table IV. Predictions of Complete Service Life Predictive Models
J. Comparisons of Adsorption Rate Coefficient Models……34
Table V. Summary of How Adsorption Rate Coefficients Calculated from Models Correlated with Experimental Ones, Flow Rates, and Reported Average Carbon Granule Sizes.
K. Comparisons of Adsorption Capacity Model Predictions…….….48
Table VI. Comparisons of Adsorption Capacities from Models with those from Experimental Data
L. Comparisons of Affinity Coefficient Models…….……50
Table VII. Supplemental Values of Affinity Coefficients on Activated Carbons Calculated from Various Sources.
Table VIII. Results of Affinity Coefficient Correlations

III. Models for Adsorption of Mixtures of Organic Vapors

A. Fundamentals……..……58
B. Models for Adsorption Capacities of Mixture Components……..…59
1. Molar Proportionality Model
2. Volume Exclusion Model
3. Lewis Equation Model
4. Greenbank and Manes Model
5. Polanyi Adsorption Potential Model
6. Ideal Adsorbed Solution Theory (IAST) Model
7. Vacancy Solution Model (VSM)
8. Multicomponent Langmuir Equation
9. Multicomponent Freundlich Equation

10. Multicomponent Langmuir/Freundlich Equation
11. Multcomponent John Equation
12. Multicomponent Dubinin/Radushkevich Equations

C. Literature Comparisons of Capacity Models……..74
Table IX. Results of Comparisons by Reucroft et al of Mixture Models
Table X. Results of Comparisons by Valenzuela and Myers of Mixture Models
Table XI. Results of Comparisons by Doong and Yang of Mixture Models

D. New Comparisons of Selected Mixture Models…….76
1. Selection of Mixture Models
2. Selection of Database
3. Single Component Adsorption Isotherms for Mixture Models
4. Results of Applying Predictive Mixture Models

Table XII. Accuracies and Precisions of Predictive Models for Mixtures

E. Multicomponent Vapor Adsorption Kinetics…….……98
F. Models for Breakthrough Curves of Mixtures……..101
Table XIII. A Generic Procedure for Predicting Breakthrough Curves and Times of Components of Binary Mixtures
G. Discussion……..……104
Table XIV. Order of Increasing Difficulty of Application of Mixture Models

IV. Models for Adsorption of Organic Vapors at High Humidities

A. Fundamentals…….108
B. Empirical and Correlation Models for High Humidity Capacities……109
C. Predictive Models for High Humidity Capacities……..113
D. Predictive Models for High Humidity Rate Coefficients……..116
Table XV. Empirical Parameters for RH Effects on Adsorption Rate Coefficients
E. Candidate Databases for Model Comparisons…….…..117
Table XVI. Breakthrough Time Correction Factors of Nelson et al.
Table XVII. Relative Breakthrough Times of Trichloroethane at Various Humidities and Vapor Concentrations Calculated from Werner's Results
F. Comparisons of Selected Humidity Effect Models……...120
Table XVIII. Accuracies and Precisions of Models for Adsorption Capacities of Activated Carbons for Organic Vapor and Water Vapor Mixtures using the Data of Okazaki et al.

V. Summary Conclusions and Recommendations

A. Current Models……..137
1. Single Vapors
2. Mixtures of Vapors
3. High Humidity Cases

B. Identified Model Gaps……...140
C. Future Work for Improved Predictive Models……..141

References……....143

REVIEWS OF MODELS FOR ADSORPTION OF SINGLE VAPORS, MIXTURES OF VAPORS, AND VAPORS AT HIGH HUMIDITIES ON ACTIVATED CARBON FOR APPLICATIONS INCLUDING PREDICTING SERVICE LIVES OF ORGANIC VAPOR RESPIRATOR CARTRIDGES

I. Introduction

Worker respiratory protection against airborne vapors of organic compounds is sometimes provided using air-purifying respirators and associated air-purifying cartridges or canisters. An essential question in such applications is "How long will the cartridge(s) last (i.e., provide acceptable protection)?" Regulatory requirements for establishing change-out schedules also require objective information on "service lives." Cartridge service life ("breakthrough time") can be measured in laboratory tests under selected conditions of vapor type(s), concentration(s), air flow, relative humidity, temperature, etc. However, workplace conditions are so varied and variable that no amount of testing is adequate. Researchers have combined correlations of experimental data and developments of theoretical equations in efforts to extrapolate and interpolate available data. The resulting sets of mathematical equations are sometimes called "models," since they attempt to describe reality. Applications of such models as procedures, computer programs, or spreadsheets are also sometimes called "models".

The objective of this report is to present and evaluate mathematical models relevant to predicting service lives of air-purifying organic vapor respirator cartridges. These models often also work for larger air-purifying canisters and air-cleaning filters and may have been developed using activated carbon beds of any size. The term "cartridge" will usually be used generically to represent all of these. The scope of this report is limited to cartridges containing granular activated carbon (charcoal), the most common sorbent for removing organic vapors due to its low cost and high capacity. We will also only consider organic vapors removed by physical

adsorption and micropore condensation. The terms “vapor”, “gas”, “chemical”, “compound”, and “adsorbate” will be used interchangeably in this report, unless otherwise stated. Some activated carbons are impregnated with chemicals to make them reactive to vapors and gases for more effective removal. Models for reactive/catalytic air-purifying processes are too specific to be considered in this report. There are no adequate models for multiple use periods, so we are currently limited to single, continuous cartridge use models.

The simplest experiment, use application, or model involves a single vapor in dry air. However, in a workplace there is often a significant amount of water vapor present (i.e., relative humidity, RH, greater than 50%). There may also be a mixture of vapors (other than water) present in the air to be cleaned for breathing. Advanced predictive models must be able to take into account high humidities and mixtures of vapors.

Another technique, computer simulation of the adsorption process with time, has much potential with increasing personal computer power, but is not yet routinely applied to predicting cartridge service lives. Therefore, it is not included in the scope of this report.

Four reviews of experimental service life data and models are noteworthy as references on this topic and as helps in preparing this report. In 1976 Gary Nelson and Nicholas Correia published a summary and conclusions paper, the eighth in a series entitled “Respirator Cartridge Efficiency Studies.”[1] This classic set of experimental data and conclusions has been and continues to be extensively cited and used. In 1977 Dennis Smoot of The Bendix Corporation published a report, “Development of Improved Respirator Cartridge and Canister Test Methods,” contracted by NIOSH and NASA.[2] In 1983 Ernest Moyer published “Review of Influential Factors Affecting the Performance of Organic Vapor Air-Purifying Respirator Cartridges.” [3] In 1988 Martin Werner and Nancy Winters published “A Review of Models Developed to Predict Gaseous Phase Activated Carbon Adsorption of Organic Compounds.”[4] Since many

developments in this area have occurred since 1988, it seems timely to build on these reviews and supplement them with model analyses and recommendations.

II. Models for Adsorption of a Single Organic Vapor

A. Fundamentals

We will first assume a simple experiment where air containing one vapor contaminant is flowed through a packed bed (e.g., an organic vapor air-purifying respirator cartridge) of granules of an activated carbon. The variables set in the experiment include: average airflow rate, airflow pattern (steady or cyclic breathing simulated), vapor type, vapor concentration (usually constant), carbon type (and physical properties), and bed size (e.g., diameter and depth). If the carbon is at all effective in removing the vapor, the effluent (air coming out of the bed) at the beginning of the experiment contains none of the vapor. However, the bed has a finite capacity for the vapor, so that eventually that capacity will be used up and the vapor will appear in the effluent. If the rate of vapor removal from flowing air to the carbon granules were infinitely fast, this "breakthrough" would be immediate and complete only at the "breakthrough time" when capacity is depleted. However, this is not the case, so some of the vapor appears in the effluent before equilibrium capacity of the adsorbent for the adsorbate vapor is reached. The amount breaking through or penetrating the carbon bed increases gradually and then more rapidly until as much is coming out as is going into the bed. A graphical representation of this process, shown in Figure 1, is called a breakthrough curve. Breakthrough concentration or fraction (effluent concentration divided by influent concentration) is plotted against time.

The objective of any service life model is to describe or predict a breakthrough time at which the effluent reaches a concentration that is no longer acceptable to breathe. So, a service life model is used to predict a breakthrough curve or a point (concentration and time) on it.

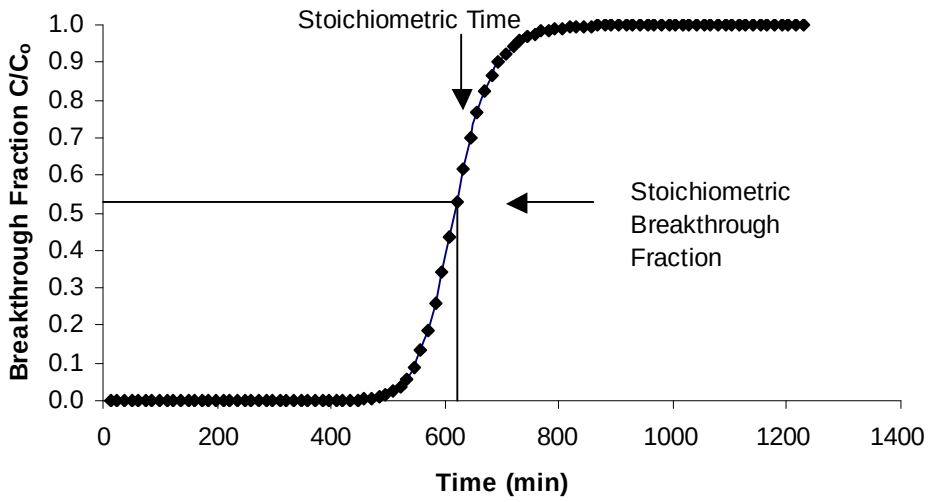

Figure 1. Components of a vapor breakthrough curve, in this case a slightly asymmetric one (stoichiometric breakthrough fraction > 0.5).

A breakthrough curve is defined by three characteristics: shape, midpoint, and steepness. Therefore, a service life model should include all of these. The midpoint is determined by the capacity of the carbon bed for the vapor at the selected vapor concentration, temperature, and other conditions. A graph, such as Figure 2, describing the relationship between equilibrium

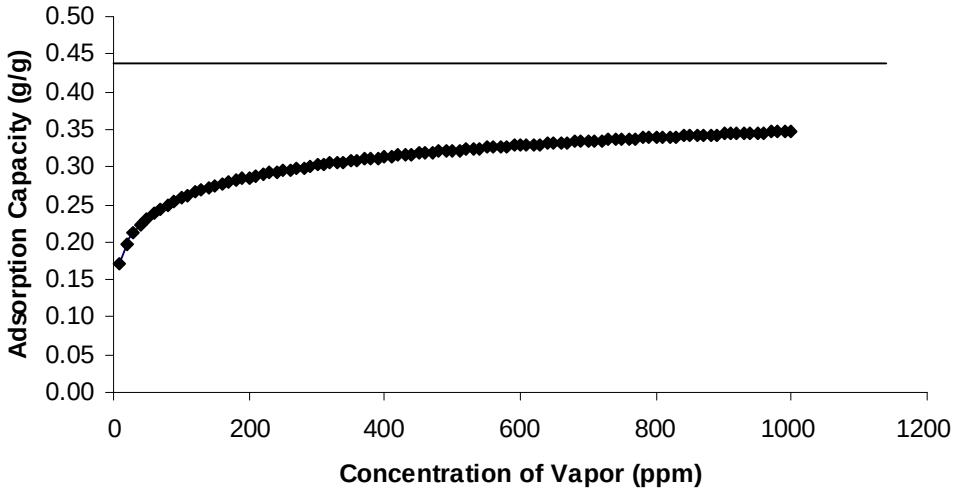

Figure 2. A sample adsorption isotherm. The horizontal line represents the maximum capacity when all the micropore volume is filled.

capacity of a given solid adsorbent and concentration of a given gas adsorbate at a given temperature is called an “adsorption isotherm.”

The steepness of a breakthrough curve is related to the rate (speed) at which the vapor is removed from air as it passes through the bed. In the simplest case steepness is described by an overall mass transfer or adsorption “rate coefficient”, which is larger for larger adsorption rates.

Service life models differ in how they describe one or more of these three breakthrough curve characteristics. Therefore, the following discussion considers them separately. A complete model requires selection from among the choices for each of these.

B. Breakthrough Curve Models

Complete breakthrough curves for physical adsorption of vapors on activated carbon from flowing air usually have what is called an “S” shape (Figure 1). They may be symmetrical or nearly so. Often they are slightly asymmetrical or skewed, usually steeper at the beginning than at the end. This is due to heterogeneity of adsorption sites and results in changes in adsorption rates and/or mechanisms as vapor loading on carbon proceeds. Highly asymmetrical breakthrough curves result from reactions and/or significant water vapor coadsorption with possible accompanying heating effects.

Bohart and Adams (1920)[5] first developed an equation describing the ideal, symmetrical breakthrough curve. It assumed mass balance and adsorption kinetics first order in vapor concentration and first order in concentration of remaining adsorption sites. With an exception of very small values of capacity and time, their equation can be rearranged to express breakthrough time t_b (min) for a breakthrough concentration of C as:

$$t_b = \frac{a_o\, z}{60\, v_L\, C_o} - \frac{1}{k\, C_o} \ln\left(\frac{C_o - C}{C}\right) \qquad (1)$$

where C_o (g/cm^3) is the entering (challenge) concentration, a_o is the volumetric capacity (g/cm^3)

of the sorbent for the vapor, z is the bed depth (cm), and v_L is the linear airflow velocity (cm/s). In this case the rate coefficient k has units of $cm^3/(g\text{-}min)$. [Note: Here and later in this report symbols and units are changed from the original references to be consistent throughout this report.] What is important to the shape is that this equation predicts that breakthrough time is on a curve centered at the first (capacity) term on the right-hand side of Equation (1) and spread symmetrically according to the logarithmic term and to an extent determined by the first-order adsorption rate coefficient, k_v. So many others [e.g., 6-8] have also derived this equation that it may be best to call it according to a generic designation, the Reaction Kinetic equation [8].

Mecklenburg [9] also used mass conservation to derive an equation with a capacity term minus a term involving an undefined "dead layer" or "critical bed depth", I:

$$t_b = \frac{a_o\, A}{C_o\, Q}\left[z - I\right] \qquad (2)$$

where Q is the volumetric airflow rate (cm^3/min) and A is the cross-section (cm^2) of the adsorbent bed. Klotz [10] combined the Mecklenburg approach with an expression derived by Gamson et al. [11] for the critical bed depth, I_t to get a breakthrough time expression:

$$t_b = \frac{a_o\, A}{C_o\, Q}\left[z - \frac{1}{a}\,\mathrm{Re}^{0.41}\;\mathrm{Sc}^{0.67}\;\ln\left(\frac{C_o}{C}\right)\right] \qquad (3)$$

(Definitions of parameters a, Re, and Sc in this equation are not important for the immediate discussion, but will be given later.) Notice that the logarithmic term is different from that in Equation (1). Klotz replaced $(C_o - C)$ with C_o, by assuming that the C_o/C is very large, i.e., that the breakthrough fraction is very small. This unnecessary assumption was copied by others [12-13] and incorporated into the best-known breakthrough equation [13], often called the Modified Wheeler Equation for breakthrough time:

$$t_b = \frac{W_e}{C_o\, Q}\left[W - \frac{\rho_B\, Q}{k_v}\, \ln\left(\frac{C_o}{C}\right)\right] \qquad (4)$$

or

$$t_b = \frac{W_e\, W}{C_o\, Q} - \frac{W_e \rho_B}{k_v\, C_o}\, \ln\left(\frac{C_o}{C}\right) \qquad (5)$$

where W_e is the gravimetric (g/g carbon) capacity, W is the weight (g) of carbon, ρ_B is the packed density (g/cm^3) of the carbon bed. The substitution of $\ln(C_o/C)$ for $\ln[(C_o - C)/C]$ makes less than 1% difference in the second (kinetic) term for breakthrough fractions C/C_o less than 0.032. However, it does change the shape of the breakthrough curve from "S"-shaped to "J"-shaped, approaching infinity instead of a maximum value at long times [Figure 11 in Reference 1]. Not realizing this and using the Modified Wheeler Equation at higher breakthrough fractions can lead to errors in analyzing data or calculating breakthrough times.

Wood and Moyer [14] have published a review of the Wheeler Equation (Modified and Reaction Kinetic variants) and comparisons of its applications to organic vapor respirator cartridge breakthrough data. Applications examined included (1) varying bed weight, (2) varying residence time, and (3) fitting the breakthrough curve. A common set of breakthrough curves was analyzed by the three methods. All three approaches produced a common capacity, but differing rate coefficients. A square-root airflow velocity dependence was found for the rate coefficients. Guidelines were given for using the Wheeler Equation to design tests and analyze experimental data.

One other approach to describing the "S"-shaped breakthrough curve is the Theory of Statistical Moments (TSM). Grubner and Burgess [15] replaced the logarithmic term with a normal probability distribution and the rate term with a standard deviation. An advantage to using the TSM is that higher statistical moment terms can be included to describe asymmetrical

breakthrough curves and calculate breakthrough times for them. A three-term TSM breakthrough time equation was expressed as:

$$t_b = t_{50\%} (1 + a \phi x_c + b \phi^2 (x_c^2 - 1)) \qquad (6)$$

where $t_{50\%}$ is the time for $C/C_o = 0.5$, x_c is the probability distribution for any C/C_o, and a, b, and ϕ are constants related to physical parameters of the adsorbent and dynamic adsorption experiment. A difficulty with using this equation is the necessity of calculating or looking up the probability distribution parameter in a table. The $t_{50\%}$ definition is exact only for symmetrical breakthrough curves (no third term of Equation (6).

Wood [16] has extended the Reaction Kinetic equation to better describe asymmetric (skewed) breakthrough curves:

$$\frac{C}{C_o} = \frac{\exp\left[\frac{t - A}{B + G(t - A)}\right]}{\exp\left[\frac{t - A}{B + G(t - A)}\right] + \left(\frac{1 - P_s}{P_s}\right)\exp\left[\frac{-H(t - A)}{B}\right]} \qquad (7)$$

where A is the time and P_s is the C/C_o ratio for the (stoichiometric, geometric) center of the breakthrough curve. Two additional terms, G and H, allow this equation to fit by nonlinear least squares regression analysis for even the most skewed breakthrough curve [16]. Equation (7) has the advantage of reducing to the Reaction Kinetic equation when G and H are zero; so, it can also describe the ideal case. A disadvantage is that the parameters G and H cannot be assigned physical meaning or be related to vapor or carbon properties for predictive purposes.

Yoon and Nelson [17] have also published an equation for describing asymmetric cartridge breakthrough curves, particularly those resulting from the presence of high humidity. They assumed that the contaminant saturation capacity, W_e, is a linear function of time: $W_e = W_b (t + W_a)$. Their resulting breakthrough curve equation can be rearranged to give a

breakthrough time expression:

$$\frac{C}{C_o} = \left(1 + \exp\left[k'' \left\{\ln(W_a + \tau) - \ln\left(W_a + t_b\right)\right\}\right]\right)^{-1} \qquad (8)$$

where A, k", and W_a are obtained by fitting breakthrough curve data to Equation (8) by nonlinear least squares regression. The 50% breakthrough time, τ, can be calculated from these fit parameters by: $A = k'' \ln (W_a + \tau)$. One disadvantage to using Equation (8) for service life predictions is that some of the fit parameters have no assigned physical meaning. Another disadvantage is that it does not reduce to the ideal Reaction Kinetic equation the same authors used previously. [18]

C. Adsorption Capacity Models

Capacity of a packed carbon bed for an organic vapor is the major property that determines breakthrough time of that vapor. The units of capacity are often moles of vapor per gram of carbon or grams of vapor per gram of carbon. Organic vapors on activated carbon containing micropores have a Type I adsorption isotherm [19], increasing rapidly at low vapor concentrations, less rapidly at moderate concentrations, and leveling off to a maximum at high concentrations (Figure 2). At vapor concentrations approaching the vapor saturation concentration at the temperature of concern, the isotherm may turn up again as larger (macro)pores begin to be filled after the micropores are filled.

Wood and Moyer [20] published a review and comparison of adsorption isotherm equations used to correlate and predict organic vapor cartridge capacities. Except for the Freundlich isotherm with ethanol, four isotherm equations described the data sets tested equally well. Other characteristics of the equations were compared.

The simplest equation describing and predicting equilibrium capacity is the Freundlich isotherm equation:

$$W_e = a\, C_o^{-b} \qquad (9)$$

where a and b are empirical coefficients. When logarithms of capacities at breakthrough times are plotted against logarithms of vapor concentrations (any units), straight lines are often obtained. Since conservation of mass for very small vapor breakthrough fractions (e.g., Equations 1-5) requires that breakthrough time is proportional to capacity divided by concentration (W_e/C) , it is expected that log-log plots of breakthrough times vs. vapor concentrations would also be linear:

$$t_b = \frac{W_e\, W}{C_o\, Q} = \left(\frac{a\, W}{Q}\right) C_o^{-(b+1)} \qquad (10)$$

$$\log t_b = \ln\left(\frac{a\, W}{Q}\right) - (b+1) \log C_o \qquad (11)$$

This has also been observed [21-22]. Such log-log plots are simple and useful for interpolations between experimental breakthrough times, but must be used with care when extrapolating beyond the data. Disadvantages of using the Freundlich isotherm are that the parameters, a and b, are empirical (must be determined by experiment for each vapor/carbon combination) and do not include temperature dependence or other conditions of an application.

Gary Nelson et al. [21-22] experimentally obtained 10% (of challenge concentration) breakthrough time Freundlich parameters for several compounds. In the first report [21] these included: acetone (2 cartridge types), hexane (2 cartridge types), vinyl chloride (3 cartridge types), and 7 other organic compounds. They obtained values of slopes (b) ranging from 0.395 to 0.937 with an average of 0.67 for nine compounds and ranging from 0.348 to 0.436 with an average of 0.39 for vinyl chloride. This led to a “Rule-of-Thumb” that, “In general, if the concentration is diminished by a factor of 10, the service life will increase by a factor of 4 or 5.” In another report [22] they listed Freundlich parameters for 20 compounds and compared

experimental and calculated breakthrough times. Values of b ranged from 0.108 (methanol) to 1.040 (xylene).

Yoon and Nelson [18] fit capacities calculated from Gary Nelson's data for 10 compounds to the Freundlich Equation (9) and reported exponents of concentration from 0.092 to 0.652. As expected from Equations (10-11), these values differed from b in Equation (9) by -1.0.

The Langmuir adsorption isotherm equation [23] is:

$$W_e = \frac{W_{max}\, K_H\, C_o}{1 + K_H\, C_o} \qquad (12)$$

where k_H is Henry's Law coefficient and W_{max} is the limit of the capacity at high concentrations. Vahdat [24] has published an extensive list of Langmuir parameters for 27 organic vapors and 11 types of activated carbons (not all vapors for all carbons). The data used to derive these parameters were taken from published sources. The Langmuir isotherm equation reduces to Henry's Law (capacity is directly proportional to concentration) at low vapor concentrations, which some find desirable for thermodynamic reasons. It is also easy to apply to mixtures [24]. However, like the Freundlich equation the parameters are empirical and vary in unknown ways with vapor properties, carbon properties, temperature, etc.

Combinations of the Freundlich and Langmuir isotherm equations have been proposed:

$$q = \frac{a\, b\, C^n}{1 + b\, C^n} \qquad (13)$$

The extra parameter (exponent n) provides better (or at least as good) fits of adsorption isotherm data a either Equations (11) or (12). One example Equation (13) is the Kisarov [25] equation:

$$q = \frac{a\, b\, (p/p_{sat})^n}{1 + b\, (p/p_{sat})^n} \qquad (14)$$

Assuming a fixed micropore volume W_o (cm^3/g) and adsorbate in liquid form with normal density and molar volume V_m (cm^3/mol), then $a = W_o / V_m$ (mol/g carbon). The equilibrium pressure of the bulk (not adsorbed) vapor is p_{sat} and of the adsorbed vapor is p. According to Kisarov [25] the exponent n is a function of temperature T, affinity coefficient β (to be defined later in this report), and a fit constant k, so that : $n = kT/\beta$. Begun et al. [26] have suggested improvement of the Kisarov Equation by replacing the b in the numerator with (1+b). This Begun/Kisarov isotherm equation did fit tested data better than the D/R at the lowest pressures of ethanol and isopropanol. In another comparison Rasmuson [27] obtained consistent micropore volumes (0.475 ± 0.015 cm^3/g) and carbon structural constants with the D/R fit to toluene and butanol data, but with the Kisarov equation (0.635 ± 0.075 cm^3/g). The Begun/Kisarov equation improved calculated micropore volume consistency (0.545 ± 0.035 cm^3/g), but discrepancies among structural and exponential constants remained (6.96 ± 2.69 vs. 1.34 ± 0.01 for D/R). Inconsistent parameters among different chemicals make such an equation less useful for capacity predictions.

Hacskaylo and LeVan [28] developed an adsorption isotherm equation based on analogy with the well-established Antoine equation for vapor pressures:

$$\ln p = A' + \ln \theta \; - \; \frac{B' + b'(1-\theta)}{C' + T} \qquad (15)$$

where *A', B', C'* are Antoine constants obtainable from many sources for many gases and vapors. Theta is the fraction of saturation capacity, $\theta = W_e / W_{sat}$ and p is the vapor concentration in pressure units at temperature T. The saturation vapor pressure, p_{sat}, can be determined from temperature and the Antoine constants. W_{sat} is the capacity at p_{sat} . Like the Freundlich and Langmuir isotherm equations, the Hacskaylo/LeVan has two unknown (fit) parameters, W_{sat} and b'. However, these have physical meanings and, therefore, there is hope of them being correlated

with physical properties of a system. Unfortunately, few values of these parameters have been published and those for light gases only.

A noteworthy empirical correlation of capacities was published by Nelson and Correia [1]. They observed that within a "class" of compounds (e.g., monochlorinated hydrocarbons) capacities measured for 10% breakthrough fraction and 1000 ppm challenge increased linearly with normal (1 atm) boiling points. They tabulated the boiling point linear fit coefficients for 10 classes of compounds: acetates, alcohols, alkanes, alkyl benzenes, amines, ketones, monochlorides, dichlorides, trichlorides, and tetrachlorides. An advantage to this approach is that normal boiling points are readily available for many compounds. Disadvantages include uncertainty as to whether these correlations apply to other activated carbons and the limited number of classes correlated.

The Polanyi or Potential Adsorption Theory [29] has been developed on a sound theoretical basis. It is consistent with the Theory of Volume Filling [30], which recognizes activated carbon as a system of micropores into which vapors can condense. An adsorption potential is taken as the reversible isothermal work (change in free energy) of compressing a vapor into a liquid in the carbon micropores. It is defined in terms of thermodynamic quantities as:

$$\varepsilon = R\,T \ln (p_{sat}/p) \qquad (16)$$

where p_{sat} is the equilibrium vapor pressure of an adsorbate in the compressed (liquid) state at a given temperature, T; p is the actual adsorbate pressure (concentration) in the vapor phase; and R is the universal gas constant. Note that $p_{sat}/p = C_{sat}/C$ in concentration units (mass/volume, e.g., mg/m^3, or moles/volume, e.g., moles/L, or volume/total volume, e.g., parts-per-million, ppm)

The Theory of Volume Filling assumes a maximum adsorption volume, W_o (cm^3/gram

carbon) filled at p_{sat}, independent of the vapor adsorbed. The Gurvitsch rule [31] assumes that the maximum capacity in gravimetric or molar units can be related to W_o by the normal liquid density d_L (g/cm^3) or the normal liquid molar volume V_m (cm^3/mole) of the vapor, respectively:

Maximum capacity (grams vapor/gram carbon) $W_v = W_o \; d_L$ (17)

Maximum capacity (moles vapor/gram carbon) $W_v = W_o / V_m$ (18)

where $V_m = M_w / d_L$ for molecular weight M_w. Below the maximum capacity the actual adsorbed capacity can likewise be expressed in gravimetric or molar units.

Polanyi [32] added the observation that for a fixed adsorption volume, adsorption potentials for different vapors are related by constants:

$$\varepsilon_1 / \beta_1 = \varepsilon_2 / \beta_2 = \varepsilon_3 / \beta_3 = \varepsilon_{reference} / \beta_{reference} \quad (19).$$

The β are called “affinity coefficients” or “similarity coefficients”. Often benzene is taken as the reference compound and $\beta_{benzene} = 1$ is assumed. The relationship of Equation (19) leads to the idea that plots of adsorption capacity vs. adsorption potential for different vapors produce different curves that can be coalesced into one “characteristic curve” by applying the appropriate affinity coefficients. This process characterizes an activated carbon independent of any vapor.

An example of development and use of a characteristic equation is an application by Grubner and Burgess [15] of the Theory of Statistical Moments to the data of Nelson and Harder [21, 33]. Midpoints of breakthrough curves were used to obtain adsorption capacities (mL/g) for five vapors. When these capacities y were plotted vs. $x = [\ln (p_{sat} /p)]/ V_m$, with one exception the data fell on the same line. Therefore, molar volume was used as a surrogate for the affinity coefficient β (more on this later). A polynomial equation of three terms in x was fit to the data to give:

$$y = 0.749 – 8.307 \; x + 14.826 \; x^2 \quad (20)$$

Nelson and Carlson [34] applied the Theory of Statistical Moments and this empirical adsorption isotherm to calculate breakthrough curves of four vapors at four concentrations. They found that at low concentrations (< 10 ppm) calculated capacities y, and therefore breakthrough times, were negative. This is a result of the characteristic equation in polynomial form not being fit to capacity data at such low concentrations. A different carbon will likely have a different characteristic curve than Equation (20).

A major contribution by Dubinin et al. [35] was to develop a general mathematical form for the Polanyi characteristic equation applicable to volume filling of microporous adsorbents, including activated carbon. The well-known Dubinin-Radushkevich (DR) equation first published in 1947 can be stated in terms defined above as:

$$W_e = W_V \exp[- B(T/\beta)^2 \{\ln (p_{sat}/p)\}^2] \qquad (21)$$

where B, the carbon structural constant, in terms of a reference characteristic free energy E_o is:

$$B = (R / E_o)^2 \qquad (22)$$

Again, the reference is often benzene for which β is taken to be = 1.0. A more general equation is the Dubinin-Astakhov (DA) [36]:

$$W_e = W_V \exp[- (R T/\beta E_o)^n \{\ln (p_{sat}/p)\}^n] \qquad (23)$$

The exponent n is a measure of the heterogeneity of the micropore distribution in the carbon; typical values of for organic vapors on activated carbons range from 1.5 to 3.[37]. For carbons molecular sieves with narrow pore size distributions, n is at the upper end of this range; for highly activated carbons it is a the lower. [38] However, the DR (n = 2) equation well describes the adsorption capacity isotherm for typical industrial activated carbons.[39]

Using the DR equation and a database of β obtained or calculated from many sources, Wood [40] developed a correlation for β in terms of molar polarization, P_e, and a correlation for

B in terms of micropore volume, W_o . These correlations were combined to give:

$$W_e = W_o\, d_L \exp[-\, b\, W_o\, P_e^{-1.8}\, R^2\, T^2\, \{\ln (p_{sat}/p)\}^{\,2}] \qquad (24)$$

Equation (24) was fit to another database, including 1350 capacity data sets from 10 sources for about 140 different compounds and 15 activated carbons measured by seven techniques over 20 – 200 ^{o}C, to get the best fit value of:

$$b = 3.56 \times 10^{-5}\ \mathrm{mol^2\ cal^{-2}\ cm_o^{-3}\ (cm_L^3 / mol)^{1.8}} \qquad (25)$$

where the subscripts o and L on the units refer to carbon micropore volume and adsorbate liquid volume, respectively. Equations (24) and (25) allow estimations of vapor adsorption capacities without experimental data for a reference compound. Micropore volume for the activated carbon can be measured, obtained from its manufacturer, or estimated. Molar polarizability, liquid density, and saturation vapor pressure of can be obtained or easily calculated for many compounds from data in common references. [41, 42] A disadvantage of using Wood's correlations is that they represent only averages; actual carbon and vapor interaction properties in an application may differ from these averages.

D. Affinity Coefficient Models

The Polanyi Potential Theory predicts a characteristic curve upon which adsorption capacities will coalesce for many different compounds [29, 32]. A coalescence factor for each chemical is used to adjust the calculated adsorption potential to cause this to happen. This factor, the ratio of a chemical potential to that of a reference compound (often benzene), came to be called an "affinity coefficient of the characteristic curve" or a "similarity coefficient" and to be represented by the Greek letter beta, β. Several equation models have been used to correlate and predict β values.

Polanyi [32] and Berenyi [43] first attempted to correlated β as ratios of the square roots

of Van der Waals constants. This worked well for gases (except hydrogen) for which these constants were known. Dubinin and Sawerina [44] assumed that London forces were responsible for adsorption, The London potential for a molecule near a surface includes polarizability of the molecule. Therefore, they proposed that affinity coefficients be approximated by ratios of molecular polarizabilities:

$$\beta = P_e / P_{e\,(reference)} \qquad (26)$$

if polarizabilities of the surface and ionization potentials are assumed equal. Later, Dubinin and Timofeyev [45] proposed that polarizabilities could be approximated by molar volumes V_m in the liquid state, so that:

$$\beta = V_m / V_{m\,(reference)} \qquad (27)$$

Next, Vaskovsky [46] reported that ratios of molecular parachors gave better correlations with experimental βs than ratios of polarizabilities (the latter are often too high). Parachors Ω are obtained from surface tension measurements on pure liquids or can be calculated for organic compounds from Sudgen's increments [47, 42]. Therefore, according to Vaskovsky:

$$\beta = \Omega / \Omega_{(reference)} \qquad (28)$$

Various authors [48-51, 40] have debated which of Equations (26-28) is the best model for estimating β for one compound relative to a reference compound. Fits to experimental data and ranges of applicability (e.g., to non-liquids and inorganic gases) have been discussed. Wood [40] published an extensive database of experimental β and β^2 values. Using this database Wood found β^2 to be proportional to $P_e^{1.8}$, rather than directly proportional to P_e^2. Therefore,

$$\beta = [P_e / P_{e\,(reference)}]^{0.9} \qquad (29)$$

can be used. This reduced dependence on P_e explains the observation of Dubinin (mentioned above) that using polarizabilities often give β that are too high.

Another correlation parameter proposed [52] for β is the critical temperature T_c:

$$\beta = T_c / T_{c\,(reference)} \qquad (30)$$

This correlation has not been extensively tested, but appears to work better for gases than for compounds that are liquids at normal temperatures.

E. Adsorption Rates Models

The adsorption rate (or mass transfer) coefficient k_v determines (or describes) a third characteristic of a breakthrough curve, its steepness. It appears as an inverse factor of the (usually) logarithmic curve shape factor, as in Equation (1). Since the adsorption rate from flowing air is not infinitely fast (infinitely large k_v), the effect of a finite adsorption rate (coefficient) is to reduce the capacity that the carbon would have at equilibrium (see Equation (1)). The parameter k_v is more properly called a "coefficient" than a "constant", since it depends on several parameters of the adsorption system, particularly linear air flow velocity, v_L (see below).

Mecklenburg [9] introduced the concept of a "dead layer," I, more commonly know as a "critical bed depth," for removal of a gas or vapor from air flowing through a packed sorbent bed. It reduces the adsorbent bed breakthrough time from what would be predicted by equilibrium adsorption capacity:

$$t_b = \frac{W_e\ \rho_B}{60\ v_L\ C_o}[z - I] \qquad (31)$$

where in SI units t_b = breakthrough time (min), v_L = linear velocity (cm/s), ρ_B = packed bed density (g/cm^3), W_e = equilibrium capacity (g/g carbon), C_o = vapor influent concentration (g/cm^3 air), z = bed depth (cm), and I = critical bed depth (cm). The factor of 60 is to reconcile units as given.

Gamson et al. [11] derived semi empirical equations for mass transfer correlated with

Reynolds Number Re = (d_p G / η) and Schmidt Number Sc = (η / ρ_a D_v). For the case of external mass transfer (diffusion to the sorbent granule) being rate limiting (slowest step) and for turbulent flow, the height of a transfer unit (HTU) was expressed as:

$$\text{HTU} = \frac{1.011}{a}\left(\frac{d_p\, G}{\eta}\right)^{0.41}\left(\frac{\eta}{\rho_a\, D_v}\right)^{0.67} \qquad (32)$$

where in SI units *a* (cm^2/cm^3) = the effective surface area of adsorbent granules per unit bed volume, d_p = diameter of spherical granules (cm), G = superficial mass flow velocity (g/cm^2-s), η = viscosity of the air mixture (g/cm-s), ρ_a = density of the air mixture (g/cm^3), D_v = diffusion coefficient of the gas in air (cm^2/s), and 1.011, 0.41, and 0.67 are empirical coefficients without units. For cylindrical adsorbent granules with cylinder height h_c and diameter d_c, the effective d_p can be estimated by

$$d_p = [d_c\, h_c + (d_c^2/2)]^{0.5} \qquad (33)$$

Gamson et al. also tabulated maximum values of *a* for ideal spherical particles from the formula:

$$a = (6/d_p)(1- \varepsilon_e). \qquad (34)$$

Fractional void bed volume (or space or external porosity) ε_e measurements yielded average values of 0.42 for spherical granules 0.23-1.2 cm diameter and 0.38 for cylindrical granules 0.41-1.9 cm average diameter. The data showed no trends.

Klotz [10] combined the Mecklenburg and Gamson equations (with 1.011 rounded off to 1) and assumed C_o/C very large to get an expression for critical bed depth due to external mass transfer:

$$I_t = \frac{1}{a}\,\text{Re}^{0.41}\,\text{Sc}^{0.67}\,\ln\left(\frac{C_o}{C}\right) \qquad (35)$$

Klotz also observed that critical bed depth due to internal (to the adsorbent granules) mass

transfer (reaction, diffusion, etc.) rate is a complex function of structure and nature of the carbon and of the gas or vapor. For an assumed first-order transfer rate he generalized it with the expression:

$$I_r = k_r v_L \ln(C_o/C) \qquad (36)$$

This has a different velocity function and is not a function of granule size, so that theoretically the limiting rate and mechanism can be identified by dependence of the total critical bed depth, $I = I_t + I_r$, on these parameters. From Equations (1-5):

$$I = (Q / k_v A) \ln(C_o/C) = (60\ v_L / k_v) \ln(C_o/C) \qquad (37)$$

So that the apparent first order adsorption rate coefficient for external mass transfer can be expressed as:

$$k_v = 60\ v_L\ a\ Re^{-0.41}\ Sc^{-0.67} \qquad min^{-1} \qquad (38)$$

For both external and internal mass transfer rate limiting, Klotz gave a more general equation:

$$I = g\ v_L^{\,n} \ln(C_o/C) \qquad (39)$$

where g is a constant depending on (mesh) size of the carbon granules and n is a constant depending on the gas being removed. Then:

$$k_v = (60 / g)\ v_L^{\,1-n} \qquad (40)$$

Nelson et al. [1, 21, 33] used Klotz' breakthrough time equation for external mass transfer (only), which they referred to as the Mecklenburg equation:

$$t_b = \frac{W_e\ \rho_B}{C_o\ v_L}\left[z - \frac{1}{a} Re^{0.41}\ Sc^{0.67}\ \ln\left(\frac{C_o}{C}\right)\right] \qquad (41)$$

with $a = a_c\ \rho_B$ (cm^2 surface area/ cm^3 bed volume) (42)

for a_c = specific surface area (cm^2/g) of the carbon granules. [Note: this is not the same as the BET "surface area" determined by equilibrium adsorption capacity measurements.] For carbons in two of the cartridges (Types 1 and 2) tested the fractional bed void volumes (0.42 and 0.38

cm^3/g), average granule diameters (0.165 and 0.117 cm), and specific surface areas (45 and 77 cm^2/g) are known [33]. Therefore, we can calculate $a = 2.8/d_p$ for Type 1 carbon and $a = 3.5/d_p$ for Type 2. These can be compared with maximum values of $a = 3.6/d_p$ for perfect spheres, a fractional void volume of 0.40 and no effects of surface porosity on *a*.

Xiang et al. [53] simplified the Mecklenburg/Klotz Equation (41) containing Reynolds and Schmitt numbers into more familiar parameters to get the equivalent of :

$$t_b = (W_e A \rho_B / C_o Q)[z - m\, d_p^{1.41} (Q/1000A)^{0.41} M_w^{0.335} \ln (Co/C)] \quad (43)$$

in symbols and units defined previously. They obtained a best-fit value of 0.45 for *m* using experimental data for 23 vapors, two bed depths, three breakthrough fractions, and three airflows; granule size was not varied. Capacity W_e was determined using the DA equation, benzene as a reference, and affinity coefficients calculated from molecular parachors. The apparent constant *m* is actually:

$$m = 3.17\, (a\, d_p)^{-1} (\eta/\rho_a)^{0.26} (D_v\sqrt{M_w})^{-0.67} \quad (44)$$

The $(a\, d_p) \leq 3.6$ is a carbon-specific parameter and a weak function (see above); $(\eta/\rho_a)^{0.26}$ and $(D_v\sqrt{M_w})^{-0.67}$ are weak functions of the vapor-air mixture. Therefore, it is not surprising that *m* appeared to be constant and vapor invariant. [Note: The ln (C/C_o) approximation was incorrectly used at breakthrough ratios as high as 0.5 (see breakthrough curve shape discussion above).] The rate coefficient corresponding to Equation (43) is:

$$k_v = 1000\, (m)^{-1} d_p^{-1.41} (Q/1000A)^{0.59} M_w^{-0.335} \ \ min^{-1} \quad (45)$$

Using this approach Xiang et al. reported mean relative errors for breakthrough times of 4-8 % for their data and 13-18 % for data of Nelson and Harder [31]. Equation (45) can be expressed as a function of linear flow velocity v_L (cm/s) since $Q/(1000A) = 0.06\, v_L$.

The Gamson et al. [11] correlation for external mass transfer has been updated by Wakao

and Funazkri [54] with additional data and corrected for axial dispersion to give:

$$I_t = (1/a)[2.0 + 1.1\,(Sc)^{0.33}(Re)^{0.60}] \qquad (46)$$

The range of the new correlation is Re = 3 to 10,000; however, it must be used with care, especially at low Re, since the contributions of axial dispersion are not included. Following the same approach as Xiang et al., we obtain:

$$k_v = (Q/A)\,[0.56\,d_p + m'\,d_p^{1.6}\,(Q/1000A)^{0.6}\,M_w^{0.165}]^{-1} \quad min^{-1} \qquad (47)$$

with

$$m' = 1.65\,(\eta/\rho_a)^{-0.27}\,(D_v\sqrt{M_w})^{-0.33} \qquad (48)$$

for the external surface area per unit bed volume approximated by $a = 3.6/d_p$.

Wheeler [55] simplified the same correlations used by Klotz, but taken from Hougen and Watson [56]. Maximum adsorption rate coefficient k_∞ was defined as that due to external mass transfer rate limiting, i.e., much faster surface adsorption and subsequent diffusion. He also assumed that there is no desorption and that all gas-air mixtures have the same viscosity and Schmidt number. Wheeler gives the resulting rate coefficient as:

$$k_\infty = 10\;\; v_L^{0.5}\,M_m^{-0.5}\,d_p^{-1.5}\,P_T^{-0.5} \quad s^{-1} \qquad (49)$$

Jonas and Rehrmann [57] further reduced this to:

$$k_\infty = 111.6\;v_L^{0.5}\,d_p^{-1.5} \quad min^{-1} \qquad (50)$$

assuming 1 atm pressure P_T and an average molecular weight M_m of 28.8 g/mole for air containing dilute vapor. Experimental values of adsorption rate coefficients for five organic vapors in air ranged 20.6-28.0 min^{-1} with an average of 24.1; this compared well with a calculated k_∞ of 23.5 min^{-1}.

In subsequent work Jonas and Rehrmann [58] reported a different linear flow velocity (cm/min) dependence observed for benzene:

$$k_v = 24420.6 / [\ 1 + 7.688 \exp(-0.005275\ v_L)]\ \ min^{-1} \qquad (51)$$

This approached a maximum value for linear flow velocity above 15 cm/s for a 12-30 mesh granular carbon (0.104 cm mean diameter). The general form of Equation (51):

$$k_v = (a + b) / [\ 1 + (a/b) \exp(-(a + b)\ c\ v_L)] \qquad (52)$$

was also fit by Rehrmann and Jonas [59] to experimental data for dimethyl methylphosphonate (DMMP) vapor. In this case the maximum rate coefficient (2600 s^{-1} or 156000 min^{-1}) was attained above v_L = 50 cm/s or below d_p = 0.02 cm. They explained these results and the form of Equation (52) as being due to changes in the rate controlling (limiting) step with changes in flow velocity and granule size. In a subsequent study with a 6-10 mesh (0.268-cm diameter granules) carbon, Jonas et al. [60-61] assumed that internal (pore) diffusion was rate limiting and that the molecular weight of the air mixture M_m in Equation (49) could be replaced with the molecular weight of the vapor M_w. Thus, the overall rate adsorption coefficient becomes inversely proportional to the square root of the molecular weight M_w. If the rate coefficient for a reference compound is known, then:

$$k_v = k_{v\ (reference)} [M_{w\ (reference)}\ /M_w\ ]^{1/2} \qquad (53)$$

This relationship was tested for seven compounds with molecular weights ranging over (only) a factor of two with a mean relative deviation of 9%. Wood and Stampfer [62] tested this relationship and found that it did not hold for a wider range of compounds.

Grubner and Underhill [63] presented mass transfer terms for the Statistical Moments Theory. Three combinations of rate limiting mechanisms were considered. The simplification for mass transfer resistance controlled by internal (pore) diffusion resulted in this breakthrough time expression:

$$t_b = t_{50} (1 + a\ \phi\ x_c + b\ \phi^2\ (x_c^2 - 1)) \qquad (54)$$

with $\phi = (R^2 u/ \varepsilon D_i L)^{1/2}$, where L (= z in cm) is the length of the bed, u (= v_L / ε_e in cm/s) is the average interparticle linear flow velocity, ε is the ratio of fractional internal porosity ε_i to fractional external porosity ε_e of the bed, D_i (in cm^2/s) is the internal (granule) pore space diffusion coefficient, and R (= d_p / 2 in cm) is the effective sorbent granule radius. The constants are granule shape factors a = 0.365 and b = 0.0477. For highly microporous carbons internal porosity ε_i (cm^3/ cm^3 of carbon bed) can be estimated from the micropore volume (cm^3/g) multiplied by the packed bed density (g/cm^3): $\varepsilon_i = W_o \rho_B$. For external porosity Gamson [11] showed (see above discussion) $\varepsilon_e = 0.40 \pm 0.02$.

Grubner and Burgess [15] applied this SMT approach with only two moments to breakthrough curve data. They used a relative standard deviation, $\sigma / t_{50} = a \phi$, to describe the spreads of the breakthrough curves and showed it to be apparently independent of challenge vapor concentration (100 – 2000 ppm) and almost proportional to granule size. They assumed $\varepsilon_i = \varepsilon_e$ (i.e., $\varepsilon = 1$) and $D_i = D_v$ (both actually upper limits) and replaced ε in the definition of ϕ with $2(1 + \varepsilon)$ (for unexplained reasons). Then ϕ became $(d_p / 4) (v_L/ \varepsilon_e D_v z)^{1/2}$. Assuming no breakthrough curve asymmetry (neglecting the third term of Equation (54)) and setting $(a \phi) = (60 v_L/k_v z)$ gives:

$$k_v = 658 (v_L/z)^{1/2} (\varepsilon_e D_v)^{1/2} dp^{-1} = 26884 (Q/V_B)^{1/2} (\varepsilon_e D_v)^{1/2} dp^{-1} \quad (55)$$

Wood and Stampfer [62] measured 165 breakthrough curves for 27 hydrocarbons and fluorocarbons. They also obtained breakthrough curves from the extensive work of Nelson et al. [1, 21, 33]. Adsorption rate coefficients were extracted from these using a form of Equation (3) and correlated with molar polarizations P_e to give:

$$k_v = [(v_L^{-1} + 0.027) (I + S_b / P_e)]^{-1} \quad min^{-1} \quad (56)$$

for I = 0.000825 min-(cm/s) and $S_b = 0.063 – 0.0055 \ln [(C_o – C) /C]$ and P_e = molar

polarizability (cm^3/mol). The increase of k_v with linear flow velocity was almost linear. Most breakthrough curves were at least slightly asymmetrical, so that rate coefficients calculated at 1% breakthrough were larger than those at 10%. This is the source of the breakthrough fraction dependence of the parameter S_b in Equation (56). In these sets of data there were no apparent effects of challenge concentration or granule size on reciprocal rate coefficients. Combined uncertainty in calculated reciprocal rate coefficients due to the empirical model and due to experimental data used was $\pm$ 50 % (2 standard deviations).

Lodewyckx [64] has derived an empirical equation for k_v as a function of linear flow velocity, average carbon granule diameter, and affinity coefficient:

$$k_v = 60\ (0.8)\ \beta^{0.33}\ v_L^{0.75}\ dp^{-1.5} \quad min^{-1} \qquad (57)$$

This is based on 55 tests of packed carbon beds for 7 carbons, 12 chemicals, 9 linear airflow velocities ranging 2 – 33 cm/s and 6 average granule sizes ranging 0.10 – 0.34 cm diameter.. Most values of β were obtained relative to benzene using assumed proportionality with molar polarizations. Values of k_v were calculated from measured 0.1% breakthrough times and capacities calculated by the Wood [40] correlations. Breakthrough curve asymmetry is not included. The observed velocity dependence is closer to that observed by Wood and Stampfer [62] than to the theoretical square root dependence in Equations (49, 50 and 55) and observed experimentally [14, 65, 73]. Since Lodewyckx assumed β proportional to P_e and referenced to benzene (P_e = 26.274), Equation (57) can be expressed as:

$$k_{v\ 0.1\%} = 16.3\ P_e^{0.33}\ v_L^{0.75}\ d_p^{-1.5} \quad min^{-1} \qquad (58)$$

Nelson and Correia [1] summarized adsorption and breakthrough data and developed a single-term equation for estimating service lives of respirator cartridges at 10% breakthrough. No adsorption rate coefficient is included; however, by comparing it with the Wheeler and

Reaction Kinetic breakthrough equations, we conclude that this model inherently assumes that the rate term is proportional to the capacity term:

$$\frac{W_e\ \rho_B}{C_o\ k_v}\ \ln\left(\frac{C_o - C}{C}\right) = k_1\ \frac{W_e\ W}{C_o\ Q} \qquad (59)$$

At 10% breakthrough:

$$k_v = \frac{Q\ \rho_B}{W\ k_1}\ \ln\left(\frac{C_o - C}{C}\right) \qquad \text{min}^{-1} \qquad (60)$$

where the proportionality constant k_1 can be defined by using the experimental rate coefficient for a reference (e.g., benzene).

F. Effects of Temperature on Rate Coefficients

Jonas and Svirbely [66] measured adsorption rate coefficients for carbon tetrachloride and chloroform at 25-50 ^{o}C. Assuming a relation between adsorption rate coefficient and the adsorption equilibrium constant and assuming a rate limiting mechanism, they calculated equilibrium heats of adsorption that were 4 % and 2 % higher, respectively, than the heats of liquefaction. However, simple Arrhenius plots ($\ln[k_v]$ vs 1/T with T in ^{o}K) of their experimental adsorption rate coefficients give activation energies of adsorption of –6392 cal/mol and –5879 cal/mol, respectively. These are 88% and 85% of the heats of liquefaction, respectively. Heats of liquefaction are negatives of heats of vaporization, which can be obtained from Arrhenius plots of vapor pressures of the pure substances. These relatively large negative values of the activation energies reflect the experimentally observed large decreases in k_v with increasing temperature.

A similar calculation of the effect of temperature on the adsorption rate coefficient by Jonas et al. [67] for DMMP predicted decreasing k_v with increasing temperature. However, no measurements were made for this comparison. A temperature 3/2-power function was assumed for molecular diffusivity, the DR equation was used for the temperature dependence of

equilibrium capacity, and the heat of adsorption was assumed equal to the heat of liquefaction. The resulting calculated k_v values, when plotted on an Arrhenius plot, give a slope equivalent to an activation energy of adsorption which is 92% the heat of liquefaction. The validity and generality of this approach to calculating effects of temperature need to be further tested with data.

G. Breakthrough Time Models (Dry Conditions, Single Vapor)

An equation model for predicting breakthrough time of a packed carbon bed or service life of a carbon-filled cartridge requires these sub-models:

1) An adsorption isotherm equation with at least 2 input parameters
2) A breakthrough curve shape term as a function of breakthrough fraction
3) An adsorption rate coefficient value or equation

In addition, these are desired for better description of actual breakthrough curves:

4) A way to incorporate asymmetry (skew) in the curves
5) Temperature effects for the adsorption isotherm
6) Temperature effects for the adsorption rate coefficient
7) Relative humidity effects on both capacity and adsorption rate
8) Effects of other vapors in mixtures in air

Various authors have selected from (usually) items 1) – 3) to put together breakthrough time equation models. A distinction can be made between a predictive model and a correlative model. A predictive model is one that provides all the necessary equations and input parameters (or sources to obtain needed input parameters). Some parameters, such as temperature or breathing rate, will need to come from the application. But, ideally, the others, such as molecular weight of the vapor, can be found in reference handbooks or may be calculated from data in such resources. The range of applicability of the model will depend on the availability of input

parameters. For example, if a Freundlich isotherm is specified in the model and the available list of Freundlich parameters includes only 8 vapors, then the model is limited to only those 8 vapors. A less empirical isotherm model, such as the Dubinin/Radushkevich, allows extension to other vapors only by knowing the β parameter, which can be calculated from molar polarization, which can in turn be calculated from molecular weight, diffractive index, and liquid density obtained from a handbook.

A correlative (or descriptive) model differs in that it requires experiments to be performed to obtain some of the parameters needed to extrapolate to an application. For example, if the model doesn't include a way of calculating an adsorption rate coefficient, it may be necessary to measure at least one breakthrough curve to get a value for k_v. On the other hand, an actual measurement with the cartridge and/or vapor of concern will likely make the estimate of service life for the application more reliable.

These two model descriptors actually represent the extremes of a spectrum. All predictive models are developed from experimental data as well as theoretical concepts. When combined with a measurement they can be made even more reliable. An equation used for correlating experimental data can require less experimental data as the input parameters become better understood.

Table I lists six complete predictive equation models which have been used to estimate breakthrough times for comparison with experimental data. Table II lists correlative models that have been proposed and used to extrapolate from data at one or more conditions to breakthrough times or curves at other conditions. Only two of these [Wood and Yoon/Nelson] include asymmetry parameters. None of these addresses relative humidity or mixtures.

Table I. Predictive Models Used to Estimate Breakthrough Times (Service Lives)

Designation	Capacity Equation	Rate Equation	Shape Term	Use References
Mecklenburg/ Klotz	Dubinin/Radushkevich with β calculated from molar volume, molecular parachor, or measured	Gamson et al. [10], external mass transfer	ln (C/Co)	Nelson [21, 33] Smoot [2]
Modified Wheeler	Dubinin/Radushkevich with β calculated from molar volume or molecular parachor,	Jona-/Rehrmann [57], maximum external mass transfer rate, $k_v = 111.6\ v_L^{1/2}\ d_p^{-3/2}\ min^{-1}$	ln (C/Co)	Nelson [1, 68, 69] Smoot [2, 70]
Nelson Empirical	Boiling point correlations plus Freundlich with $C^{2/3}$. Parameters tabulated for 10 classes of compounds.	Included in capacity term, i.e., rate term is proportional to capacity term	Included in the capacity term; This model is for 10% breakthrough only	Nelson [1] Smoot [2]
Statistical Moments	Polanyi plot characteristic equation expressed as a polynomial	Internal pore diffusion rate per Grubner and Underhill [63]	Normal distribution function with 2 moments	Grubner and Burgess [15], Nelson and Carlson [34]
Wood	Dubinin/Radushkevich with β calculated from molar polarization $P_e^{0.9}$ and the carbon structural constant from micropore volume by correlation data	k_v an empirical function of molar polarization, flow velocity, and breakthrough fraction	ln {C/(Co-C)}	Wood [71]
Xiang	Dubinin/Astakhov with β calculated from molecular parachor	Reduced Gamson for external mass transfer, fit to only one carbon	ln (C/Co)	Xiang et al. [53]

Table II. Correlative Models Used to Estimate Breakthrough Times (Service Lives)

Designation	Capacity Equation	Rate Equation	Shape Term	Use References
Yoon/Nelson	Freundlich with parameters empirically determined by measuring breakthrough curves. Values for 9 vapors from Gary Nelson data are reported.	k_v and asymmetry parameters empirically determined by fitting equations to breakthrough curves. Capacity and rate fit parameters are reported for 121 compounds from Gary Nelson data.	ln {C/(Co-C)} with asymmetry incorporated by an equation for capacity change with time.	Yoon and Nelson [7, 17, 18,72]
Balieu	Langmuir with parameters empirically determined by measuring breakthrough curves at different concentrations.	k_v empirically determined by fitting equation to breakthrough curves. k_v proportional to $v_L^{1/2}$	ln {C/(Co-C)}	Balieu [73]
Residence Time	Freundlich with Nelson's average power of 0.67.	Breakthrough time determined experimentally as a function of bed residence time for ond size bed is applied to another.		Cohen and Garrison [75], Ackley [74]

H. Review of Single Vapor Breakthrough Time Databases

We examined published and unpublished sources, many discussed previously, for listings (databases) of breakthrough times of varieties of chemical vapors. It was anticipated that these could be used for testing service life models. The preliminary criteria for selection were:

- Breakthrough time data given, not merely correlation parameters.
- Complete set of testing (or use) conditions and description of the cartridge(s) or carbon bed(s) given.
- At least 9 vapors studied.

Desirable characteristics were:

- Concentration varied over a wide range.
- Flow velocity varied over a wide range.

Table III lists the most promising databases found and some of their characteristics.

I. Comparisons of Complete Predictive Models

We have compared five of the service life predictive models listed in Table I. The Xiang model could not be included, since the DA parameter B given in their paper [53] is incorrect and does not give reasonable values for capacities. The database selected for comparing breakthrough times was taken from Table IV of Nelson and Correia [1]. Only data for 50% or 65% relative humidity were used. Included were 32 chemicals, 3 types of organic vapor cartridges (and their carbons), and vapor concentrations ranging 100-2000 ppm. We used average carbon weights and densities given in that reference.

The original table of Nelson and Correia included experimental 10% breakthrough times and those calculated by the Mecklenburg/Klotz, Wheeler/Jonas, and Nelson models described previously. To this we have added $t_{10\%}$ predictions of the Wood and Statistical Moments Theory

Table III. Candidate Single-Vapor Breakthrough Time Databases for Evaluations of Service Life Models

Data Resource	Ref.	Number of Organic Vapors	Concentration Varied?	Flow Velocity Varied?	Relative Humidity Varied?	Other Comments
MSA (1999)	76	15	Yes, Usually x 5 or more range	No	Yes	3 cartridges; 75 ^{o}F, 64 L/min
Smith (1996)	77	12	Yes, Usually 1000-10000 ppm	No	Yes	22 – 80% RH; 10 ppm breakthrough times
Smoot (1977)	2	12	No, 1000 ppm	No	Yes	0, 50, 80% RH; 1%, 10%, 50%, and 99% breakthrough times
Xiang (1998)	53	23	No, 2000 ppm	Yes	No	2 bed depths;3 Flow velocities; 5%, 10%, and 50% breakthrough times
Tanaka (1993)	78	46	No, 300 ppm	No	No	1.67 % breakthrough times
Freedman(1973)	79	29	No, 1000 ppm	No	No	0.5% breakthrough times
Nelson, Carlson, and Johnson (1980)	22	20	No, 10 TLVs	No	No	10% breakthrough times and Freundlich correlations
Nelson V (1974)	33	121	No, 1000 ppm	No	No	1%, 10%, 99% breakthrough times and equilibrium capacities
Nelson VI (1976)	21	9	Yes, 50-2000 ppm	Yes	Yes	10% breakthrough times and equilibrium capacities
Nelson VII (1976)	69	36	Yes, 100-2000 ppm	Yes	Yes	10% breakthrough times
Nelson VIII (1976)	1	32	Yes	No	Yes	10% breakthrough times

models for dry conditions. The results are listed in Table IV. Figure 3 shows graphical comparisons of the five models with each other and with experimental breakthrough times.

The Mecklenburg/Klotz and Wheeler/Jonas results were very close to each other for all data points. This is because they were based on capacity predictions using the same D/R equation and parameters. The rate terms of Equations (3) and (5) are much smaller than the corresponding capacity terms, so differences in the former affect the total breakthrough times very little. This shows the weakness of using total breakthrough time to determine success of rate coefficient models, as has often been done.

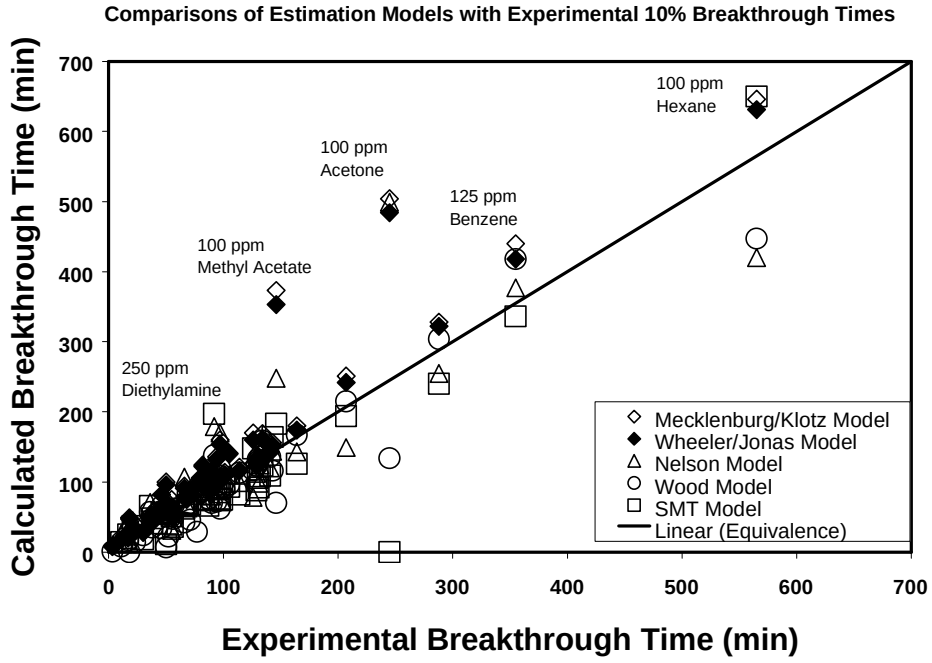

Figure 3. Comparisons of five predictive single-vapor models with experimental 10% breakthrough times.

Table IV. Predictions of Single-Vapor Service Life Predictive Models.

				10% Breakthrough Time (min)					
Cartridge Type	Chemical Vapor	Flow (L/min)	Conc (ppm)	Exptl.	Meckl./ Klotz	Wheeler/ Jonas	Nelson	Wood	SMT
1	Benzene	53.3	125	355	440	418	377	418	336
1	Benzene	53.3	500	134	169	161	150	159	123
1	Benzene	53.3	2000	42	59	56	59	55	41
3	Benzene	53.3	1000	101	114	110	127	90	100
1	Toluene	20.6	1000	288	328	322	255	304	240
1	Toluene	36.7	1000	164	180	174	143	167	126
1	Toluene	53.3	1000	114	121	116	99	113	82
1	Methanol	53.3	1000	3.2	8.6	7.9	-0.5	1	-15
1	Isopropanol	53.3	500	126	170	160	78	117	148
1	Isopropanol	53.3	2000	55	75	63	31	51	51
1	Butanol	53.3	1000	141	150	143	120	136	109
1	Pentanol	53.3	1000	130	137	134	139	132	106
3	Vinyl Chloride	40	50	77	99	96	-69	29	-2016
1	Vinyl Chloride	40	250	52	58	57	-24	22	-221
1	Vinyl Chloride	40	1000	23	32	31	-9	14	-10
1	Ethyl Chloride	53.3	1000	11	22	18	26	8	14
1	1-Chlorobutane	53.3	1000	87	90	87	73	76	66
1	Chlorobenzene	53.3	1000	131	132	128	98	130	92
1	Dichloromethane	53.3	500	30	30	28	44	24	18

1	Dichloromethane	53.3	1000	17	21	20	18	17	25
1	o-Dichlorobenzene	53.3	1000	132	132	130	124	136	108
1	Chloroform	53.3	1000	52	70	67	52	61	57
1	Methyl Chloroform	53.3	250	207	251	242	149	215	194
1	Methyl Chloroform	53.3	2000	56	51	50	37	47	36
1	Trichlorethylene	53.3	1000	83	108	103	73	96	74
1	Carbon Tet	53.3	1000	69	82	79	87	84	67
1	Perchloroethylene	53.3	1000	129	128	123	112	123	88
1	Methyl acetate	53.3	100	146	373	353	248	70	183
1	Methyl acetate	53.3	1000	46	74	82	53	34	56
3	Ethyl acetate	53.3	1000	90	115	111	80	70	97
1	Propyl acetate	53.3	1000	99	110	106	72	93	75
1	Butyl acetate	53.3	1000	97	106	104	87	109	76
3	Acetone	53.3	100	245	504	484	499	134	0
3	Acetone	53.3	500	97	160	154	170	62	85
3	Acetone	53.3	1000	66	94	91	107	42	62
2	2-Butanone	53.3	1000	94	136	132	103	72	96
2	Diisobutyl ketone	53.3	1000	94	97	97	103	90	92
2	Pentane	53.3	1000	71	86	84	68	46	68
3	Hexane	53.3	100	565	646	631	420	447	650
3	Hexane	53.3	500	143	156	152	144	116	164
3	Hexane	53.3	2000	38	44	43	57	35	48
1	Hexane	53.3	1000	68	78	75	67	67	65
2	Cyclohexane	53.3	1000	82	124	122	90	87	89
2	Heptane	53.3	1000	80	106	104	87	85	83
2	Methylamine	53.3	1000	18	49	47	13	0	-120
2	Ethylamine	53.3	1000	50	100	96	57	7	11
1	Diethylamine	53.3	250	92	117	110	179	138	197
1	Diethylamine	53.3	1000	36	53	50	71	57	66
1	Diethylamine	53.3	2000	21	34	32	45	35	37
2	Dipropylamine	53.3	1000	105	141	140	110	96	93

These two models overestimated breakthrough times at the lowest concentrations. We attribute this to failure of the DR capacity predictions using molar volume ratios for affinity coefficients β. The Nelson model also gave large overestimates for low concentrations in some cases.

The Statistical Moments Theory application of Grubner and Burgess [15] often gave values close to experimental ones (i.e., close to the equivalence line of Figure 3); however, it can give zero or negative capacities and breakthrough times when $x = [\ln(p_{sat}/p)]/V_m \geq 0.114$; i.e., for low concentrations and/or very volatile chemicals.

Figure 3 shows the Wood model predictions to be near or lower than experimental values. For service life predictions underestimates are preferable to overestimates. This model gave no negative breakthrough time predictions, even with vinyl chloride, as occurred with the Nelson and SMT models.

J. Comparisons of Adsorption Rate Coefficient Predictions

Nine models for calculating adsorption rate coefficients were discussed in a previous section and are listed in Table V. In this section we will compare their predictions with rate coefficients obtained from two sets of experimental data.

The first database is from Table I of Nelson and Harder [33]. It includes 1% and 10% breakthrough times and equilibrium capacities for 121 chemicals and two brands of cartridges with differing dimensions and carbons. In order to test rates separately, we will assume the capacities W_e (g/g), bed volumes V_B (cm^3), and bed carbon weights W (g) listed in this table. Vapor pressures and diffusion coefficients are also listed. Flow rate Q= 53300 cm^3/min and vapor concentrations C_o = 1000 ppm = M_w/24.210 g/cm^3 at 22 ^oC are fixed. Using the Reaction Kinetic form of the Wheeler Equation, the experimental rate coefficient at 10% breakthrough becomes:

$$k_{v10\%}\ (min^{-1}) = \frac{[\ln(9)]/V_B}{\frac{1}{Q} - \left(\frac{t_b\, C_o}{W_e\, W}\right)} \qquad (61)$$

Xiang et al. [53] provided the second database we used. It includes 10% and 50% breakthrough times for three volumetric flow velocities (Q/1000A in L/(min-cm^2)), two bed depths (we will only use z = 2 cm), and 23 chemicals at 2000 ppm. The $t_{50\%}$ are taken as the

stoichiometric centers of the breakthrough curves and as measures of capacity, so that:

$$k_{v10\%}\ (\text{min}^{-1}) = \frac{1000[\ln(9)]\,V_v\,t_{50\%}}{z\,(t_{50\%} - t_{10\%})} \qquad (62)$$

Comparisons of calculated rate coefficients with experimental ones are given in Figures 4 – 14 for the Nelson data and in Figures 15 – 22 for the Xiang data.

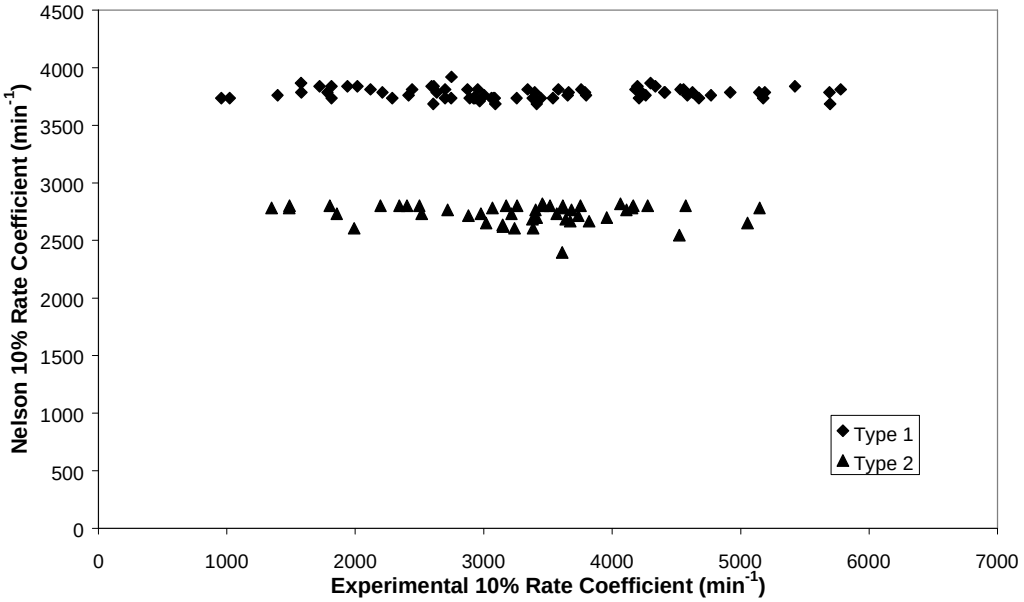

Figure 4. Comparisons of predictions of rate coefficients from the Nelson 10% breakthrough model with experimental rate coefficients [33].

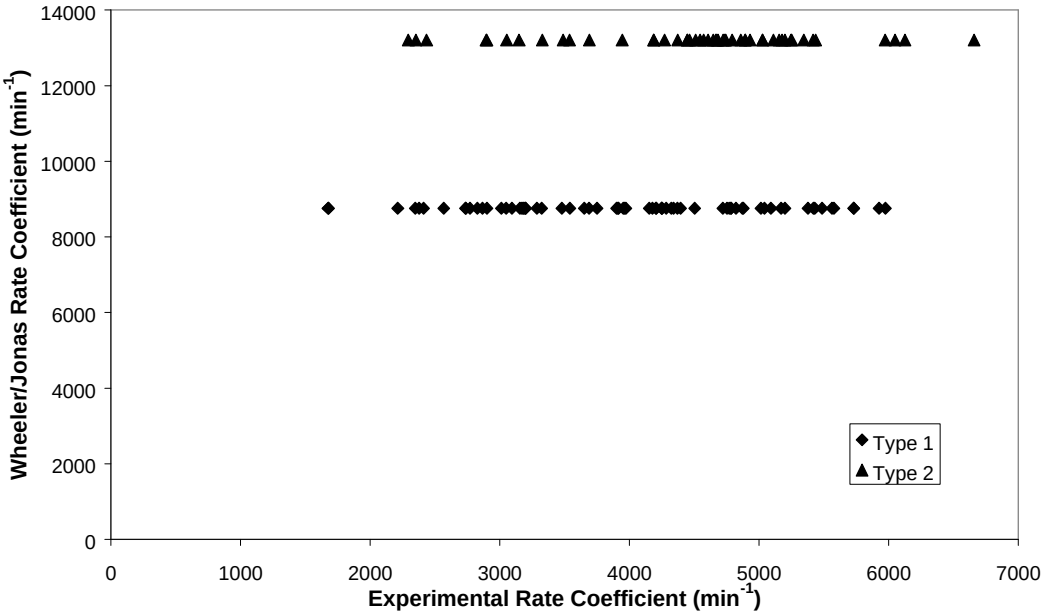

Figure 5. Comparisons of predictions of rate coefficients from the Wheeler-Jonas equation with experimental rate coefficients [33].

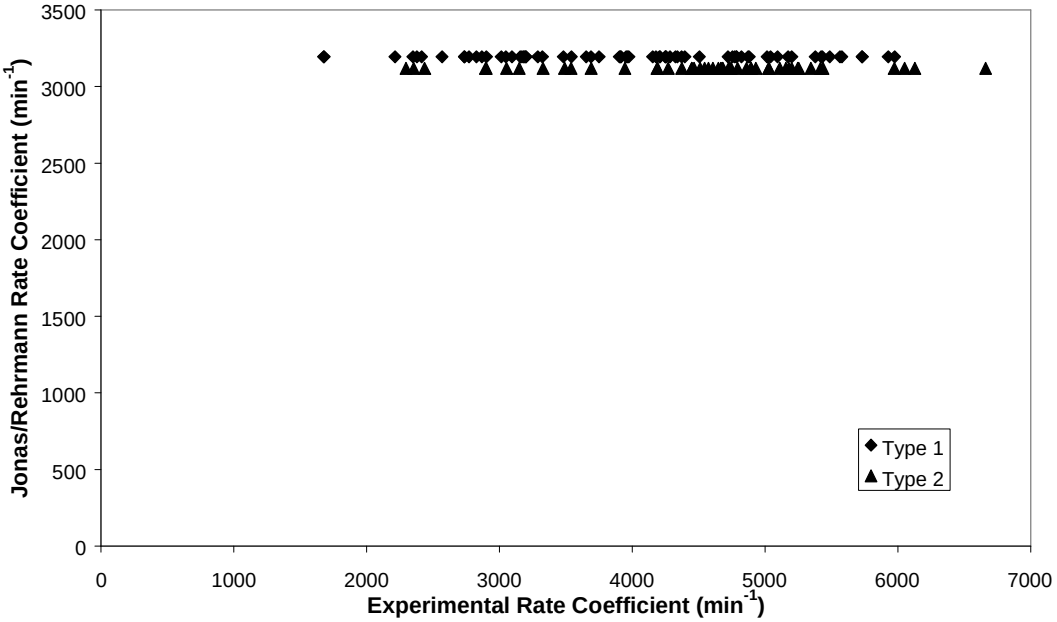

Figure 6. Comparisons of predictions of rate coefficients from the Jonas-Rehrmann equation with experimental rate coefficients [33].

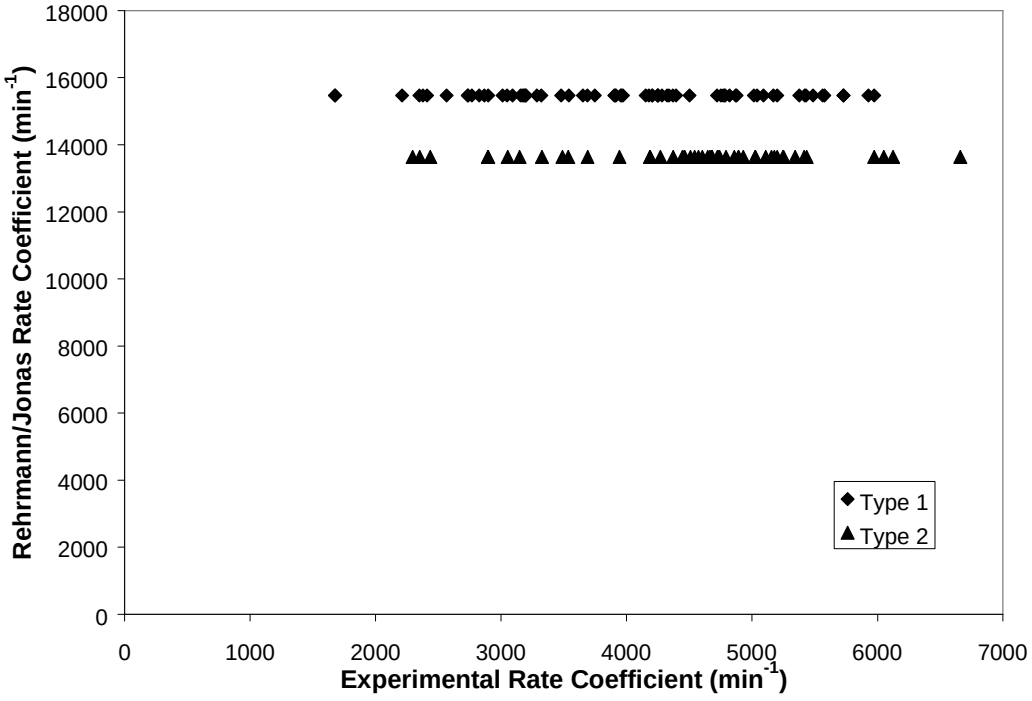

Figure 7. Comparisons of predictions of rate coefficients from the Rehrmann-Jonas equation with experimental rate coefficients [33].

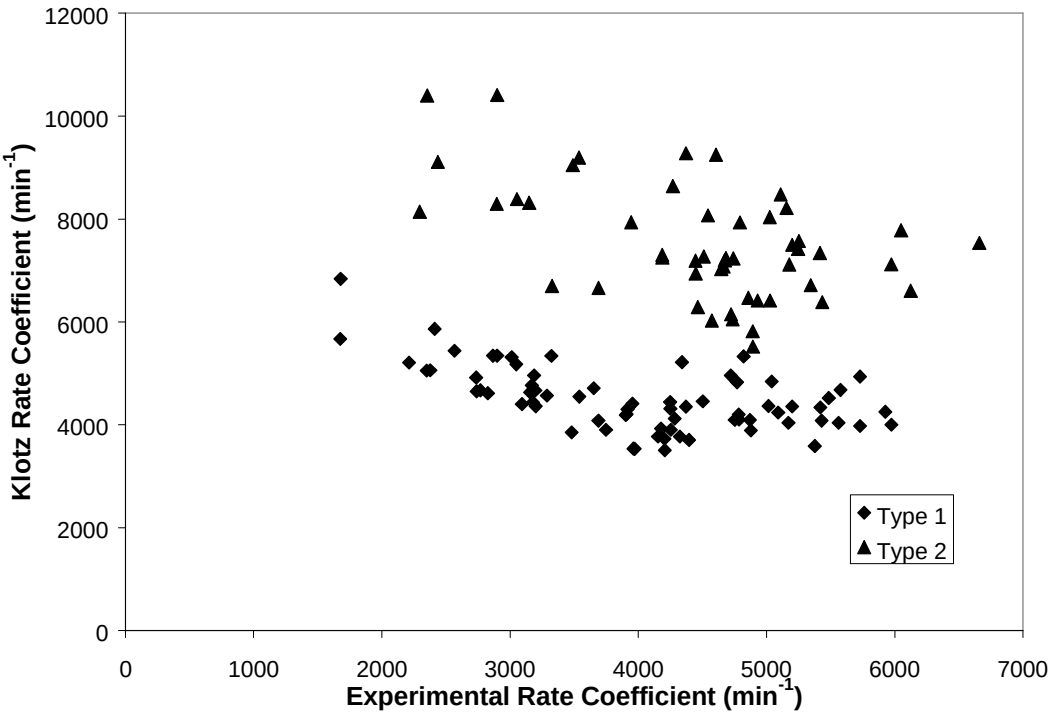

Figure 8. Comparisons of predictions of rate coefficients from the Klotz equation with experimental rate coefficients [33].

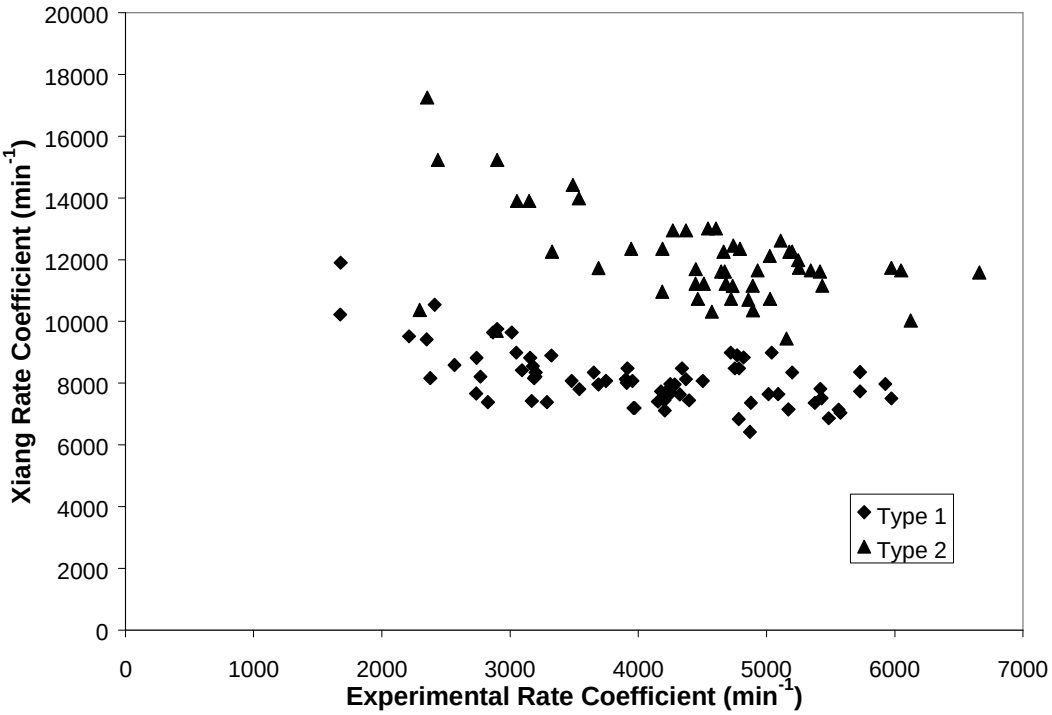

Figure 9. Comparisons of predictions of rate coefficients from the Xiang equation with experimental rate coefficients [33].

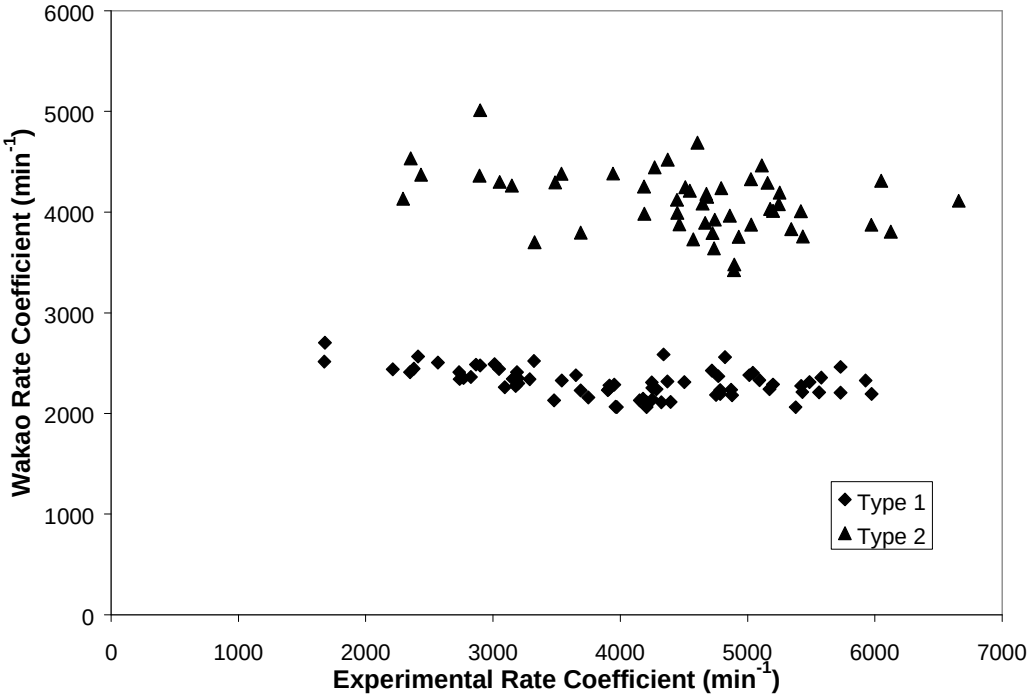

Figure 10. Comparisons of predictions of rate coefficients from the Wakao equation with experimental rate coefficients [33].

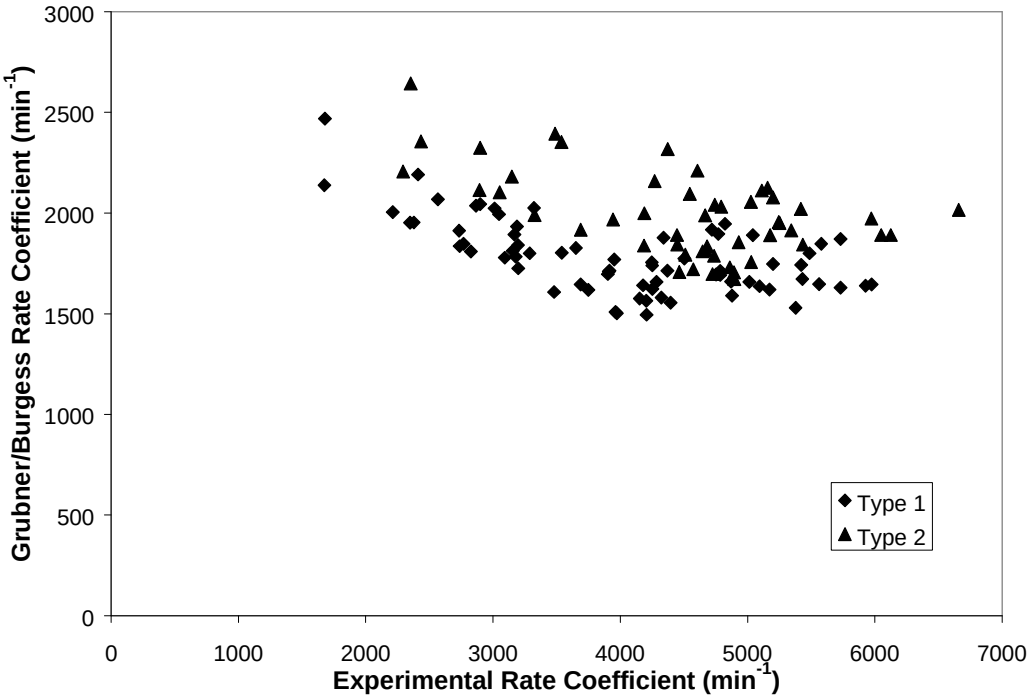

Figure 11. Comparisons of predictions of rate coefficients from the Grubner-Burgess equation with experimental rate coefficients [33].

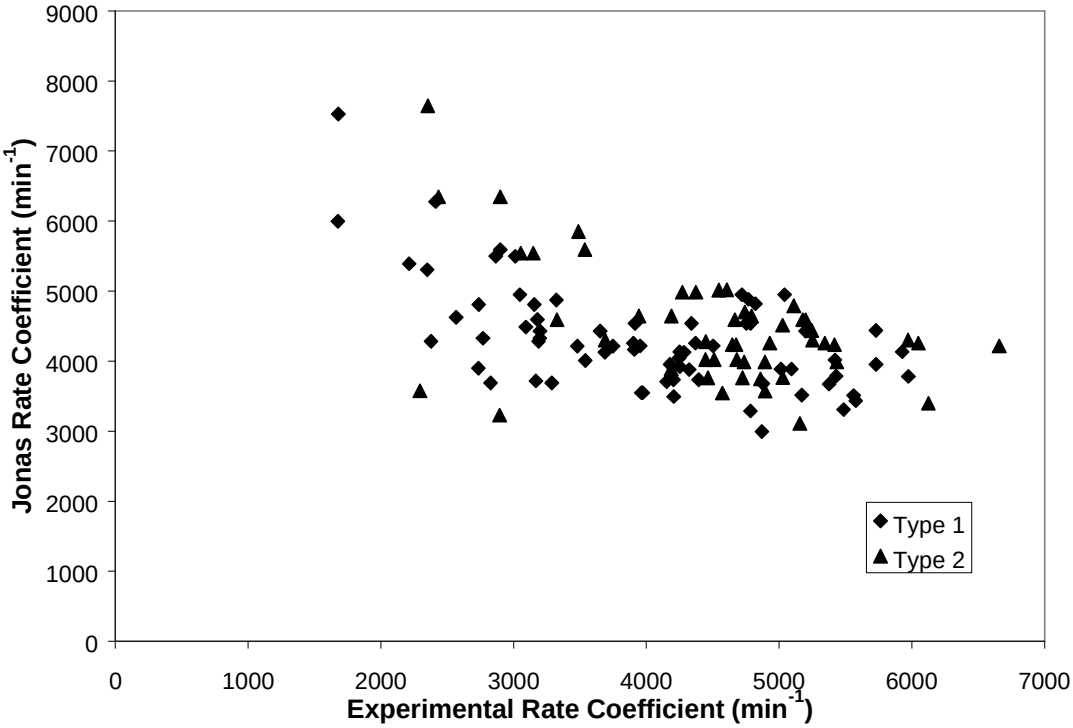

Figure 12. Comparisons of predictions of rate coefficients from the Jonas equation with experimental rate coefficients [33].

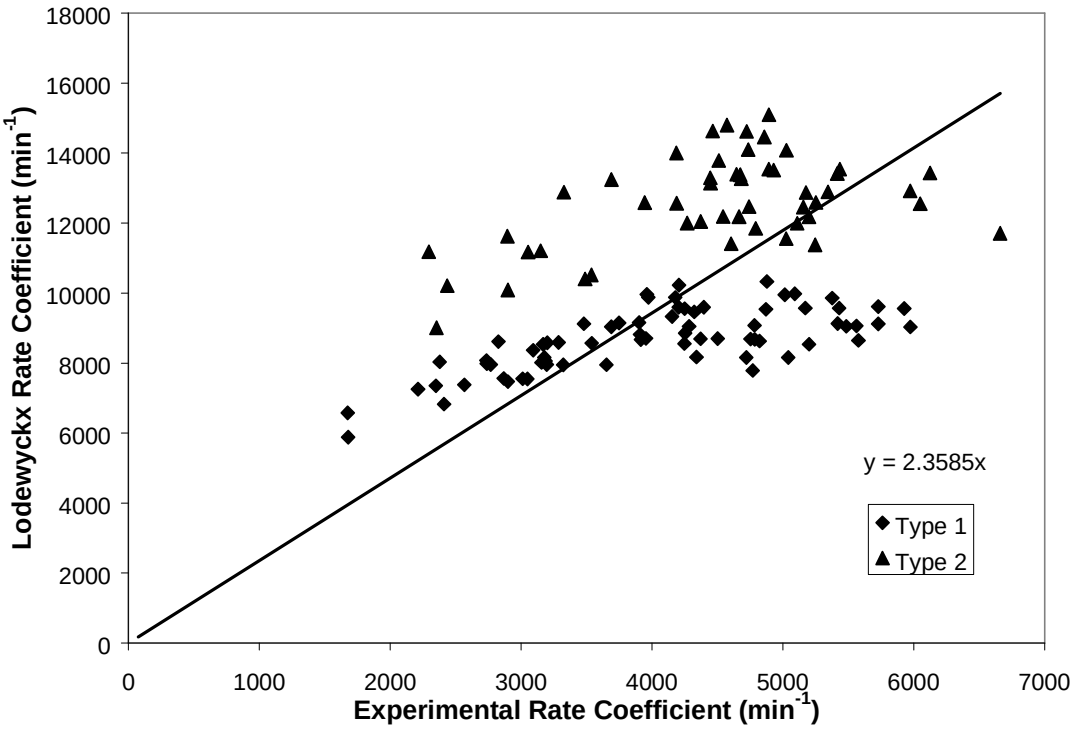

Figure 13. Comparisons of predictions of rate coefficients from the Lodewyckx equation with experimental rate coefficients [33].

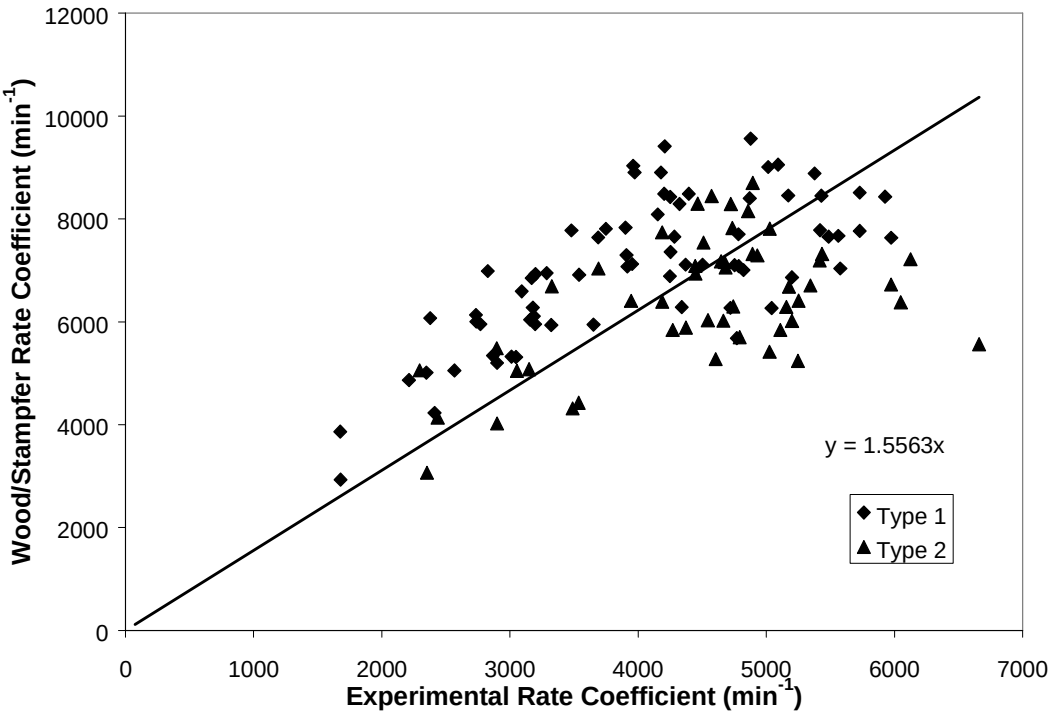

Figure 14. Comparisons of predictions of rate coefficients from the Wood-Stampfer equation with experimental rate coefficients [33].

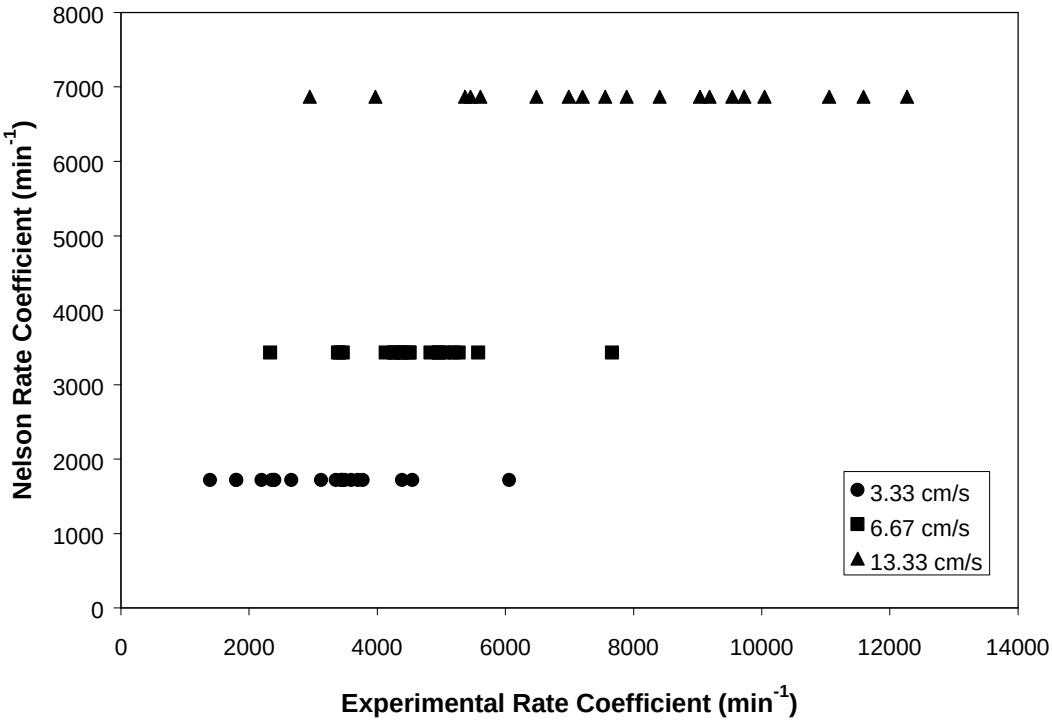

Figure 15. Comparisons of predictions of rate coefficients from the Nelson 10% breakthrough model with experimental rate coefficients [53].

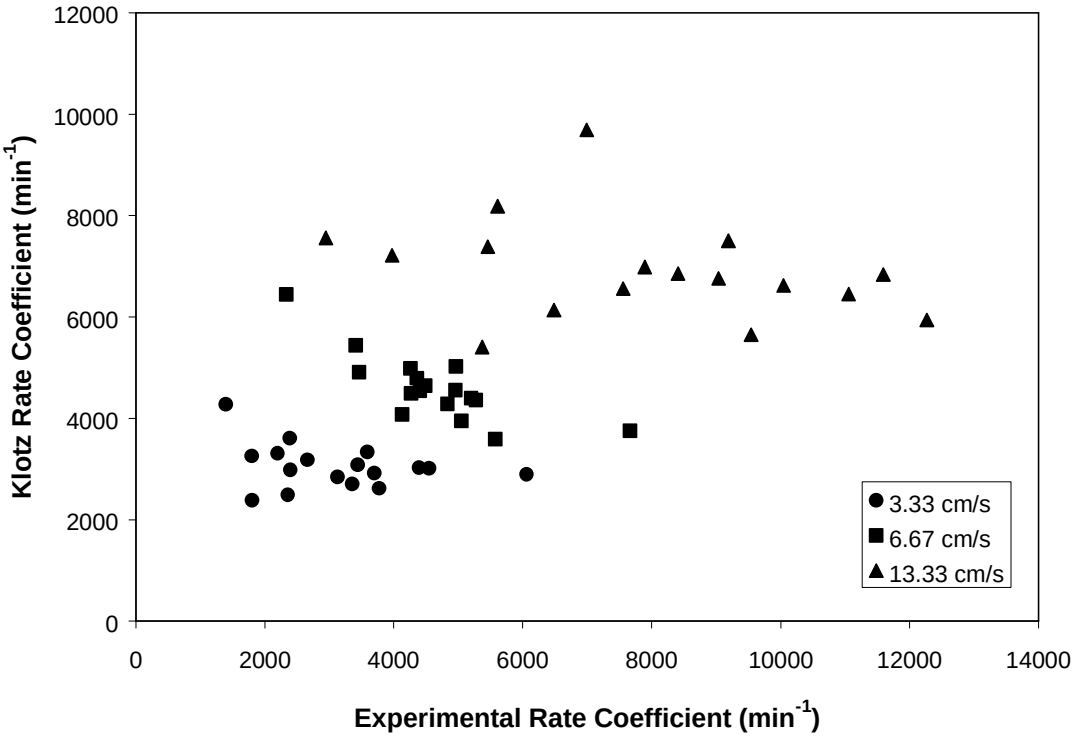

Figure 16. Comparisons of predictions of rate coefficients from the Klotz equation with experimental rate coefficients [53].

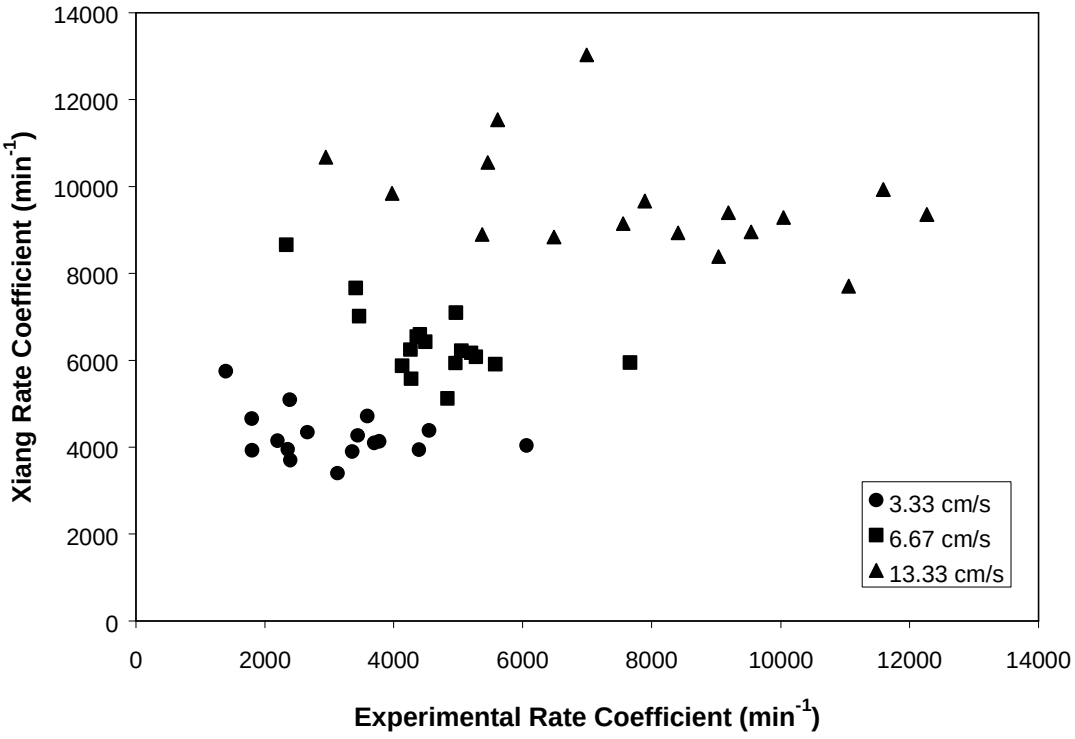

Figure 17. Comparisons of predictions of rate coefficients from the Xiang equation with experimental rate coefficients [53].

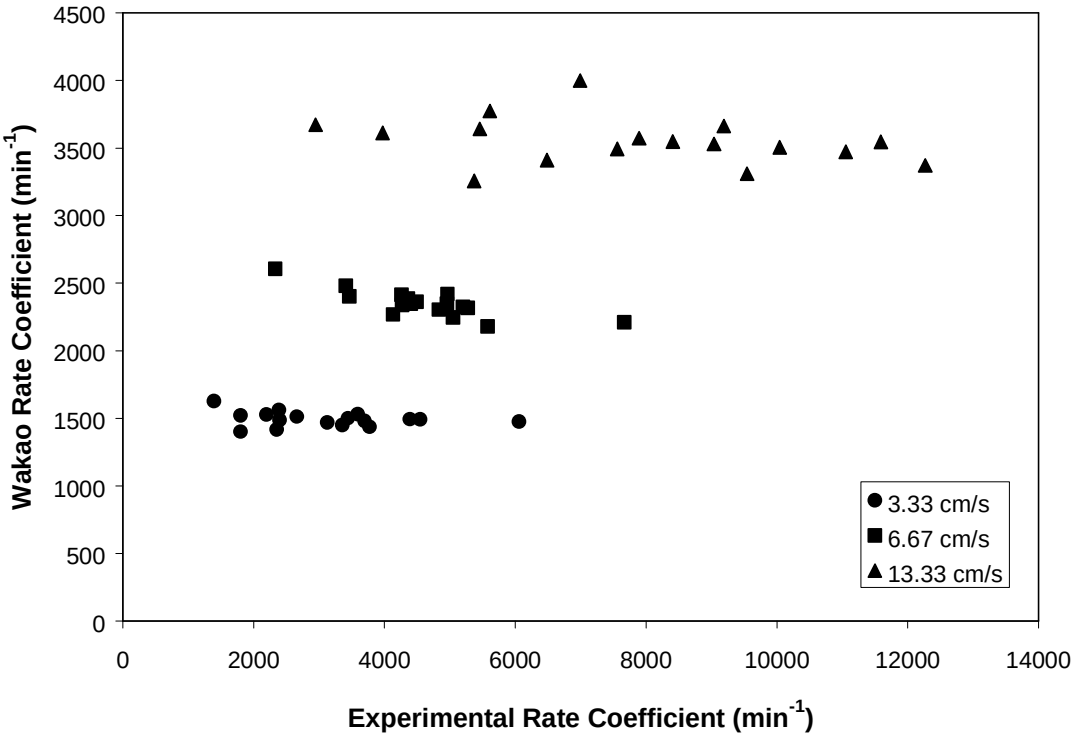

Figure 18. Comparisons of predictions of rate coefficients from the Wakao equation with experimental rate coefficients [53].

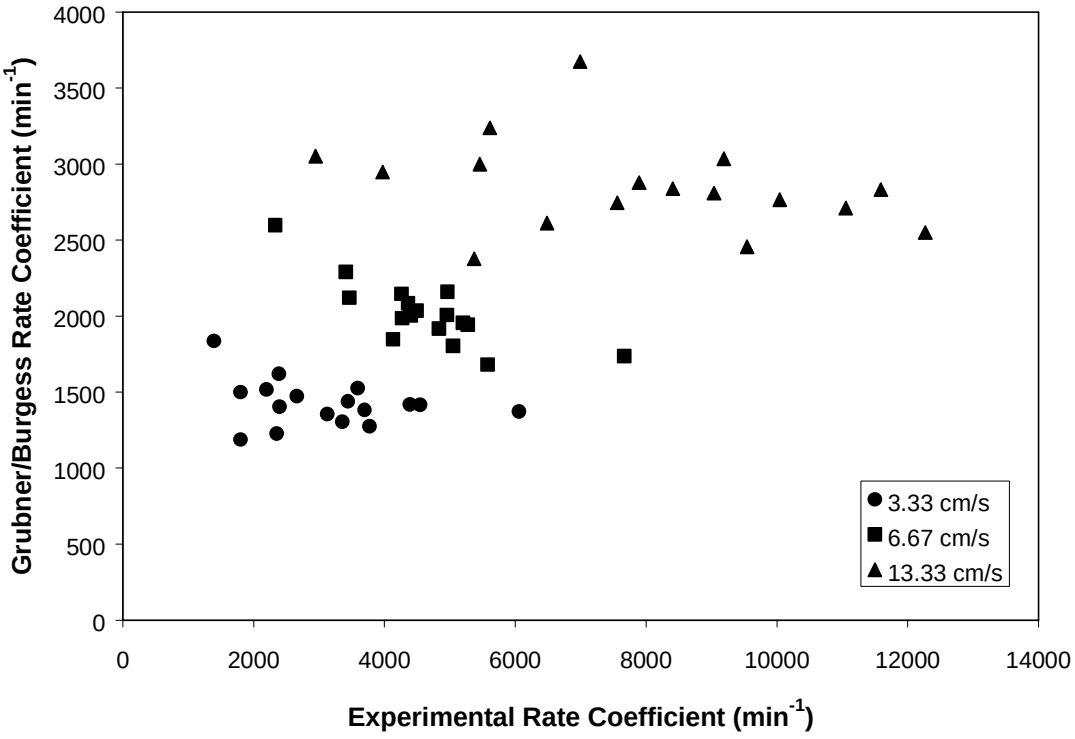

Figure 19. Comparisons of predictions of rate coefficients from the Grubner-Burgess equation with experimental rate coefficients [53].

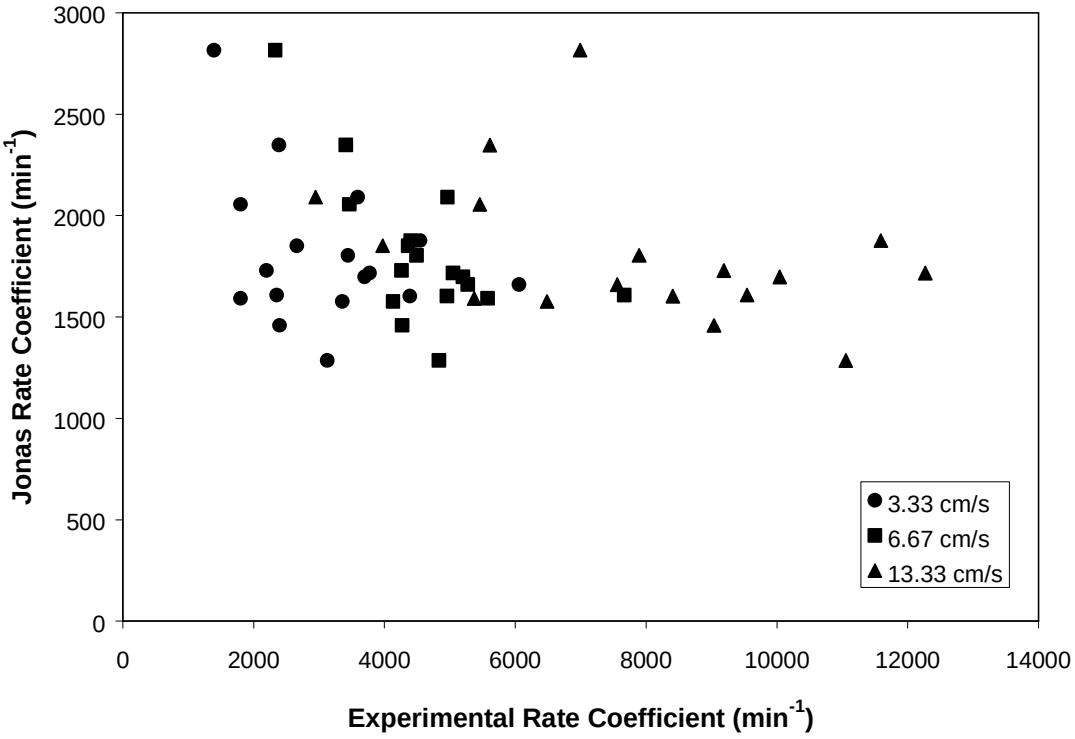

Figure 20. Comparisons of predictions of rate coefficients from the Jonas equation with experimental rate coefficients [53].

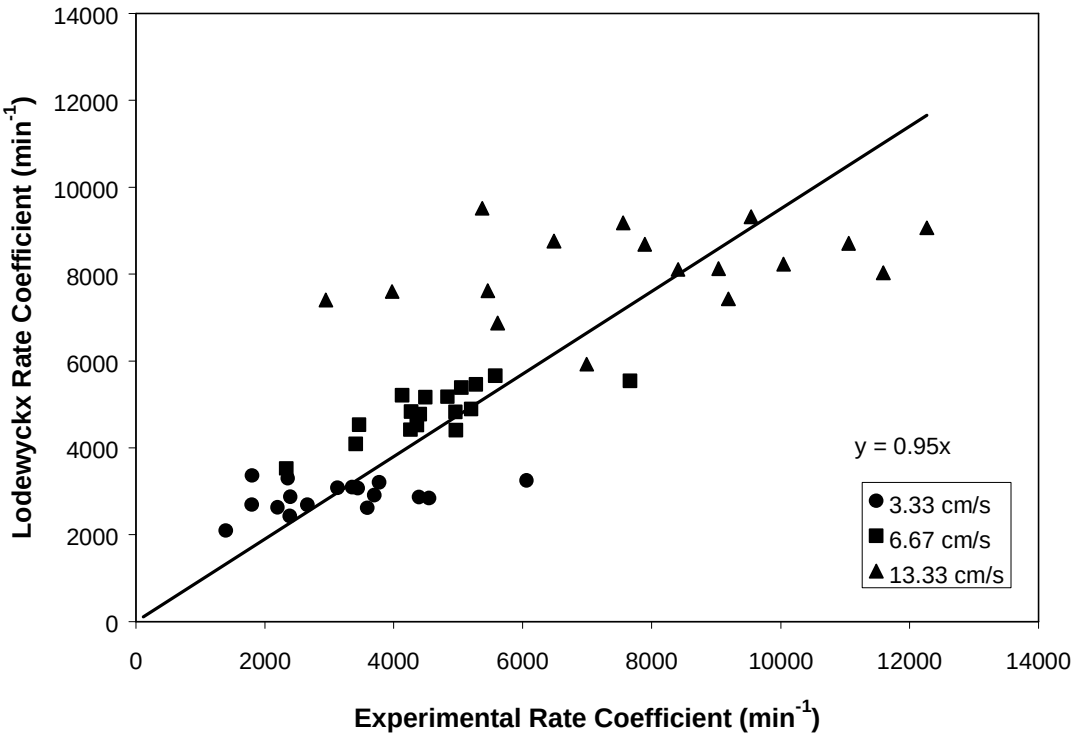

Figure 21. Comparisons of predictions of rate coefficients from the Lodewyckx equation with experimental rate coefficients [53].

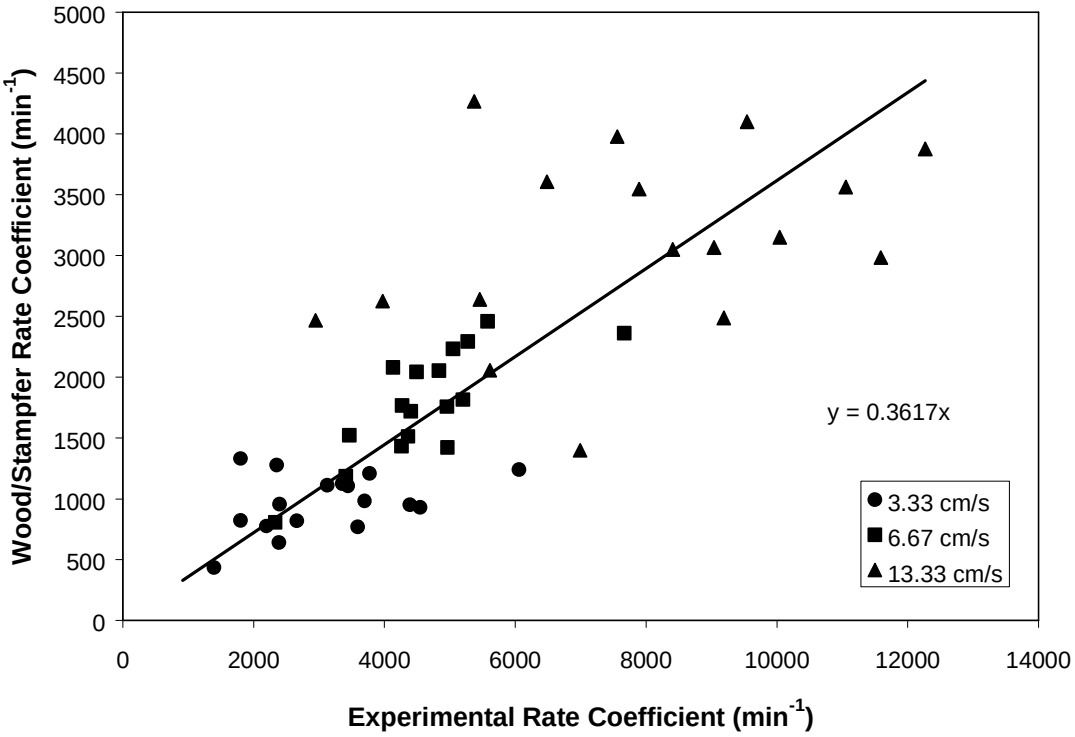

Figure 22. Comparisons of predictions of rate coefficients from the Wood-Stampfer equation with experimental rate coefficients [53].

All the preceding graphs have large data scatter due more likely to the experimental results than to the calculated values. As seen in the Equations (61) and (62) the calculated k_v depend on small differences between relatively larger breakthrough times (e.g., at 10% and 50% breakthroughs). Even though the precisions of the breakthrough times may be relatively good, the precisions of the differences will be worse. A second observation is that the experimental rate coefficients at 10% breakthrough cover wide ranges for the different chemicals: 959 to 5778 min^{-1} for Nelson's data and 1394 to 12268 min^{-1} for Xiang's. Therefore, a model that doesn't include chemical-specific parameters is expected to be inadequate.

Table V summarizes the comparisons shown in these figures. We found three groups of models distinguished by abilities to 1) correlate with the experimental rate coefficients for different chemicals, 2) correlate with carbon granule size, and 3) correlate with flow velocity.

Table V. Summary of How Adsorption Rate Coefficients Calculated from Models Correlated with Experimental Ones, Flow Rates, and Reported Average Carbon Granule Sizes.

Model	Correlation with Experimental Rate Coefficients (see graphs)	Vapor Parameters used for Rate Coefficient Calculations	Correlation with Flow Rates (overlap of Xiang data sets)	Correlation with Granule Size (overlap of Nelson data sets)
Nelson	None	None	None	None
Wheeler/Jonas	None	None	Not Tested	None
Jonas-Rehrmann	None	None	Not Tested	None
Rehrmann-Jonas	None	None	Not Tested	None
Gamson/Klotz	Inverse	Diffusivity	None	None
Xiang	Inverse	Molecular Weight	None	None
Wakao	Inverse	Molecular Weight	None	None
Grubner-Burgess SMT	Inverse	Diffusivity	None	None
Jonas	Inverse	Molecular Weight	Yes*	Yes*
Lodewyckx-Vansant	Positive	β from Polarizability	Yes	None
Wood-Stampfer	Positive	Polarizability	Yes	Yes

* Overlaps due only to the absence of velocity and granule size parameters.

The models (Nelson, Wheeler/Jonas, Jonas/Rehrmann, and Rehrmann/Jonas) that do not include vapor parameters failed completely to correlate k_v predictions with experimental ones. Those (Gamson/Klotz, Xiang, Wakao, Grubner/Burgess SMT, and Jonas) that include molecular weight or diffusivity as a parameter actually showed inverse correlations of calculated rate coefficients with experimental ones, i.e. the former decreased as the latter increased. The only rate coefficient models that showed positive correlations were the Lodewyckx and Wood-Stampfer models, which include molar polarizability (or its surrogate, affinity coefficient) as a parameter. Other molecular size parameters (e.g., molar volume or molecular parachor) should give similar positive correlations.

The Xiang data correlations show whether the models can account for differences in

airflow rates. Separation of data by flow velocity implies failure of a model for this parameter. Only the Lodewyckx, Wood-Stampfer, and Jonas models showed overlap of the results for the three flow velocities. The Jonas model did so only because it does not include velocity as a parameter.

Likewise, the Nelson data correlations should show whether the models account for differences in average carbon granule sizes d_L. Surprisingly, only the Wood-Stampfer and Jonas models, which are two that do not include this parameter, showed overlap of results for the two cartridges and their carbons. In analyzing a larger database Wood and Stampfer [62] observed an apparent lack of granule size dependence.

On the other hand, granule size effects on adsorption rate coefficients have been clearly demonstrated [64, 59]. The former [64] showed this with original carbons, while the latter [59] did so with size fractions obtained by sieving. An alternate explanation is that the carbons in the two cartridges tested by Nelson and Harder were more alike in effective granule sizes than the manufacturers' information indicated. In that case models like the Lodewyckx that include d_L as a parameter would have overcompensated for a reported difference that was not significant.

Figures 13 – 14 and 21 – 22 show best fit lines through the graph origins and their equations. Slopes of these lines can be considered as average accuracies of the model predictions, taking 1.0 as ideal. Accuracies for the Wood-Stampfer model (1.56 and 0.79 were better for both data sets than for the Lodewyckx model (2.36 and 2.09). Lodewyckx's correlation was done with k_v calculated from 0.1% breakthrough times. For skewed (asymmetric) breakthrough curves k_v is often larger for smaller breakthrough times. For example, for all of the Nelson data set the average $k_{v1\%} / k_{v10\%}$ ratio was 1.3; it would be expected to be even greater for $k_{v0.1\%} / k_{v10\%}$. The Wood-Stampfer model includes skew adjustments, so that $k_{v10\%}$ could be calculated and compared directly with experimental ones.

Precisions of model predictions were compared after "correcting" the calculated values with the accuracy factors and by calculating standard deviations σ of corrected calculated rate coefficients from experimental ones. The Wood-Stampfer model results were slightly more precise than the Lodewyckx model (σ = 938 vs 1029 min^{-1}) for the Nelson data set, but less precise (σ = 1838 vs 1685 min^{-1}) for the Xiang data set.

K. Comparisons of Adsorption Capacity Model Predictions

Six adsorption isotherm models (listed in Table VI and discussed above) were tested for their abilities to predict experimentally determined capacities of vapors on activated carbons. The three experimental data selected were:

- At 2000 ppm benzene, 0.0194 g/g capacity was calculated from the experimental breakthrough curve midpoint $t_{50\%}$ = 74.6 min for a 2-cm-deep bed and a 0.4 L/(min-cm2) flow rate from the paper of Xiang et al. [53].
- At 100 ppm hexane, 0.242 g/g capacity was reported by Nelson and Harder [21] for a Type 3 (AO) respirator cartridge.
- At 35.5 ppm ethanol, 0.0255 mL/g, which equals 0.0201 g/g capacity was reported by Robell et al. [80] for dry conditions at 26 ^{o}C and 0.5 atm pressure. This is assumed equivalent to 17.75 ppm at 1 atm.

Table VI also shows the results. There was no clear "winner" in these comparisons.

- The Kisarov model prediction was closest to the experimental capacity for 2000 ppm benzene;
- The Gruber-Burgess model prediction was closest (next to one of the Vahdat/Langmuir) for 100 ppm hexane;
- The Nelson/Freundlich model prediction was closest for 17.75 ppm ethanol.

For one carbon in Vahdat's list the prediction was closest to the experimental hexane capacity; however, three others weren't. The practical question is, "How does one choose which carbon (and its Langmuir parameters) to use?

The Grubner-Burgess quadradic equation for capacity gives negative values at low concentrations (see previous discussion). The Kisarov/Langmuir-Freundlich implementation [25] has general parameters that are proposed to be used for all chemical; but, Begun et al. [26] list parameters for only eight chemicals, mostly alcohols, for the modified Begun-Kisarov/Langmuir-Freundlich equation. Likewise, the Nelson/Freundlich and Vahdat/Langmuir model implementations have limited lists of parameters to use.

Table VI. Comparisons of Adsorption Capacities from Models with Experimental Ones.

Compound	Benzene	Hexane	Ethanol	Comments
Concentration (ppm)	2000	100	35.5	Ethanol data at 0.5 atm converted to 17.75 ppm at 1 atm.
Experimental Value (g/g)	0.194	0.242	0.0201	For benzene, calculated from 74.6 min breakthrough time.
Reference	Xiang	Nelson VI	Robell	
Micropore Volume (cm^3/g)	0.385	0.454	0.4	Assumed for ethanol
Affinity Coefficient	1.00	1.25	0.60	Experimental average value (Ref. Wood).
Calculated Values:				
Nelson/Freundlich	0.40 or 0.37	0.11 or 0.20	0.023	For average or measured exponent, respectively.
Vahdat/Langmuir	0.11 to 0.35	0.05 to 0.24	0.008 to 0.009	For various carbons for which parameters are listed.
Kisarov/Langmuir-Freundlich	0.19	0.11	0.0095	Used micropore volumes given above.
Begun-Kisarov/ L-F	0.21		0.0029	Parameters not given for hexane.
Wood/Dubinin-Radushkevich	0.28	0.16	0.0087	
Grubner-Burgess/Polanyi	0.37	0.22	-0.112	Negative values obtained at low concentrations.

The Wood/Dubinin-Radushkevich, Grubner-Burgess/Polanyi, and Kisarov/Langmuir/Freundlich models should be most useful for prediction of capacities for more chemicals, since they have general parameters that include vapor properties. They predicted ethanol capacities too low; however, for respirator cartridge or air-cleaning bed service life applications, too low is better than too high.

L. Comparisons of Affinity Coefficient Models

Wood [40] published an extensive tabulation of affinity coefficients for gases and vapors on activated carbons. We have supplemented this with the experimental affinity coefficients listed in Table VIII. Sources and means of extracting affinity coefficients β from published and unpublished data are given in a paper [81] recently submitted for publication; therefore, these details will not be repeated here.

Table VII. Supplemental Values of Affinity Coefficients on Activated Carbons Calculated from Various Sources.

Compound	Activated Carbon	DA Exponent	βE kJ/mol	Experimental β vs. Reference	Molar Polarizability	Liquid Molar Volume	Parachor
Methane	Nuxit AC	2.02	3.954	0.71	6.541		73.2
Ethylene	Nuxit AC	1.86	4.386	0.79	10.726		101.2
Ethane	Nuxit AC	1.89	4.456	0.80	11.225		112.2
Propylene	Nuxit AC	1.89	5.547	1.00	15.791	81.884	140.2
Propane*	Nuxit AC	1.85	5.568	1.00	15.967	88.092	151.2
Methane	BPL	1.55-1.93	3.52-4.12	0.81	6.541		73.2
Ethylene*	BPL	1.48-1.75	4.05-5.35	1.00	10.726		101.2
Ethane	BPL	1.56-1.79	4.17-5.78	1.05	11.225		112.2
Ethylene	Carbon Mol Sieve	2.68	6.740	0.59	10.726		101.2
Ethane	Carbon Mol Sieve	2.85	6.670	0.58	11.225		112.2
Propylene	Carbon Mol Sieve	2.78	8.410	0.73	15.791	81.884	140.2
Propane	Carbon Mol Sieve	3.02	7.81	0.68	15.967	88.092	151.2
Methanol	Carbon Mol Sieve	1.81	4.651	0.40	8.236	40.485	82.2
Acetone	Carbon Mol Sieve	2.00	9.774	0.85	16.177	73.528	162.0
Hexane	Carbon Mol Sieve	1.62	14.968	1.30	29.898	130.486	271.0
Benzene*	Carbon Mol Sieve	1.78	11.52	1.00	26.274	89.116	206.1
Cyclohexane	CAL AC	2	18.73	1.03	27.735	108.105	240.1
Benzene*	CAL AC	2	18.23	1.00	26.274	89.116	206.1
Methanol	CAL AC	2	8.06	0.44	8.236	40.485	82.2
Ethanol	CAL AC	2	10.55	0.58	12.922	58.368	121.2
2-Propanol	CAL AC	2	12.57	0.69	17.623	76.512	166.2
2-Butanol	CAL AC	2	15.75	0.86	22.177	91.926	205.2
Acetone	CAL AC	2	13.21	0.72	16.177	73.528	162.0
Acetonitrile	CAL AC	2	9.85	0.54	11.069	52.246	121.9
Sulfur Dioxide	CAL AC	2	12.64	0.69	10.090		88.2
Ammonia	CAL AC	2	17.28	0.95	5.460	25.609	63.8
1-Hexanol	BPL	2	24.55	1.04	31.636	125.590	280.0

2-Hexanol	BPL	2	22.22	0.94	31.321	125.236	280.0
DMMP**	BPL	2	17.90	0.76	28.181	108.300	
Hexane*	BPL	2	23.59	1.00	29.898	130.486	271.0
Heptane	BPL	2	27.86	1.18	34.552	146.556	307.2
Nonane	BPL	2	32.80	1.39	43.846	178.635	385.2
R-113**	BPL	2	18.22	0.77	26.166	116.875	249.6
Dichloromethane	BPL	2	14.43	0.61	16.338	64.021	147.6
R-123**	BPL	2	18.61	0.79	20.911	103.192	212.4
R-11**	BPL	2	15.90	0.67	21.241	91.700	193.4
R-134**	BPL	2	13.72	0.58	11.225		146.6
Toluene	BPL	2	22.49	0.95	31.054	106.287	245.6
R-22**	BPL	2	13.99	0.59	11.521		127.6
R-318	BPL	2	16.28	0.69	18.197		236.4
1-Butanol	BPL	2	18.29	0.78	22.154	91.529	205.2
1-Propanol	BPL	2	15.55	0.66	17.529	74.798	166.2
Ethanol (UVa)	BPL	2	11.21	0.47	12.922	58.368	121.2
Ethanol	BPL	2	12.84	0.54	12.922	58.368	121.2
Methanol	BPL	2	10.15	0.43	8.236	40.485	82.2
Acetone	BPL	2	15.48	0.66	16.177	73.528	162.0
Cyanogen Chloride	BPL	2	14.85	0.63	11.326	51.405	120.1
Perfluorocyclo-hexane	BPL	2	19.27	0.82	27.735		240.1
Ammonia	BPL	2	7.28	0.31	5.460	25.609	63.8
Nitrogen	Carbon Mol Sieve	2.6	11.72	0.41	4.390		50.0
Carbon Dioxide	Carbon Mol Sieve	2.3	11.30	0.39	7.344		91.2
Oxygen	Carbon Mol Sieve	2.3	9.21	0.32	3.989		40.0
Hydrogen	Carbon Mol Sieve	2.5	5.44	0.19	2.029		34.2
Neon	Carbon Mol Sieve	3.0	4.06	0.14	0.998		
Argon	Carbon Mol Sieve	2.9	10.04	0.35	4.140		
Krypton	Carbon Mol Sieve	2.8	11.30	0.39	6.267		
Xenon	Carbon Mol Sieve	2.8	14.23	0.49	10.202		
Methane	Carbon Mol Sieve	2.8	13.39	0.46	6.541		73.2
Ethylene	Carbon Mol Sieve	3.0	15.48	0.54	10.726		101.2
Ethane	Carbon Mol Sieve	2.9	16.74	0.58	11.225		112.2
Propylene	Carbon Mol Sieve	3.0	21.34	0.74	15.791	81.884	140.2
n-Butane	Carbon Mol Sieve	2.9	23.43	0.81	20.624	100.415	190.2
n-Hexane	Carbon Mol Sieve	2.8	30.55	1.06	29.898	130.486	271.0
Benzene*	Carbon Mol Sieve	3.1	28.87	1.00	26.274	89.116	206.1
Ethyl Acetate	Carbon Mol Sieve	3.1	27.62	0.96	22.267	97.867	216.0

p-Xylene	Carbon Mol Sieve	3.3	37.66	1.30	36.005	123.298	282.4
Trichlorethylene	Carbon Mol Sieve	3.2	31.38	1.09	25.369	89.735	212.8
Tetrahydrofuran	Carbon Mol Sieve	3.0	24.27	0.84	19.876	81.095	184.5
Dichloromethane	Carbon Mol Sieve	3.0	20.92	0.72	16.338	64.021	147.6
Cyclohexane	Carbon Mol Sieve	2.8	25.11	0.87	27.735	108.105	240.1
Acetone	Carbon Mol Sieve	2.8	20.92	0.72	16.177	73.528	162.0
Carbon Disulfide	Carbon Mol Sieve	2.6	20.92	0.72	21.494	60.694	147.4
Methanol	Carbon Mol Sieve	2.7	10.88	0.38	8.236	40.485	82.2
Ethanol	Carbon Mol Sieve	2.7	17.16	0.59	12.922	58.368	121.2
1-Butanol	Carbon Mol Sieve	2.6	25.53	0.88	22.154	91.529	205.2
Acetic Acid	Carbon Mol Sieve	3.0	20.92	0.72	13.008	57.234	138.0
Pyridine	Carbon Mol Sieve	3.0	28.45	0.99	24.074	80.558	196.7
Benzene*	Shirasagi S	2		1.00	26.274	89.116	206.1
Acetone	Shirasagi S	2		0.86	16.177	73.528	162.0
Toluene	Shirasagi S	2		1.36	31.054	106.287	245.6
Methanol	Shirasagi S	2		0.40	8.236	40.485	82.2
Benzene*	HG I-780	2		1.00	26.274	89.116	206.1
Acetone	HG I-780	2		0.85	16.177	73.528	162.0
Methanol	HG I-780	2		0.36	8.236	40.485	82.2
Chloroform*	BPL	2	26.5	1.00	21.462	80.488	184.8
Phosgene	BPL	2	24.1	0.91	18.391	72.104	132.4
Cyanogen Chloride	BPL	2	16.9	0.64	11.326	51.405	120.1
Hydrogen Cyanide	BPL	2	10.8	0.41	6.370	39.311	82.9
Carbon Tetrachloride*	BPL	2	18.2-25.8	1.00	26.435	96.499	219.7
Acetone	BPL	2	15.5-19.4	0.81	16.177	73.528	162.0
Ammonia	BPL	2	6.8-10.2	0.38	5.460	25.609	63.8
Hydrogen Sulfide	BPL	2	9.24-13.46	0.50	9.750		82.4
m-Xylene*	Coconut BS	2.0	32.2	1.00	35.962	122.854	284.2
MIBK**	Coconut BS	2.4	28.0	0.87	30.179	123.456	278.7
Argon	Coconut BS	2.4	6.2	0.19	4.140		
Ethane*	Carbon C	2.03	12.3	1.00	11.225		112.2
Ethylene	Carbon C	1.98	11.7	0.95	10.726		101.2
Xenon	Carbon C	1.90	10.9	0.89	10.202		
Ethane*	Carbon D	1.91	11.5	1.00	11.225		112.2
Ethylene	Carbon D	1.98	11.9	1.03	10.726		101.2
Xenon	Carbon D	1.93	11.0	0.96	10.202		
Ethane*	MSC-5A	2.45	16.0	1.00	11.225		112.2
Ethylene	MSC-5A	2.53	15.6	0.98	10.726		101.2
Xenon	MSC-5A	2.30	14.0	0.88	10.202		
Ethane*	MSC-7A	2.17	14.1	1.00	11.225		112.2
Ethylene	MSC-7A	2.16	13.7	0.97	10.726		101.2

Xenon	MSC-7A	2.11	12.7	0.90	10.202		
n-Butane*	BPL	2	18.3	1.00	20.624	100.415	190.2
Propane	BPL	2	14.8	0.81	15.967	88.092	151.2
Ethane	BPL	2	12.3	0.67	11.225		112.2
n-Butane*	Columbia	2	17.1	1.00	20.624	100.415	190.2
Propane	Columbia	2	14.5	0.85	15.967	88.092	151.2
Ethane	Columbia	2	12.1	0.71	11.225		112.2
n-Butane*	PA	2	23.3	1.00	20.624	100.415	190.2
Propane	PA	2	17.0	0.73	15.967	88.092	151.2
Ethane	PA	2	12.8	0.55	11.225		112.2
Benzene*	Calgon PCB	2		1.00	26.274	89.116	206.1
Methanol	Calgon PCB	2		0.50	8.236	40.485	82.2
Benzene*	Y-25	2		1.00	26.274	89.116	206.1
Methanol	Y-25	2		0.58	8.236	40.485	82.2
Benzene*	AC			1.00	26.274	89.116	206.1
Hexane	AC			1.08	29.898	130.486	271.0
n-Pentane*	AC			1.00	25.278	115.219	231.0
Pyridine	AC			0.75	24.074	80.558	196.7
Argon	AC			0.26	4.140		
Carbon Monoxide	AC			0.24	5.279		61.6
Benzene*	U-02	2	17.00	1.00	26.274	89.116	206.1
1,2,-Dichloro-ethane	U-02	2	14.23	0.84	21.316	80.123	188.5
Carbon Tetrachloride	U-02	2	15.51	1.03	26.435	96.499	219.7
Chlorobenzene	U-02	2	18.39	1.082	31.150	101.791	244.3
Benzene*	Ajax 976	2		1.00	26.274	89.116	206.1
Propane	Ajax 976	2		0.68	15.967	88.092	151.2
Methyl Mercaptan*	BPL 2026			1.00	14.919	55.522	121.4
Ethyl Mercaptan	BPL 2026			1.24	19.344	74.732	160.4
n-Propyl Mercaptan	BPL 2026			1.79	23.770	90.548	199.4
Ethyl Ether*	BPL No. 2			1.00	22.493	103.839	210.2
Carbon Tetrachloride	BPL No. 2			0.84	26.435	96.499	219.7
Ethylene Oxide	BPL No. 2			0.48	10.963	49.938	144.7
Ethyl Chloride	BPL No. 2			0.68	16.158	72.467	149.5
Benzene*	BPL			1.00	26.274	89.116	206.1
Carbon Disulfide	BPL			0.52	21.494	60.694	147.4

* Reference compound in a set

** DMMP = Dimethyl methylphosphonate; R-113 = 1,1,1-Trichlorotrifluoroethane; R-123 = 2,2-Dichloro-1,1,1-trifluoroethane; R-11 = Trichlorofluoromethane; R-134 = 1,1,2,2-Tetrafluoroethane; R-22 = Chlorodifluoromethane; R-318 = Perfluorocyclobutane

The β values in Table VII plus those in the previously published table [40] have been correlated with molar polarizability, molar volume, molecular parachor, and critical temperature. We chose power functions $\beta = a X^m$ of each parameter, X, with coefficients, a, that defined benzene as the reference, so that $\beta = 1$ for the value of the parameter for benzene. When the

reference chemical for a set of data in Table VII was not benzene, we used the appropriate ratio of β for comparison with experimental data.

A Sum of the Squares of Deviations analysis resulted in standard deviations for experimental values vs. correlation values. Selected values of power exponents m were used first and then varied until the standard deviation was minimized. This data fitting process is equivalent to the "floating reference" approach used previously [40]. Numbers of data differed for the three parameters, since some parameter values were not available (e.g, parachors for inert gases or liquid molar volumes for gases). One questionable β = 0.95 for ammonia (see above) was excluded from all correlations. Figures 23 – 26 and Table VIII show the results of these correlations.

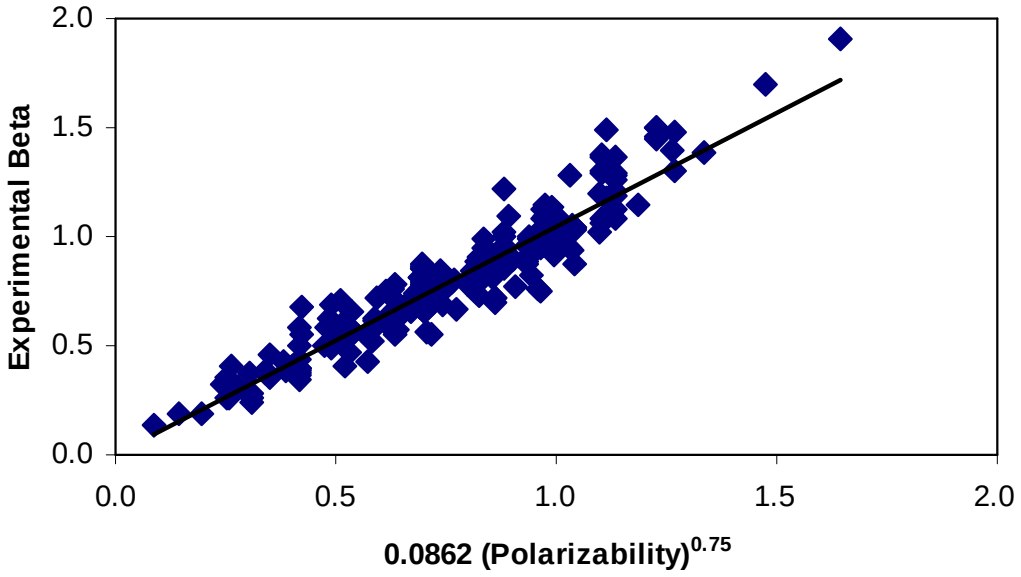

Figure 23. Comparison of experimental affinity coefficients with those calculated by the optimum molar polarizability correlation. Triangles represent data for carbon molecular sieves. The line is the trend for all the data.

One observation from these results is that affinity coefficients for carbon molecular sieves (CMS) did not differ significantly from those of more ordinary activated carbons.

Figure 23, the optimum polarizability correlation, shows CMS results as triangles. There seems to be no trend distinguishing ordinary activated carbons from molecular sieve carbons for either small or large molecules.

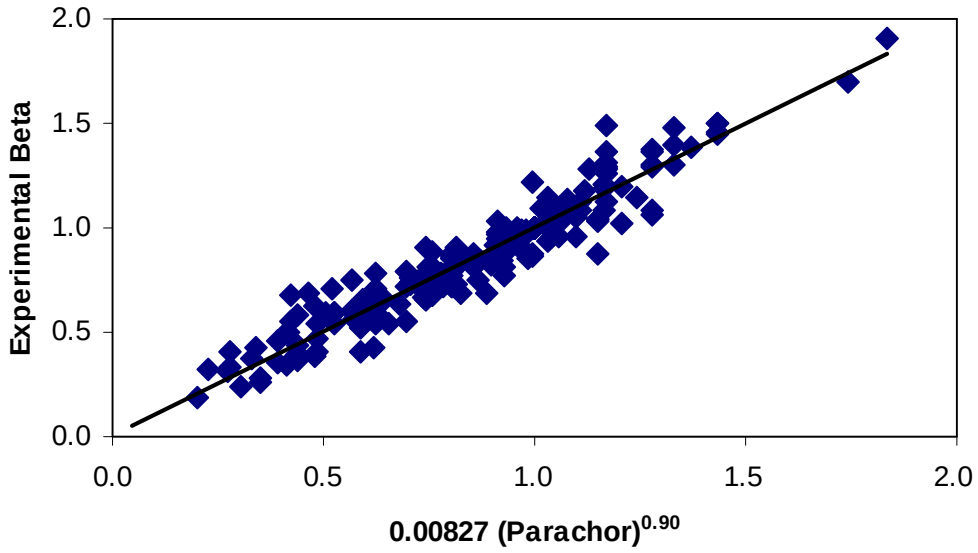

Figure 24. Comparison of experimental affinity coefficients with those calculated by the optimum molecular parachor correlation. The line is the trend for all the data.

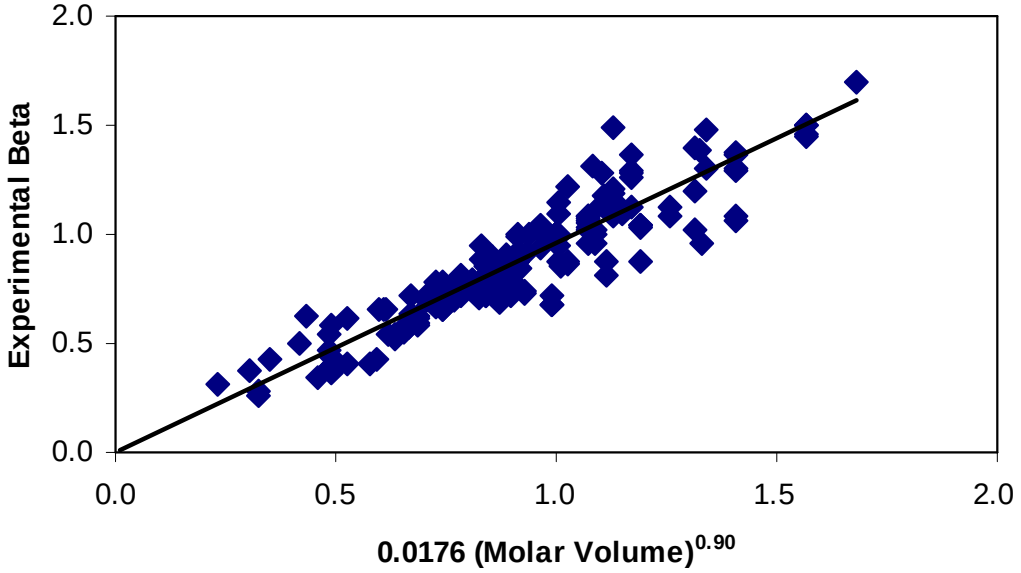

Figure 25. Comparison of experimental affinity coefficients with those calculated by the optimum molar volume correlation. The line is the trend for all the data.

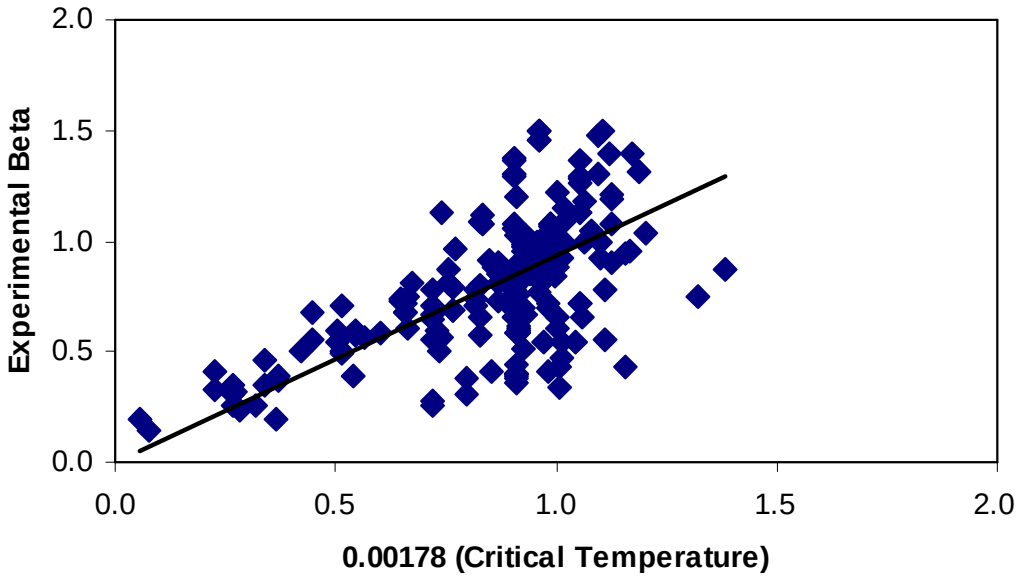

Figure 26. Comparison of experimental affinity coefficients with those calculated by the optimum critical temperature correlation. The line is the trend for all the data.

Table VIII. Results of Affinity Coefficient Correlations: $\beta = a\ X^m$

Parameter X	Power m	Coefficient a	Number of Data	Standard Deviation in β
Molar Polarizability	1.00	0.0381	263	0.12
	0.90	0.0528	263	0.11
	0.75*	0.0862	263	0.10
Molecular Parachor	1.00	0.00485	247	0.09
	0.90*	0.00827	247	0.08
Molar Volume	1.00	0.0112	203	0.12
	0.90*	0.0176	203	0.11
Critical Temperature	1.00*	0.00178	254	0.24

* Power that produced the best fit to data

From Table VIII we see that molecular parachor was the parameter that produced the best β correlations. Since liquid surface tensions and/or liquid densities are unknown or cannot be measured for many chemicals, molecular parachor is usually calculated from sums of Sugden atomic and structural constants. We have used parachors tabulated in American Chemical Society references or calculated from the Sugden tables in them [42]. However, there are no Sugden constants for less common atoms such as phosphorus and inert gases.

The work of Reucroft [48] has suggested that using parachor to calculate β might not properly account for dipole moments in polar molecules. The analyses of our more extensive database do not indicate any worse correlations of polar compounds than nonpolar ones. Figure 27 shows comparisons of experimental β for the most polar compounds, alcohols, with those calculated using the best correlations (Table IX) for the complete dataset. Within experimental scatter there are no trends or significant deviations from equivalence using parachor, polarizability, or molar volume parameters.

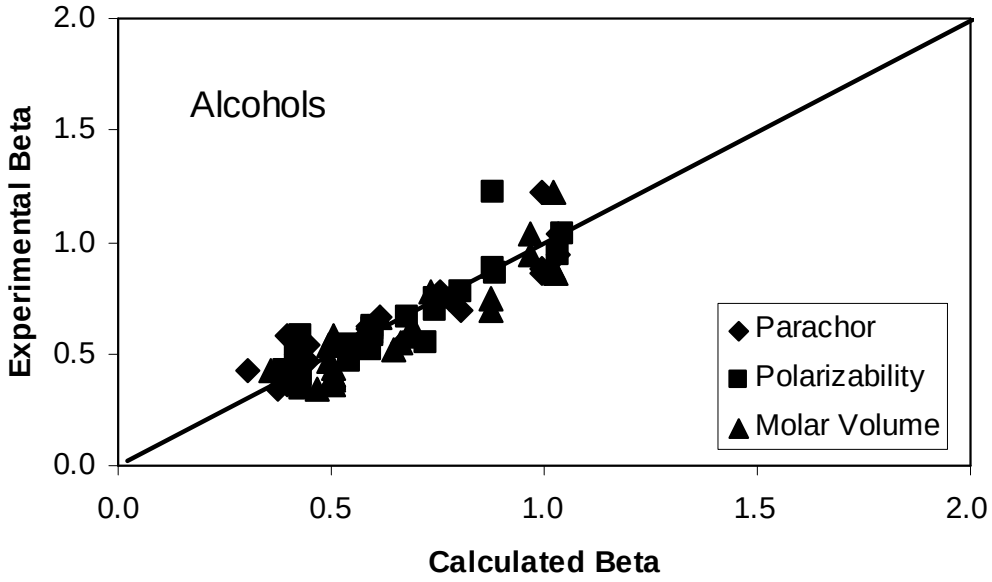

Figure 27. Comparisons of experimental and calculated affinity coefficients for alcohols.

III. Models for Adsorption of Mixtures of Organic Vapors

A. Fundamentals

The goal of a theoretical model should be to describe and predict actual physical situations using mathematical equations (models). In the case of service life (breakthrough time) models this means one must be able to predict the major contributors to breakthrough curves: a) adsorption capacities and b) adsorption rates. Often the first step in developing a theoretical and practical model is to start with ideal (simple and thermodynamically consistent) cases and add additional parameters (complications) only as required. For the adsorption of mixtures of vapors in air onto an adsorbent surface the following *ideal* cases can be defined :

1) *Ideal gas mixture*: All gas (or vapor) components i and their mixtures follow the Ideal Gas Law,

$$p_i V = n_i R T \quad \text{and} \quad p_T V = n_T R T \qquad (63)$$

and the Ideal Gas Mixture Law (Dalton's Law):

$$p_i = y_i p_T \quad \text{and} \quad p_T = \Sigma p_i \qquad (64)$$

2) *Ideal concentrated solution*: The adsorbed mixture of vapors on the adsorbent follow Raoult's Law:

$$p_i = x_i p_T \text{ and } p_T = \Sigma p_i \qquad (65)$$

where the components of a carrier gas (usually air) are ignored.

3) *Ideal pore-filling solution*: The volumes W_i occupied by components are additive (no volume change upon mixing) and exist at the same densities as if not adsorbed (e.g., normal bulk liquid densities, $d_{L\,i}$. in g/cm^3).

4) *Ideal porous adsorbent*: It is thermodynamically inert and has a fixed maximum adsorption volume (space or micropore volume W_o in cm^3/g) that may be filled to the extent V_{ads}

Combining 3) and 4) gives the Gurvitsch [31] rule:

$$W_o = (\Sigma V_{ads\,i})_{max} \qquad (66)$$

p_i = partial pressure exerted by n_i moles of vapor I

p_T = total pressure of n_t total moles of a gas/vapor mixture

R = ideal gas constant, e.g., 8.31451 j/mol-deg

T = absolute temperature (^{o}K)

V = total volume of gas/vapor mixture

y_i = mole fraction of chemical i in the gas phase

x_i = mole fraction of chemical i in the adsorbed phase

V_{ads} = total occupied adsorption volume (or space) in cm^3/g

M_w = molecular weight in g/mol

The number of moles of each vapor adsorbed is given by:

$$n_i = W_i \, d_{L\,i} / M_{w\,i} \qquad (67)$$

with adsorbate mole fractions:

$$x_i = n_i / \Sigma n_i \qquad (68)$$

and gas phase mole fractions:

$$y_i = p_i / \Sigma p_i \qquad (69)$$

B. Models for Adsorption Capacities of Mixture Components

1. **Molar Proportionality Model**. The simplest model for predicting adsorption capacities of mixtures is the Molar Proportionality Model (or Method). It incorporates these ideal cases (especially $x_i = y_i$) and the assumption that the amounts adsorbed from a vapor mixture are proportional by adsorbate (and equivalent vapor) mole fractions to the amounts W_i^o that would have been adsorbed from a pure vapor at the same partial vapor pressure (or concentration). In other words, the different components do not interact except to "deny" adsorption to one another. This assumes a limited number of moles (adsorption sites or surface area) can be covered (the Langmuir isotherm assumption). For a binary vapor mixture (two vapors excluding air components) the total W_{12} and individual amounts W_i adsorbed (in any consistent units) can be expressed as:

$$W_{12} = x_1 W_1^o + x_2 W_2^o = y_1 W_1^o + y_2 W_2^o \qquad (70)$$

$$W_i = y_i W_i^o \qquad (71)$$

This can easily be extended to any number of vapor components. Known component vapor pressures (concentrations) are used to calculate mole fractions.

Any single-vapor isotherm (see discussion in a previous section) or measurements can be used to calculate the pure vapor adsorption capacities W_i^o. For example, Jonas et al. [82] used the Dubinin/Rasdushkevich isotherm with carbon tetrachloride as the reference compound to predict individual and total adsorption volumes (and corresponding gravimetric capacities in g/g

carbon) from gas phase mole fractions by the Molar Proportionality Method. They found good agreement (-10 to +20% individual deviations) with experimental kinetic capacities obtained from slopes of plots of 1% breakthrough times vs. carbon bed weights. Figure 28 shows a comparison (least squares trend line and standard deviation of 0.02 g/g) of calculated and experimental capacities for binary mixtures of benzene, chloroform, and carbon tetrachloride.

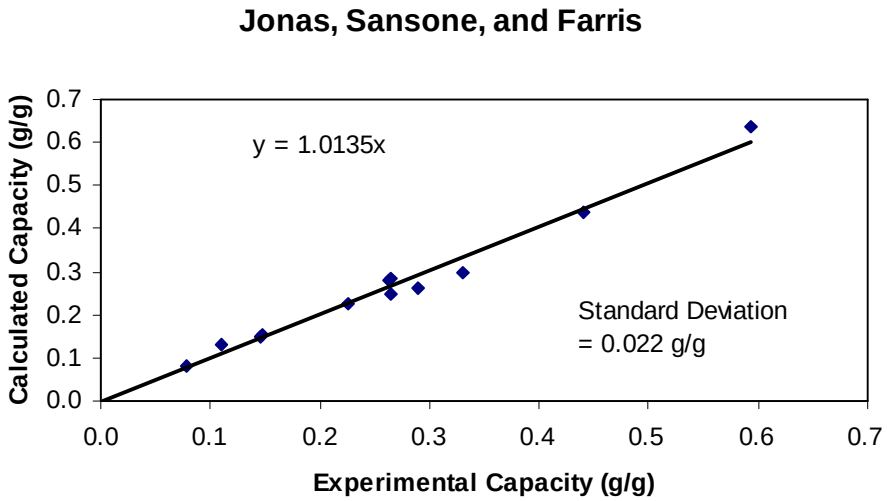

Figure 28. Comparison of capacities calculated by the Molar Proportionality Model with experimental ones for binary mixtures including carbon tetrachloride, benzene, or chloroform [82].

Robbins and Breysse [83] similarly measured single-vapor gravimetric adsorption capacities for p-xylene and pyrrole from breakthrough curves and used them with the Molar Proportionality Method to predict capacities and breakthrough times in the presence of other vapors (o-dichlorobenzene, p-dichlorobenzene, p-fluorotoluene, and toluene). Average capacity deviations from experimental values ranged from 0 to –35% for p-xylene and from –13 to +32% for pyrrole. Figure 29 shows precision of the predictions similar to those of Jonas et al. [82], but an average 20% underestimate for p-xylene capacities.

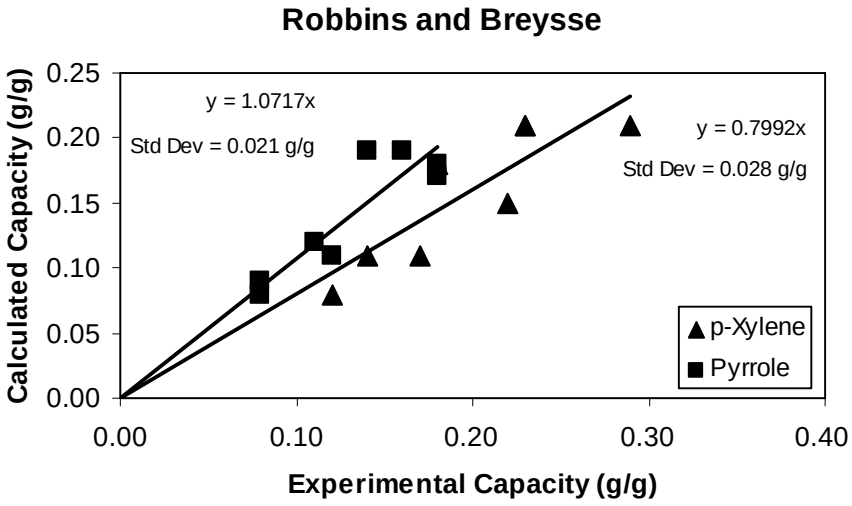

Figure 29. Comparisons of capacities calculated by the Molar Proportionality Model with experimental ones for binary mixtures including p-xylene or pyrrole with four other vapors [83].

Reucroft et al. [84] applied the Molar Proportionality Method with three other models (Dubinin/Polanyi, John's, and IAST—see discussions below) to predicting adsorption capacities from measured pure vapor adsorption capacities. They measured total equilibrium capacities of mixtures of chloroform/methylene chloride, n-hexane/methylene chloride, benzene/n-hexane, and chloroform/carbon tetrachloride. Figure 30 shows that only the hexane/methylene chloride total weights were overestimated.

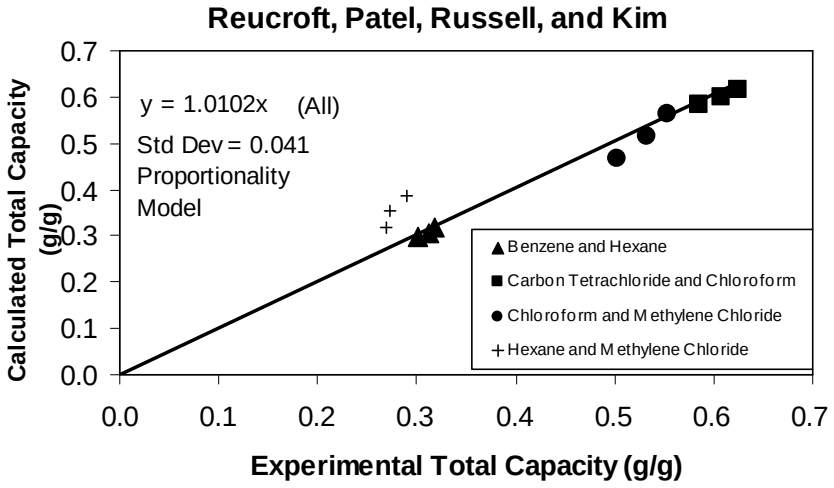

Figure 30. Comparisons of total binary vapor capacities calculated by the Molar Proportionality Model with experimental ones for four binary mixtures [84].

Individual kinetic capacities from breakthrough time vs bed weight plots are compared with predictions in Figure 31. Chloroform capacities in mixtures with methylene chloride were grossly underestimated.

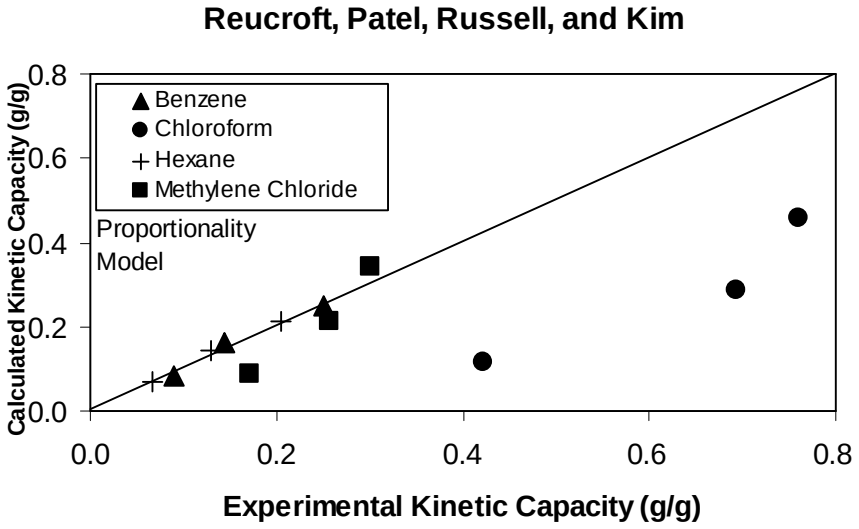

Figure 31. Comparisons of capacities calculated by the Molar Proportionality Model with kinetic capacities measured for four vapors in binary mixtures [84].

Cohen et al. [85] applied molar proportionality to predict some of their data for carbon tetrachloride/n-hexane and carbon tetrachloride/pyridine equimolar (1000 ppm each) mixtures. Deviations of predicted adsorption capacities from kinetic W_e values obtained from plots of 10% breakthrough times vs. bed residence times were –39% for carbon tetrachloride and +3% for n-hexane in one mixture and –12% for carbon tetrachloride and –39% for pyridine in another.

2. Volume Exclusion Model

There is also a Volume Exclusion Model which assumes that the adsorbates are competing for adsorption volume, rather than for number of surface sites or area. The condensed adsorbates are still considered independent and existing as if they are in the pure state; only the volume to be filled is less for each because of the presence of the other. Jonas and Sansone [86]

showed individual volumetric capacities at breakthrough times of a second vapor to be additive for mixtures of benzene and carbon tetrachloride at fixed vapor concentrations. It didn't seem to matter if the vapors were added singly, concurrently, or sequentially. Breakthrough times calculated from the assumptions of volume additivity gave only –14% to +18% deviations from predictions (Figure 32). This is an experimental confirmation of the Ideal Pore-Filling Solution assumption (above).

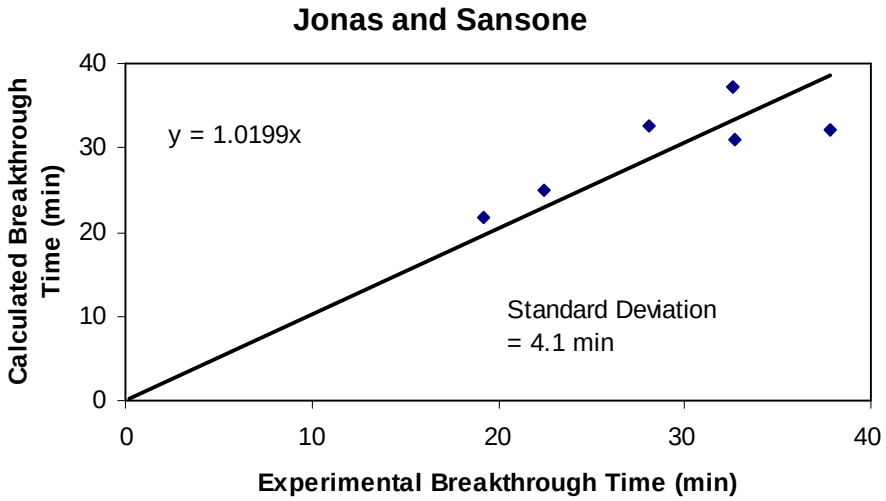

Figure 32. Comparisons of capacities calculated by the Volume Exclusion Model with capacities at breakthrough of the second vapor in binary mixtures [85].

Doong and Yang [87] proposed a simple Volume Exclusion Model for predicting mixed gas adsorption. It used the Dubinin/Astakhov single component isotherm equations and required no numerical iterations to apply.

Lavanchy and Stoeckli [88] successfully applied this model using Dubinin/Astakhov isotherms to calculate breakthrough times and curves for immiscible mixtures of water and 2-chloropropane. Miscible mixtures were handled with the Ideal Adsorption Solution Theory model discussed below.

3. Lewis Equation Model:

Another simple model for predicting quantities of adsorbed components of a mixture is based on observations by Lewis et al [89] with hydrocarbon gas mixtures that:

$$\Sigma\, n_i / n_i^o = 1 \qquad (72)$$

or for binary mixtures:

$$(n_1 / n_1^o) + (n_2 / n_2^o) = 1 \qquad (73)$$

Besides the pure gas adsorbed molar capacities n_i^o at the same pressures (concentrations), one other piece of information is required to solve the equation for binary mixtures individual adsorbate amounts; two pieces for ternary, etc. For the binary it can be the total number of moles $(n_1 + n_2)$ adsorbed or some relationship between n_1 and n_2. Lewis et al. used:

$$n_1 / n_2 = \alpha\, (p_1 / p_2) \qquad (74)$$

where α is a proportionality constant determined by trial and error. They showed that n_i ratios from binary data could be used for ternary mixture calculations. They also tried Langmuir isotherms, Freundlich isotherms, and the Polanyi adsorption potential approach to relate these molar capacities for mixture components. None of these was very satisfactory for activated carbons. The Ideal Lewis Model assumes $\alpha = 1$, which is equivalent to Raoult's Law.

In the previously cited report by Reucroft et al. [84] the Lewis Equation was used with poor predictive results for kinetic adsorption capacities of chloroform and methylene chloride in mixtures, but good for benzene and hexane (Figure 33). Grant and Manes [90] pointed out that the Lewis Equation must break down for mixtures of high relative volatility.

4. Greenbank and Manes Model

Another approach was developed by Greenbank and Manes [91] for aqueous solutions of organic compounds and activated carbon. In contrast to the Lewis Equation this model sums the

fluid (aqueous or air) phase component concentrations C_i relative to those C_i^o calculated for a pure vapor and an assumed occupied adsorption volume V_{ads} :

$$\Sigma\, C_i / C_i^o = 1 \qquad (75).$$

Any isotherm equation can be used to calculate the C_i^o. An iterative process is used to find the best V_{ads} that satisfies this sum. Then the adsorbed volume of a component is given by:

$$W_i = (C_i / C_i^o)\, V_{ads} \qquad (76)$$

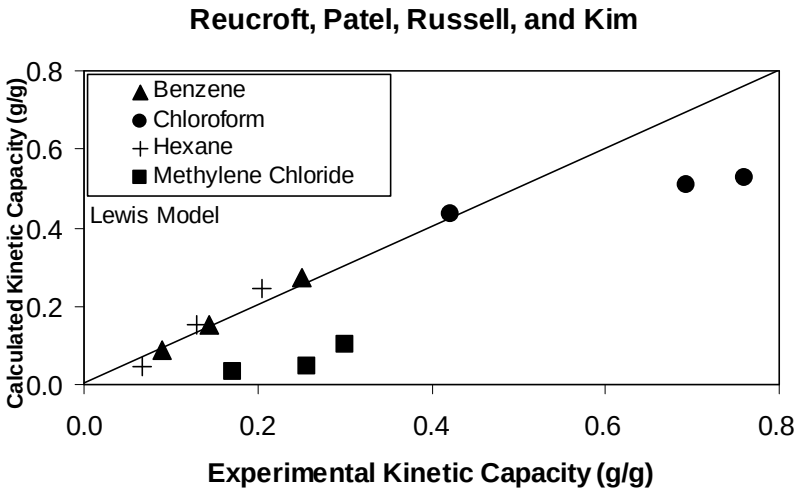

Figure 33. Comparisons of capacities calculated by the Lewis Model with kinetic capacities measured for four vapors in binary mixtures [84].

5. Polanyi Adsorption Potential Theory

Co-adsorbed vapors cannot always be considered independent, especially if they are miscible with one another. One of the most popular theories to relate adsorption of vapors singly and in mixtures is the Polanyi Theory. Lewis et al. [89] and Grant and Manes [90] have developed it for mixtures. The latter assumed: a) a liquid-like adsorbate mixture in which the adsorption potential of each pure adsorbed component is determined by the total adsorbate volume of the mixture, b) Raoult's Law as the relationship between the partial pressure of each component and its adsorbate mole fraction, and c) the adsorbate volumes are additive. According

to the Polanyi Theory all characteristic curves (adsorption capacities vs. adsorption potentials) on a given adsorbent are superimposable to a single curve by a correlating divisor for the adsorption potential. This correlating divisor can be 1) molar volume calculated at the boiling point corresponding to adsorption pressure [89], 2) normal boiling point molar volume [90], or, more generally, 3) the affinity coefficient β of Dubinin [35, 36]. This theory for mixtures states that:

$$(RT / \beta_1) \ln (x_1 f_{1s} / f_1) = (RT / \beta_2) \ln (x_2 f_{2s} / f_2) = \text{etc.} \qquad (77)$$

Fugacities f_i (and f_{is} for saturated vapors) used by Grant and Manes for high-pressure gases can be replaced with partial (and saturated vapor) pressures p_i or concentrations C_i at normal atmospheric pressures. Using the sum of mole fractions x_i in the adsorbate equal to unity and the additivity of molar volumes allows the calculation of the numbers of moles of each component adsorbed.

6. Ideal Adsorbed Solution Theory (IAST)

Myers and Prausnitz [92] are credited with the thermodynamically consistent Ideal Adsorption Solution Theory, sometimes called the Myers-Prausnitz theory**.** They assumed Raoult's Law and the concept of equality of spreading pressures Π_i for each component:

$$\Pi_i = \frac{RT}{A} \int_0^{p_i^o} \frac{n_i^o}{p_i} d\, p_i \qquad (78)$$

where n_i^o is the number of moles of pure component i in the adsorbed phase obtained from a pure component isotherm for a vapor pressure p_i. The value of p_i^o is that corresponding to the spreading pressure. A is the specific area of the sorbent.

Grant and Manes [90] point out that their adsorption theory for mixtures and the IAST are practically equivalent if the correlating divisor is molar volume.

A major difficulty with the IAST model is the requirement that the adsorption isotherms

(actually, the n_i/p_i ratios as functions of p_i) be accurately defined to zero pressure and capacity, so that they can be integrated. Kidnay and Myers [93] used the IAST with Freundlich isotherm equations to overcome this problem. They also developed a simplified method that avoids the calculation of spreading pressures, but requires Freundlich isotherms with equal powers of concentration (seldom the case). Digiano et al. [94] simplified this even further for cases of identical Freundlich isotherms (very rare). Kaul [95] used Langmuir-Freundlich isotherms with the IAST. Valenzuela and Myers [96] used Toth and Honig/Reyerson isotherms. Vahdat [24] used the easily-integrated Langmuir isotherm, because it maintains thermodynamic consistency. Others (Hill et al. [97], Myers and Prausnitz [92], Sundaram and Yang [98], Mahle [99], etc.) have fit the lower coverage portion of experimental or theoretical isotherms with empirical equations that can be integrated analytically.

Alternately, Grant and Manes [90] point out that the integration difficulties for the IAST can be overcome by using any Polanyi-type correlation. Lavanchy et al. [39] derived analytical solutions for the integrations of the Dubinin/Radushkevich and Dubinin/Astakhov equations to calculate spreading pressures. This Myers/Prausnitz-Dubinin (or IAST/DR) theory has the added advantage of not requiring the reference pure vapor isotherm to be at the same temperature as the mixture. They found it to work well with miscible mixtures of chlorobenzene/carbon tetrachloride [39], 1,2-dichloroethane/benzene [100], and the ternary mixture carbon tetrachloride/chlorobenzene/2-chloropropane, but they did not use it for immiscible 2-choropropane/water [88]. Multicomponent breakthrough times and curves, as well as equilibrium adsorbed capacities, were successfully predicted.

Reucroft [84] compared total capacities calculated for three binary mixtures with measured equilbrium capacities. Figure 34 shows the results. Hexane/methylene chloride mixtures could not be calculated by the IAST method at the experimental concentrations.

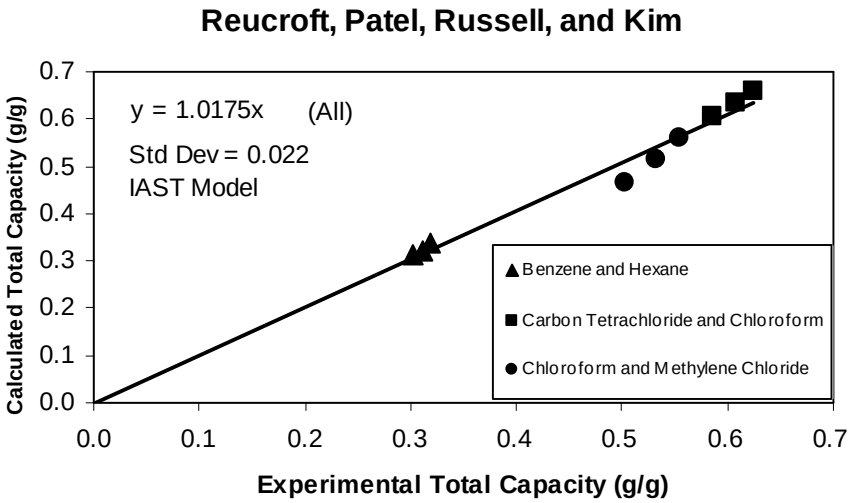

Figure 34. Comparisons of total binary vapor capacities calculated by the IAST Model with experimental ones for four binary mixtures [84].

7. Vacancy Solution Model (VSM)

The Vacancy Solution Model was proposed by Suwanayuen and Danner for single gases [101] and for mixtures [102] of any number of gases. Their four empirical parameter equation describing the equilibrium relation between the ideal gas phase and the nonideal adsorbed phase can be found in the references. It includes activity coefficients that can be calculated for gases by summing over all components and "vacancies". Mixture component and vacancy interactions are described by other coefficients. A nonlinear equation solver or iterative approach is required to obtain adsorbate loadings. Kaul [95] used a simplified version of the VSM that requires only pure component isotherm data and ignores interaction coefficients. Hydrocarbon gas mixture data were well predicted.

Costa et al. [103] similarly improved the IAST by modifying Raoult's Law with the

introduction of activity coefficients. This, of course, improved data predictions, but added to the complexity of the model and added the requirement of having binary data to obtain the activity coefficients. Gusev et al. [104] introduced a multispace adsorption model for multicomponent adsorption equilibrium. It, likewise, with an added parameter gives better fits of some mixture data, but requires binary data to establish that parameter for each pair of components.

8. Multicomponent Langmuir Equation

The next category of models for capacities of mixtures is the mixed, combined, or weighted isotherm equations. Actually, the Molar Proportionality Model can be considered as a Henry's Law multicomponent model. The next simplest mixed vapor isotherm is the Multicomponent Langmuir Equation of Glueckauf [105]:

$$q_i = \frac{a_i\ C_i}{1 + b_i\ C_i + \Sigma\, b_j\ C_j} \tag{79}$$

and for a binary mixture:

$$q_1 = \frac{a_1\ C_1}{1 + b_1\ C_1 + b_2\ C_2} \tag{80}$$

$$q_2 = \frac{a_2\ C_2}{1 + b_1\ C_1 + b_2\ C_2} \tag{81}$$

Cooney and Strusi [106] explored the conditions under which the Multicomponent Langmuir Equation could be used at nonequilibrium conditions, such as adsorption onto a sorbent bed from flowing air. They found that the requirement for this application is that the mass transfer coefficients be of the same order of magnitude. Thomas and Lombardi [107] found that for benzene/toluene mixtures at equilibrium it was necessary to use a smaller value for b_B (0.322×10^8) than that obtained from the pure benzene isotherm ($b_B = 0.455 \times 10^8$). This can be attributed to interaction (mixing) between the two adsorbed vapors.

9. Multicomponent Freundlich Equation

The empirical Freundlich isotherm can be extended to the Multicomponent Freundlich Isotherm [108]:

$$q_i = \frac{a_i \; C_i^{(n_i + n_{ii})}}{C_i^{n_{ii}} + \Sigma \, a_{ij} \; C_j^{n_{ij}}} \tag{82}$$

where the a_i and n_i are pure component Freundlich parameters and the a_{ij} and n_{ij} are mixture parameters. For one vapor of a binary mixture:

$$q_1 = \frac{a_1 \; C_1^{(n_1 + n_{11})}}{C_1^{n_{11}} + \; a_{12} \; C_2^{n_{12}}} \tag{83}$$

The binary equations introduce six more empirical parameters and require six more equations or (binary) data to solve. These equations have been used successfully to describe equilibrium data, at least over a limited concentration range, and to do numerical simulations of column dynamics; however, they have the shortcomings of being entirely empirical and failing to satisfy Henry's Law and thermodynamic consistency at low coverages [109]. The assumptions $a_{12} = a_2$, $a_{21} = a_1$, $n_{12} = n_2$, $n_{21} = n_1$, $n_{11} = 1$, and $n_{22} = 1$ simplify Equation (83) to:

$$q_1 = \frac{a_1 \, C_1^{(n_1 + 1)}}{C_1 + \; a_2 \, C_2^{n_2}} \tag{84}$$

which no longer requires binary data.

10. Multicomponent Langmuir/Freundlich Equations

Various combinations of multicomponent Langmuir and Freundlich isotherm equations have been proposed and used. Basmadjian et al. [110] developed one for binary mixtures that includes a compositional cross-term in the denominator:

$$q_1 = \frac{a_1 \; C_1}{1 + b_{11} \, C_1^{n_{31}} + \; b_{21} \; C_2^{n_{41}} \, C_i^{n_{51}}} \tag{85}$$

Sheindorf et al. [111] proposed a Langmuir/Freundlich-like multicomponent isotherm equation with competition coefficients b_{ij} obtained empirically from binary mixture data:

$$q_i = a_i C_i (C_i + \Sigma b_{ij} C_j)^{(n_1-1)} \quad (86)$$

Rudling [112] suggested using Langmuir coefficients (obtained from single-component isotherms) for the Sheindorf competition coefficients, so that only single-component isotherm data are required.

One Langmuir/Freundlich combination single component equation of special note is that of Kisarov et al. [25, 26]. It uses relative pressures in place of concentrations and an exponent, ($n_i = kT/\beta_i$) which includes temperature and affinity coefficient. A binary form without cross-terms would be:

$$q_1 = \frac{a_1 b_1 (p_1/p_{sat1})^{n1}}{1 + b_1 (p_1/p_{sat1})^{n1} + b_2 (p_2/p_{sat2})^{n2}} \quad (87)$$

11. Multicomponent John Equation

A multicomponent John isotherm equation has been proposed [113] to calculate the total volume of an adsorbed mixture. For binary mixtures:

$$\log \log p_{12} = a_{12} + b_{12} \log n_{12} \quad (88)$$

where $a_{12} = y_1 a_1 + y_2 a_2$ and $b_{12} = y_1 b_1 + y_2 b_2$ for gas phase mole fractions y_i and single-vapor John isotherm coefficients a_i and b_1; $p_{12} = 10^N (p_1 + p_2)/ (p_{1s} + p_{2s})$ for partial and saturation pressures and a constant integer N (must be the same for both pure isotherms); n_{12} = the total mixture adsorption amount. If both components have similar adsorbabilities (similar van der Waals constants), the individual adsorbed amounts can be calculated by $n_i = y_i b_i n_{12} / b_{12}$. Reucroft et al. [84] applied John's model to total mixture capacity data with the results shown

graphically in Figure 35. Total capacities of hexane/methylene chloride mixtures were greatly overestimated. The others were close to experimental.

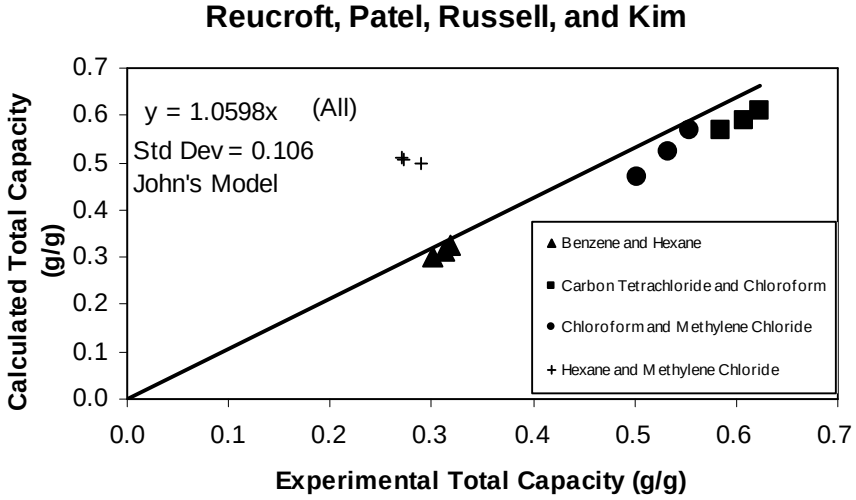

Figure 35. Comparisons of total binary vapor capacities calculated by the John Model with experimental ones for four binary mixtures [84].

12. Multicomponent Dubinin/Radushkevich Equations

Bering et al. [114, 30] extended the Dubinin/Radushkevich equation to the multicomponent case. For adsorption of a binary mixture of vapors on microporous adsorbents they expressed total moles adsorbed as:

$$n_1 + n_2 = \frac{W_o}{\Sigma x_i V_{mi}} \exp\left[- B T^2 \left\{ \frac{\Sigma x_i \ln (p_{sat\,i}/p_i)}{\Sigma x_i \beta_i} \right\}^2 \right] \qquad (89)$$

where W_o and $B = (R/E_o)^2$ are taken to be constants for both mixtures and individual components. Molar volume V_m, affinity coefficient β, and adsorption potential $RT \ln (p_{sat}/p)$ are weighted by x_i , the molar fractions of the components in the adsorption phase. Upon further defining the standard state of a mixture, they obtained an alternate equation:

$$n_1 + n_2 = \frac{W_o}{\Sigma x_i V_{mi}} \exp\left[- B T^2 \left\{ \frac{\ln (\Sigma p_{sat\,i} / \Sigma p_i)}{\Sigma x_i \beta_i} \right\}^2 \right] \qquad (90)$$

Since mole fractions are not known another equation is needed; Bering et al. [114] used the Lewis Equation (72) and obtained good agreement with experimental capacities for ethyl chloride/diethyl ether mixtures. Reucroft et al. [84] used this approach and obtained the results graphed in Figure 36. Alternately, Raoult's Law can be assumed to calculate a value for the standard state pressure $p_{12} = x_1 p_{sat\,1} + x_2 p_{sat\,2}$ (binary mixture case). If other parameters, such as W_o and B, are not the same for all pure components, it may be necessary to weight-average them with x_i also.

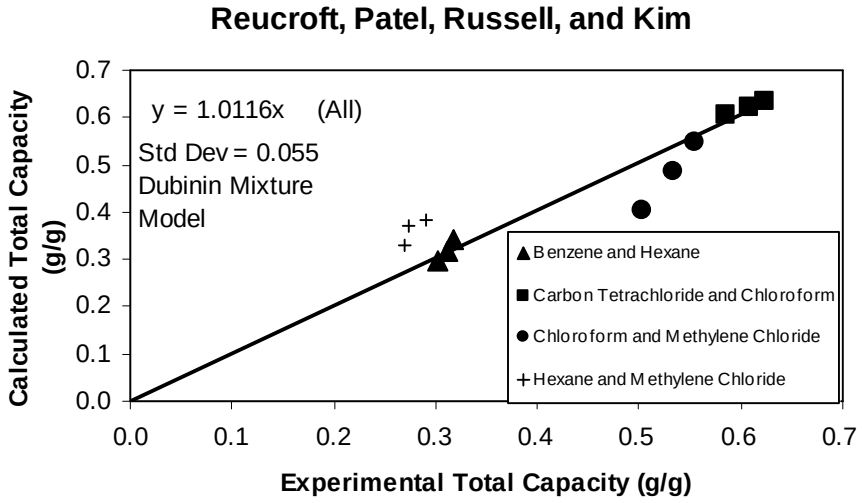

Figure 36. Comparisons of total binary vapor capacities calculated by a Dubinin Mixture Model with experimental ones for four binary mixtures [84].

C. Literature Comparisons of Capacity Models

Kaul [95] reviewed some of the above and other single vapor isotherms for suitability with mixtures and concluded: The **BET Isotherm** is known to be applicable only over a limited (low) range of pressure and mixture predictions using it are unacceptable. The **Statistical Thermodynamics Correlation** is only applicable for zeolites. The **Viral Isotherm Equation** is empirical and difficult to extrapolate and apply to mixtures, especially when enough terms are added to make it accurate for single vapors. Kaul's simplified version of the VSM gave results similar to the IAST at low coverages of hydrocarbon gases. At higher pressures and coverages and for azeotropic mixtures the original VSM predicted the data better than the IAST, since the VSM uses additional parameters (empirical binary interaction coefficients) to incorporate nonideality.

Rasmuson [27] compared the Volume Exclusion and Molar Proportionality approaches with the more complex and integration-requiring IAST. With toluene/butanol mixtures the total volume assumption overestimated butanol capacities more than the IAST, but toluene capacities less. The fixed total moles assumption gave even worse predictions for butanol and slightly better for toluene.

Figures 30 and 34-36 have shown the results of the Reucroft et al [84] study of four mixture models and mixtures of chloroform/methylene chloride, n-hexane/methylene chloride, benzene/n-hexane, and chloroform/carbon tetrachloride at three ratios each. Table IX gives them in a different format. The Molar Proportionality Model predictions were closest to the total equilibrium capacity data most of the time. Although the IAST didn't "win" any comparisons, it had the smallest range of deviations. In attempts to predict individual component kinetic capacities from total equilibrium capacities, the Molar Proportionality Method was more successful than the Lewis Equation (compare Figures 31 and 33).

Table IX. Results of the Comparisons by Reucroft et al. [84] of Mixture Models

Model Tested for Prediction	Number of Times Closest to the Data		Range of Deviations of Predictions from the Data	
	Total Mixture Equilibrium Capacity	Component Kinetic Capacities	Total Mixture Equilibrium Capacity	Component Kinetic Capacities
Molar Proportionality	7	14	-2 to +34 %	-73 to + 16 %
IAST	0		-5 to +10%	
Multicomponent DR	2		-7 to +33 %	
Multicomponent John	3		-3 to +90 %	
Lewis Equation		4		-81 to +21 %

Valenzuela and Myers [115] compared predictions of the Grant-Manes, IAST, and VSM models with experimental data for 22 mixtures of hydrocarbon and other gases on activated carbons. They calculated the average errors in selectivity shown in Table X. The average error of 35% in selectivity for IAST corresponds to an average absolute error of 0.04 in mole fraction. This table also shows the number of "bests" for each model (ties are counted twice) obtained from Appendix 3 in their article.

Table X. Results of the Comparisons by Valenzuela and Myers [115] of Mixture Models

Model Tested for Prediction	Number of Times Closest to the Data	Average Absolute Relative Errors
IAST	69	35 %
VSM	55	41 %
Grant-Manes	25	80 %

Doong and Yang [87] compared equations they developed to the IAST, the Grant-Manes Model, and the Multicomponent DR model proposed by Bering et al. They commented that latter three were more difficult to apply, since they require numerical iteration. Table XI shows a summary of their model comparison results for hydrocarbon gases on an activated carbon and a molecular sieve carbon. It can be seen that the Grant-Manes and IAST models were most

successful. However, acetone/hexane and methanol/hexane mixtures on a molecular sieve carbon the Doong-Yang Mixture Model matched the data best, though not very well. The graphs (no data tabulated) suggest that a simple Molar Proportionality model would have done (on the average) as well as or better than any of them for these latter two vapor mixtures.

Table XI. Results of the Comparisons by Doong and Yang [87] of Mixture Models

Model Tested for Prediction	Number of Times Closest to the Data	Average Absolute Relative Errors
Doong-Yang	1	20.3 %
Grant-Manes	7	16.2 %
IAST	6	17.5 %
Multicomponent DR	2	28.8 %

D. New Comparisons of Selected Mixture Models

1. Selection of Mixture Models

Twelve models (with some variations) selected from those described above for further study are listed in Table XII. The main criteria for selection were that they could be used predictively and with a minimum of input information. The minimum input should be pressures (concentrations) and adsorption isotherms (with known parameters) for the individual components of a mixture. On this basis the Vacancy Solution Model was excluded; it requires too many empirical parameters even for the single component isotherms. The VSM is also mathematically difficult to apply. Other models (e.g., Multicomponent Freundlich and Langmuir) that rigorously require binary interaction data were either excluded or used in their simplest forms with parameters from single component isotherms only.

2. Selection of Database

The sets of data mentioned in literature model comparisons were considered for a reference database to compare predictive models for mixtures of vapors. However, many of them

are data for light hydrocarbon and other gases. For respiratory protection the concern is with vapors of larger molecules, most of which condense at normal temperatures. Also, often the data given in these papers are limited in numbers and scope.

Fortunately, a Swiss group at Neuchatel and Spiez [39, 100] has published tabulations of experimental data of adsorbed capacities for mixtures of vapors for wide ranges of compositions. The two mixtures are chlorobenzene/carbon tetrachloride (very different volatilities) and benzene/1,2-dichloroethane (similar volatilities).

3. Single Component Adsorption Isotherms for Mixture Models

Lavanchy et al.[39] have also provided DR equation parameters that allow calculation of single component capacities for the four components of the two binary mixtures studied. These can be used directly as model inputs or used to obtain parameters for other isotherm equations.

Figures 37 and 38 show Polanyi characteristic curve (isotherm) plots for the two mixtures using capacities obtained from the DR equation and parameters given. Affinity coefficients were

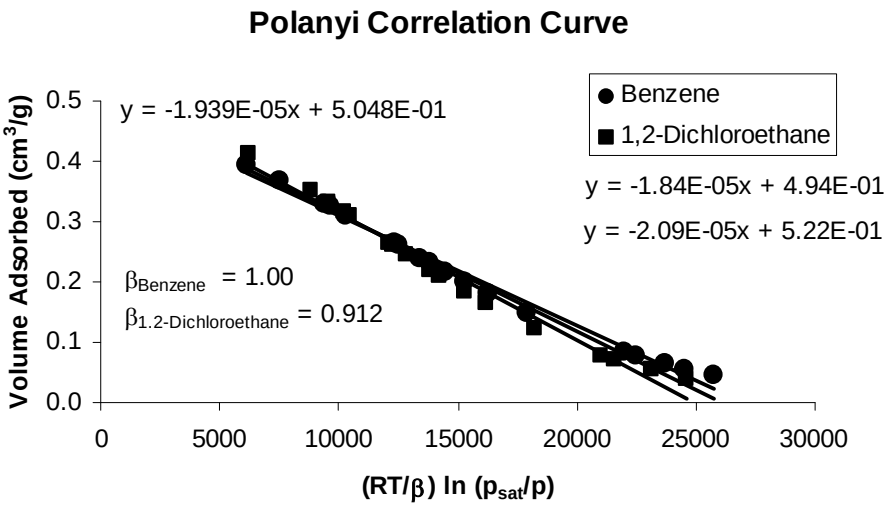

Figure 37. Polanyi correlation curve for pure benzene and 1,2-dichloroethane superimposed by the selection of relative affinity coefficients shown.

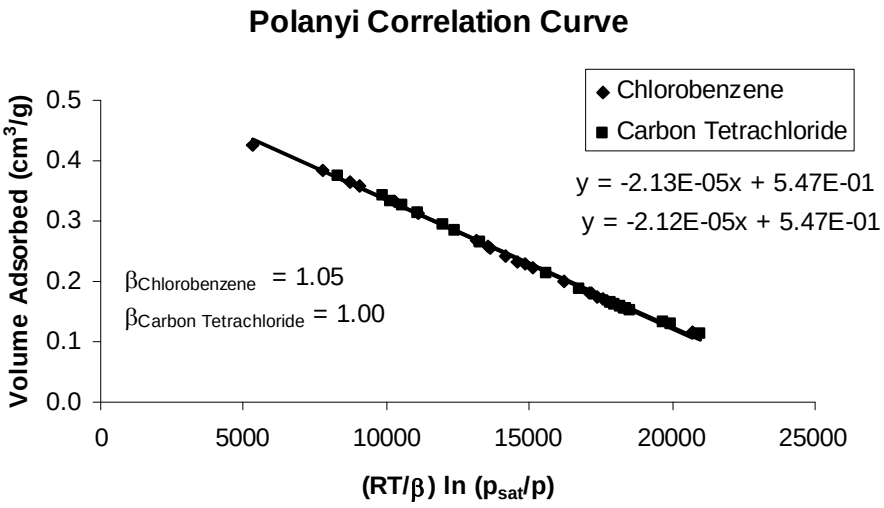

Figure 38. Polanyi correlation curve for pure chlorobenzene and carbon tetrachloride superimposed by the selection of relative affinity coefficients shown.

adjusted to coalesce the pairs of chemical in each mixture as much as possible. Linear fits were used to calculate capacities used in the Grant-Manes model.

Figures 39 and 40 show best fits of linearized Freundlich isotherms obtained by a similar procedure. In these cases there is no coalescing parameter and none is needed for the simplified Multicomponent Freundlich model (no cross-component terms). Slopes and intercepts of these isotherm plots give the single component Freundlich parameters needed.

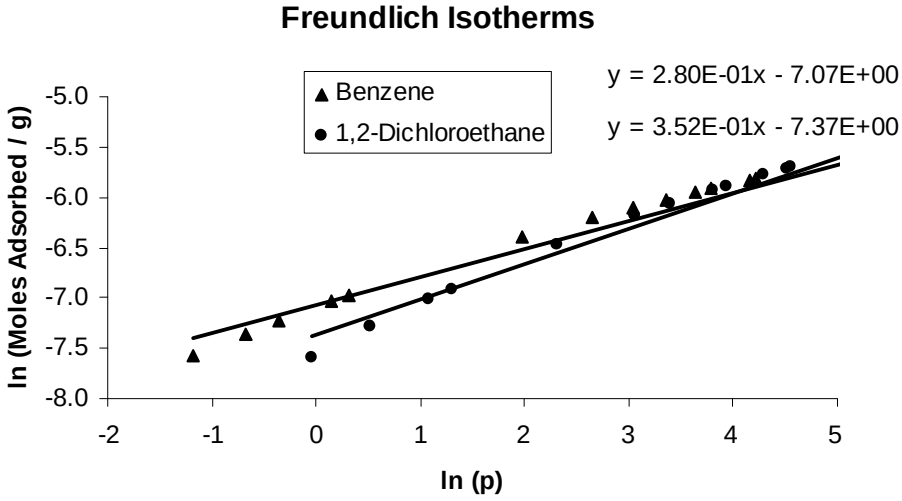

Figure 39. Linear Freundlich adsorption isotherms for pure benzene and 1,2-dichloroethane calculated from DR isotherm correlations.

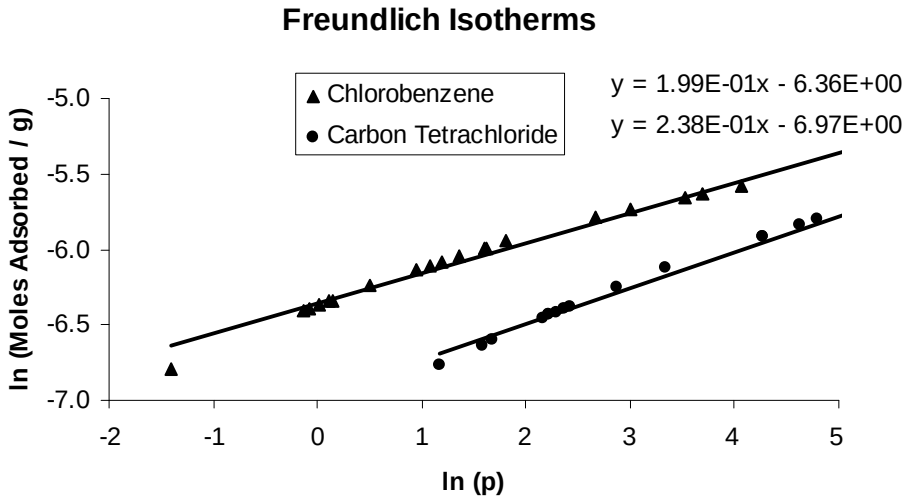

Figure 40. Linear Freundlich adsorption isotherms for pure chlorobenzene and carbon tetrachloride calculated from DR isotherm correlations.

Figures 41 and 42 show linearized Langmuir isotherm plots obtained and used similarly. The chlorobenzene, benzene, and 1,2-dichloroethane capacities clearly do not conform to the Langmuir equation, but the best-fit straight lines were used in the Multicomponent Langmuir model anyway.

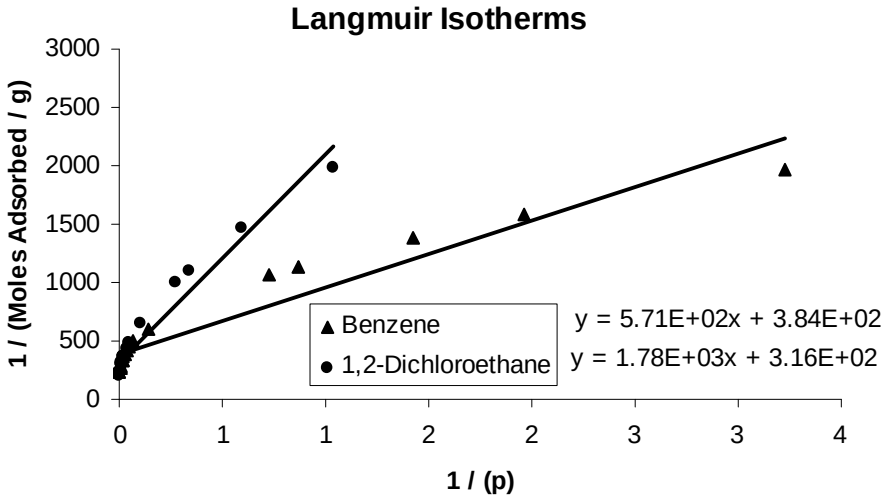

Figure 41. Linear Langmuir adsorption isotherms for pure benzene and 1,2-dichloroethane calculated from DR isotherm correlations.

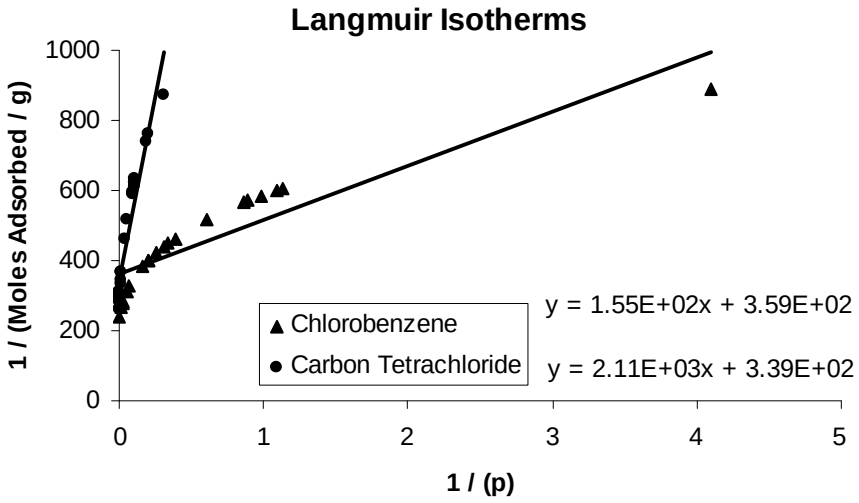

Figure 42. Linear Langmuir adsorption isotherms for pure chlorobenzene and carbon tetrachloride calculated from DR isotherm correlations.

A similar problem of nonlinearity of Kisarov (combined Langmuir and Freundlich isotherm with affinity coefficients) isotherms is shown in Figures 43 and 44. The chlorobenzene/carbon tetrachloride pair of component curves could be coalesced by selection of the KT/β parameters. This process was less successful with benzene/1,2-dichloroethane. Neither coalesced curve was linear as predicted by the Kisarov equation, but the best fits were used for testing the Multicomponent Kisarov L/F Model.

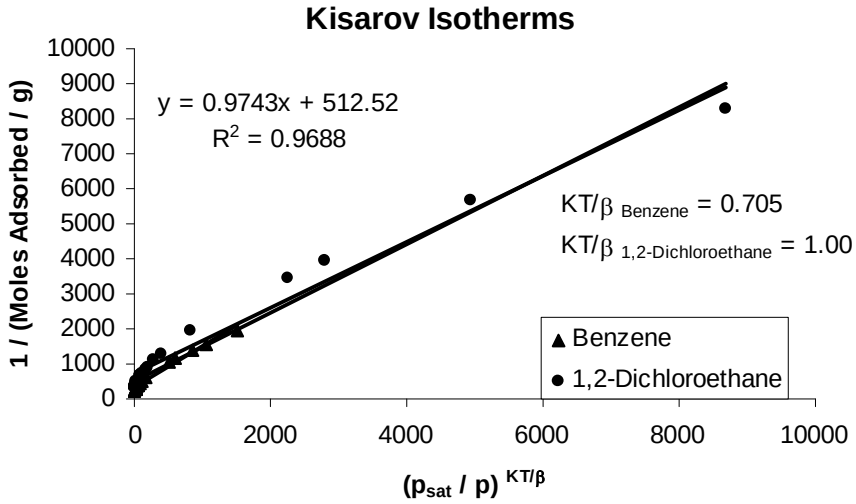

Figure 43. Linear Kisarov adsorption isotherms for pure benzene and 1,2-dichloroethane calculated from DR isotherm correlations.

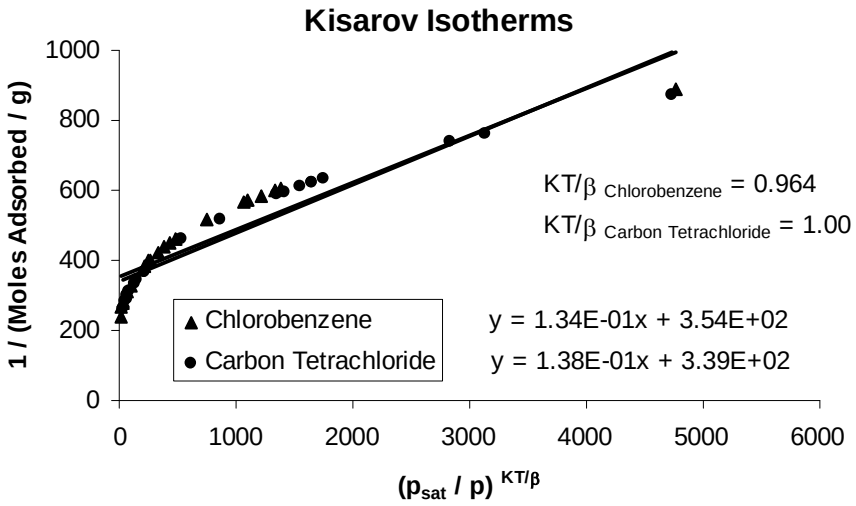

Figure 44. Linear Kisarov adsorption isotherms for pure chlorobenzene and carbon tetrachloride calculated from DR isotherm correlations.

John linearized, single-component isotherm plots in Figures 45 and 46 were linear in only certain regions for chlorobenzene and benzene. The Multicomponent John Model was tested with and without fitting the isotherm equations to only the linear regions.

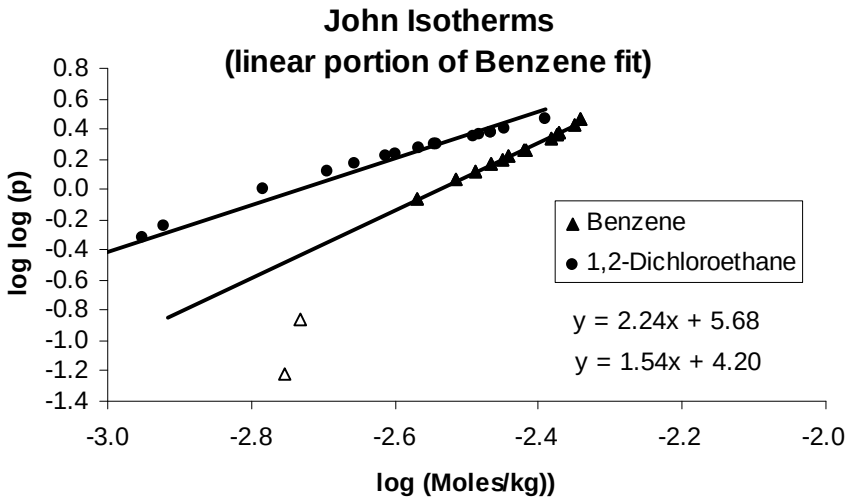

Figure 45. Linear John adsorption isotherms for pure benzene and 1,2-dichloroethane calculated from DR isotherm correlations.

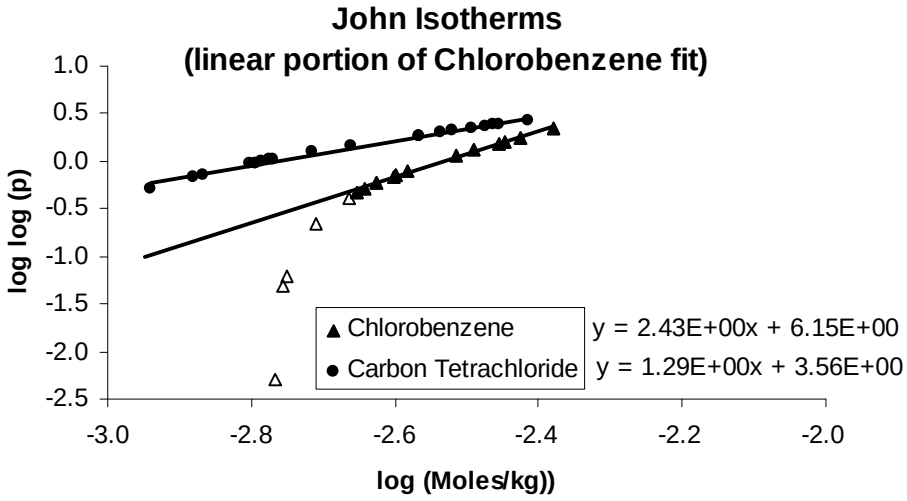

Figure 46. Linear John adsorption isotherms for pure chlorobenzene and carbon tetrachloride calculated from DR isotherm correlations.

4. Results of Applying Predictive Mixture Models

Table XII and Figures 47 - 75 show the results of applying models to the selected data.

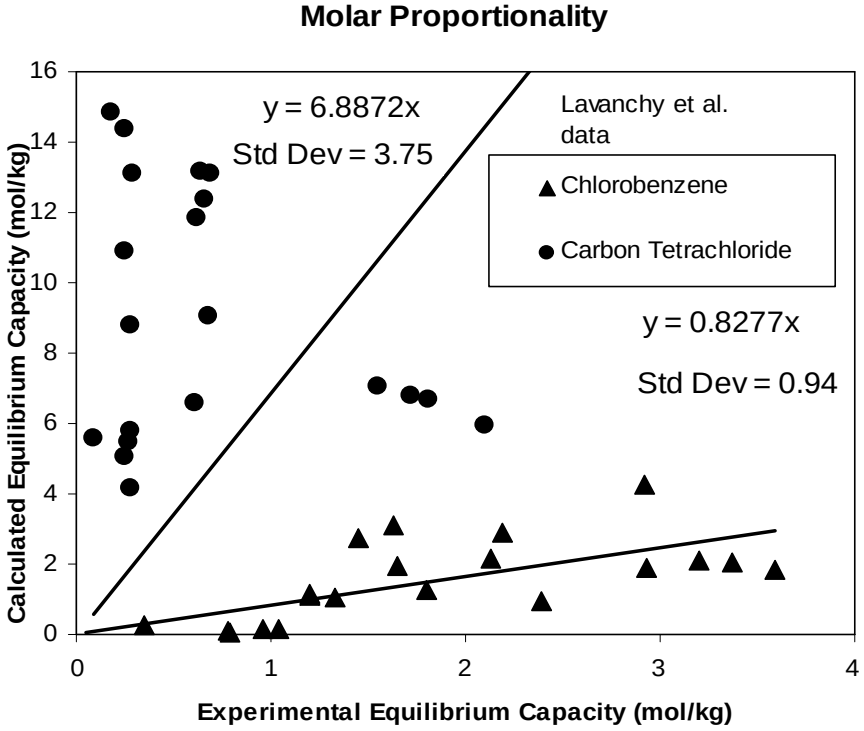

Figure 47. Results of applying the Molar Proportionality Model to equilibrium capacity data for mixtures of chlorobenzene and carbon tetrachloride [39].

Table XII. Accuracies and Precisions of Predictive Models for Mixtures

Mixture Model	Mixture Components A/B*	Component A		Component B	
		Average Accuracy (Calc/Exp)	Average Precision (mol/kg)	Average Accuracy (Calc/Exp)	Average Precision (mol/kg)
Molar Proportionality	CB/CT	0.83	0.94	6.89	3.75
Molar Proportionality	B/DCE	2.00	3.55	3.96	11.77
Volume Exclusion	CB/CT	0.86	0.96	6.85	3.73
Volume Exclusion	B/DCE	2.07	3.81	3.87	14.9
Lewis Ideal	CB/CT	*1.05*	1.30	6.68	3.60
Lewis Ideal	B/DCE	2.25	4.69	3.79	14.10
Greenbank-Manes	CB/CT	*0.97*	*0.20*	1.67	0.43
Greenbank-Manes	B/DCE	0.72	0.29	*0.94*	0.23
Grant-Manes	CB/CT	**0.98**	*0.20*	1.67	0.44
Grant-Manes	B/DCE	0.88	*0.14*	*1.08*	*0.16*
IAST/DR	CB/CT	*1.07*	**0.19**	1.45	0.40
IAST/DR	B/DCE	**0.96**	**0.11**	*1.04*	*0.13*
Freundlich Simplified	CB/CT	1.24	0.47	2.38	0.65
Freundlich Simplified	B/DCE	1.33	0.67	1.51	1.02
Langmuir Simplified	CB/CT	0.84	0.40	1.32	**0.28**
Langmuir Simplified	B/DCE	0.78	0.47	0.64	0.66
Kisarov L/F Simplified	CB/CT	0.83	0.39	**1.10**	0.53
Kisarov L/F Simplified	B/DCE	0.36	0.77	0.56	0.72
Rudling/Sheindorf L/F	CB/CT	**1.02**	0.28	1.71	0.50
Rudling/Sheindorf L/F	B/DCE	1.15	0.46	*0.99*	0.22
John-All Isotherm Data	CB/CT	0.67	0.27	2.03	0.35
Linear Isotherm Data	CB/CT	0.51	0.34	2.19	0.36
John-Linear Isotherm Data	B/DCE	*0.91*	0.34	**1.00**	0.32
Multicomponent DR - A	CB/CT	0.32	0.52	2.18	0.46
Multicomponent DR - B	CB/CT	0.32	0.52	2.20	0.42
Multicomponent DR - C	CB/CT	0.29	0.55	2.11	0.45
Multicomponent DR - A	B/DCE	0.86	*0.13*	1.13	0.17
Multicomponent DR - B	B/DCE	0.78	0.21	*1.04*	**0.08**
Multicomponent DR - C	B/DCE	0.76	*0.16*	*0.95*	0.21

* B = benzene, CT = carbon tetrachloride, CB = chlorobenzene, DCE = 1,2-dichloroethane
Numbers in bold print are the best agreements of models with data in each column for each vapor. Those in italics are $\pm$ 10 % accuracy or $\leq$ 0.20 mol/kg Standard Deviation.

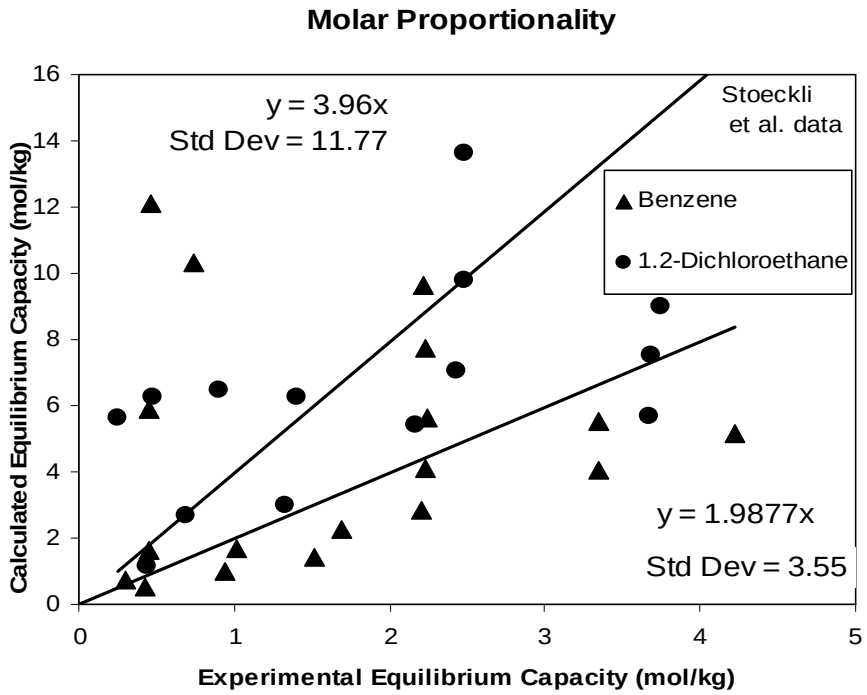

Figure 48. Results of applying the Molar Proportionality Model to equilibrium capacity data for mixtures of benzene and 1,2-dichloroethane [100].

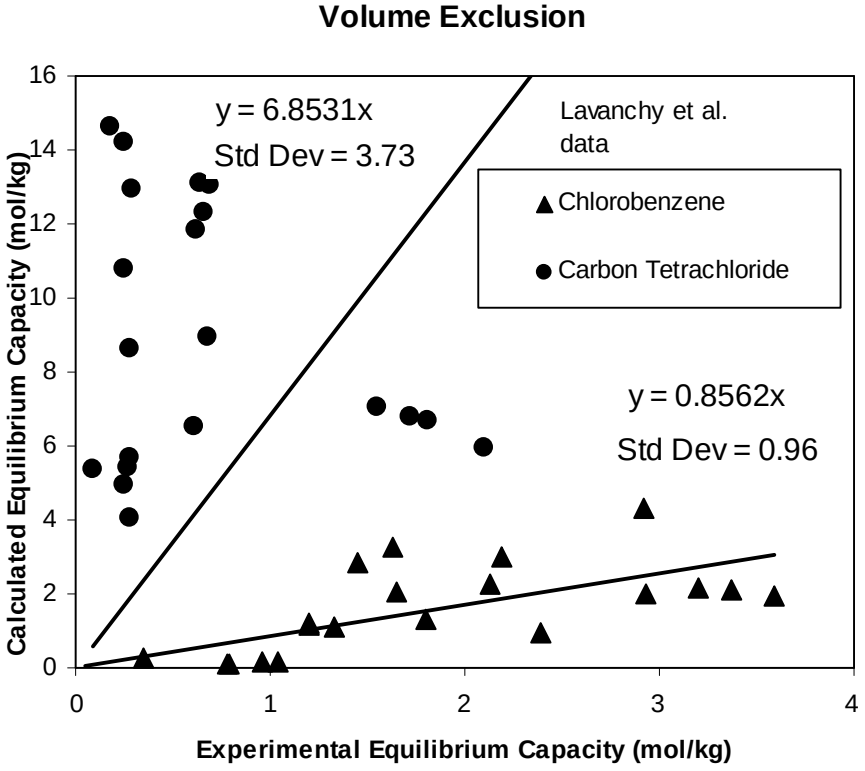

Figure 49. Results of applying the Volume Exclusion Model to equilibrium capacity data for mixtures of chlorobenzene and carbon tetrachloride [39].

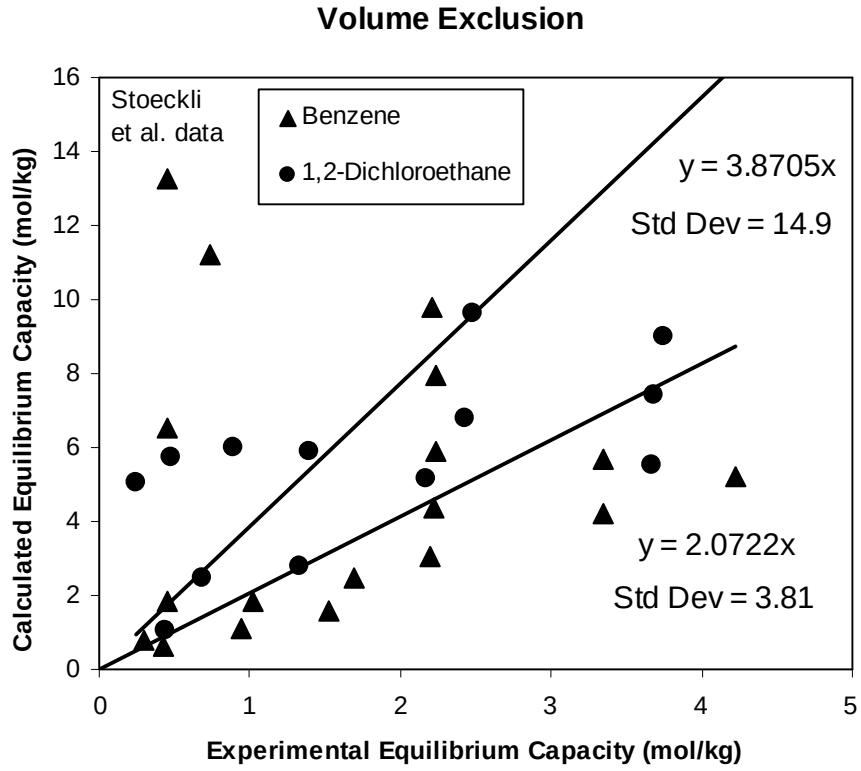

Figure 50. Results of applying the Volume Exclusion Model to equilibrium capacity data for mixtures of benzene and 1,2-dichloroethane [100].

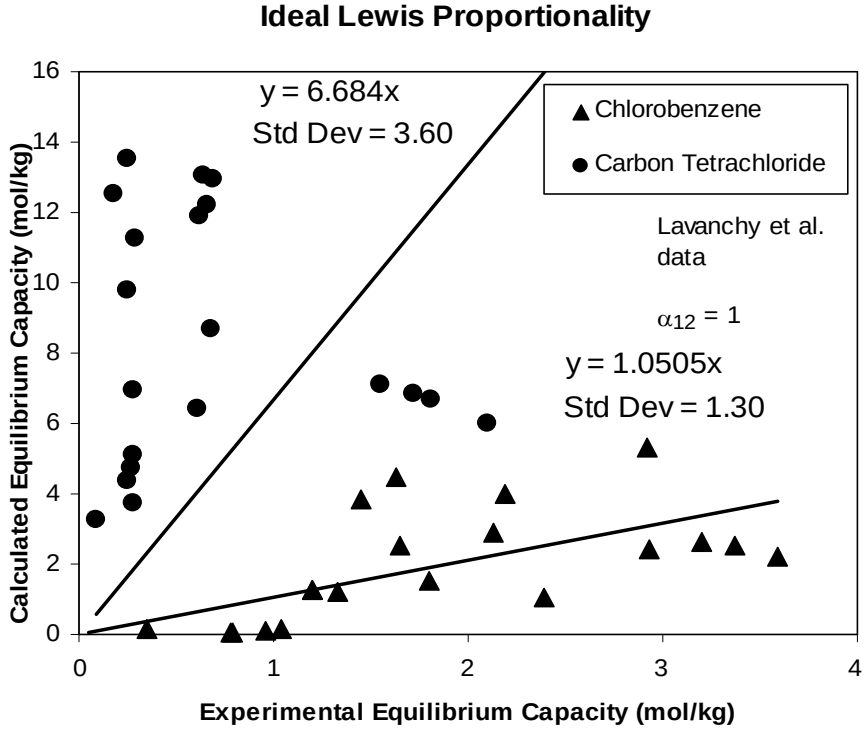

Figure 51. Results of applying the Ideal Lewis Proportionality Model to equilibrium capacity data for mixtures of chlorobenzene and carbon tetrachloride [39].

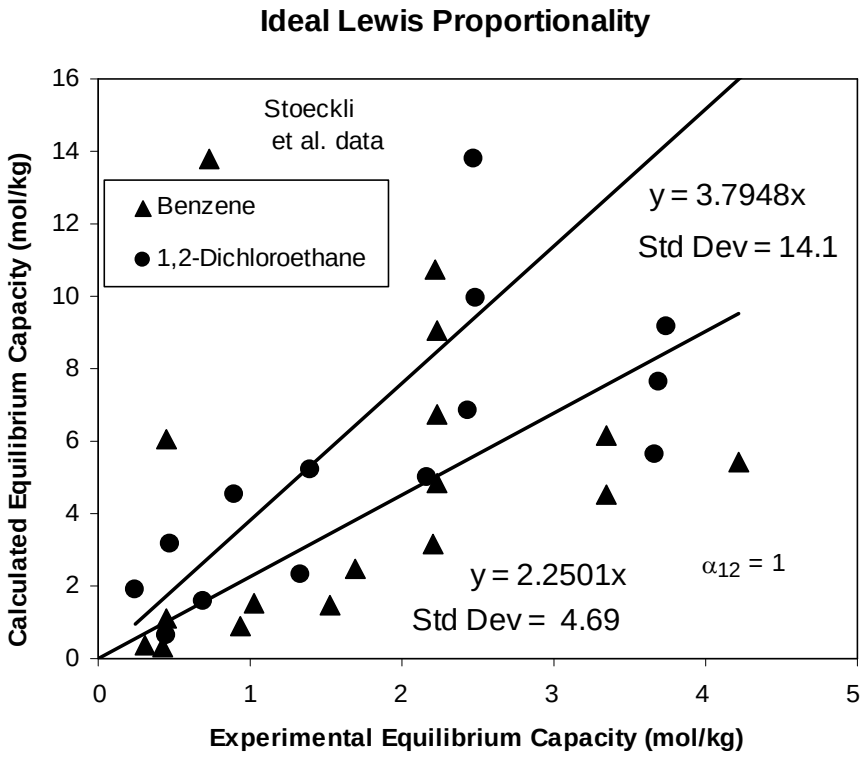

Figure 52. Results of applying the Ideal Lewis Proportionality Model to equilibrium capacity data for mixtures of benzene and 1,2-dichloroethane [100].

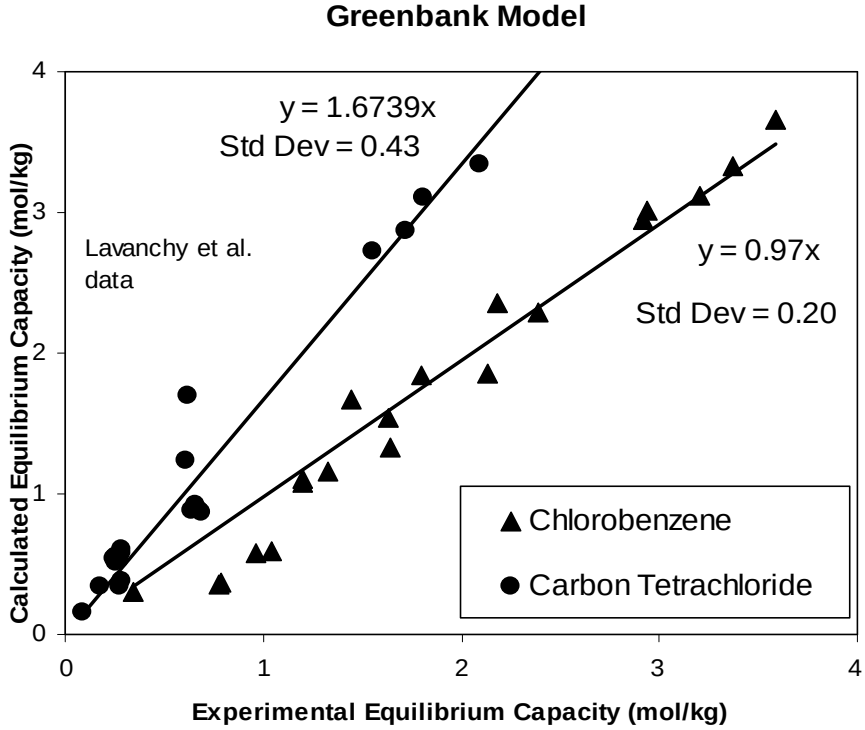

Figure 53. Results of applying the Greenbank-Manes Model to equilibrium capacity data for mixtures of chlorobenzene and carbon tetrachloride [39].

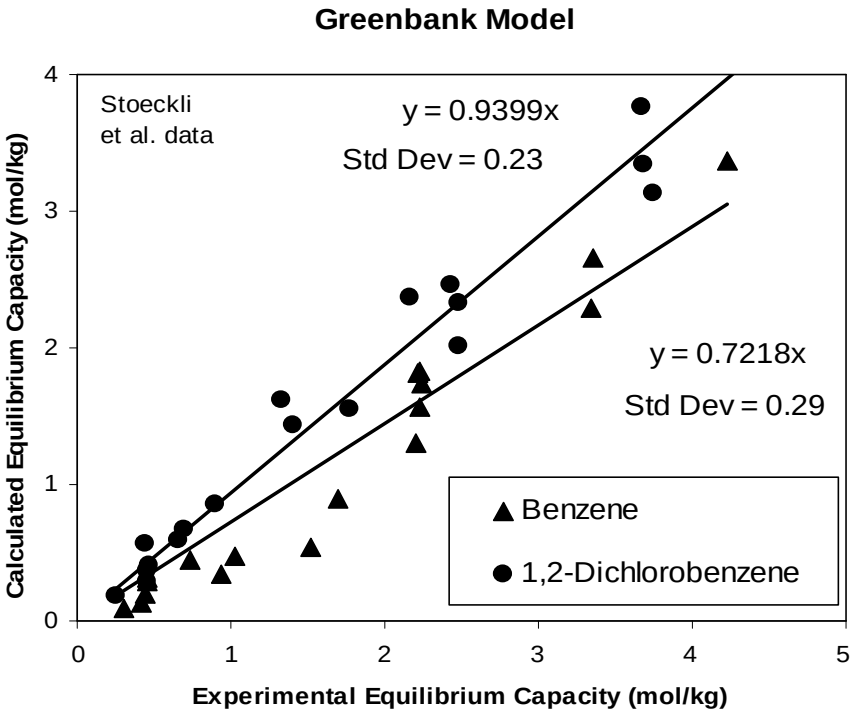

Figure 54. Results of applying the Greenbank-Manes Model to equilibrium capacity data for mixtures of benzene and 1,2-dichloroethane [100].

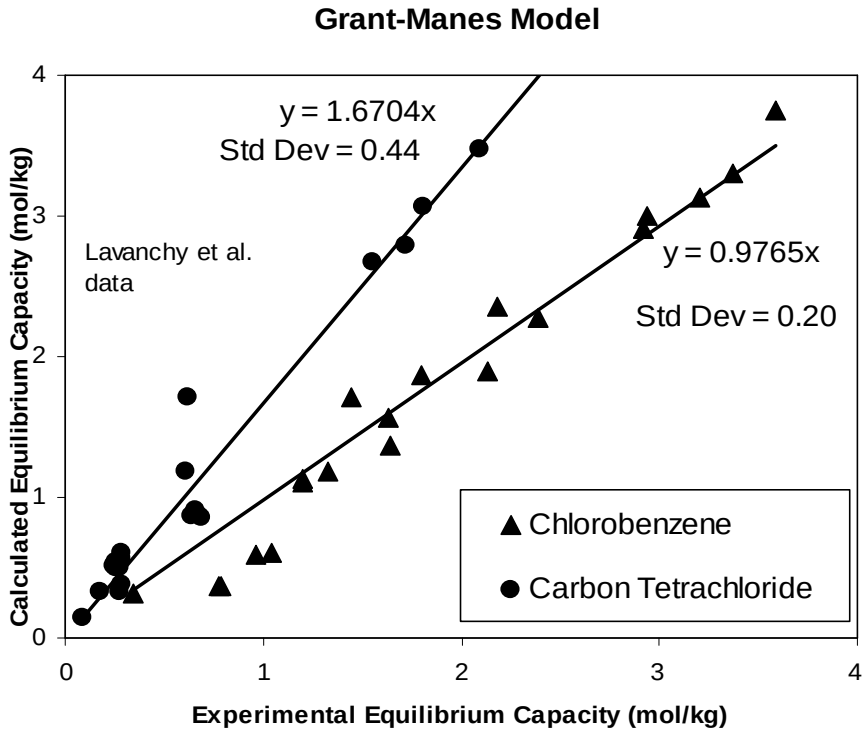

Figure 55. Results of applying the to Grant-Manes equilibrium capacity data for mixtures of chlorobenzene and carbon tetrachloride [39].

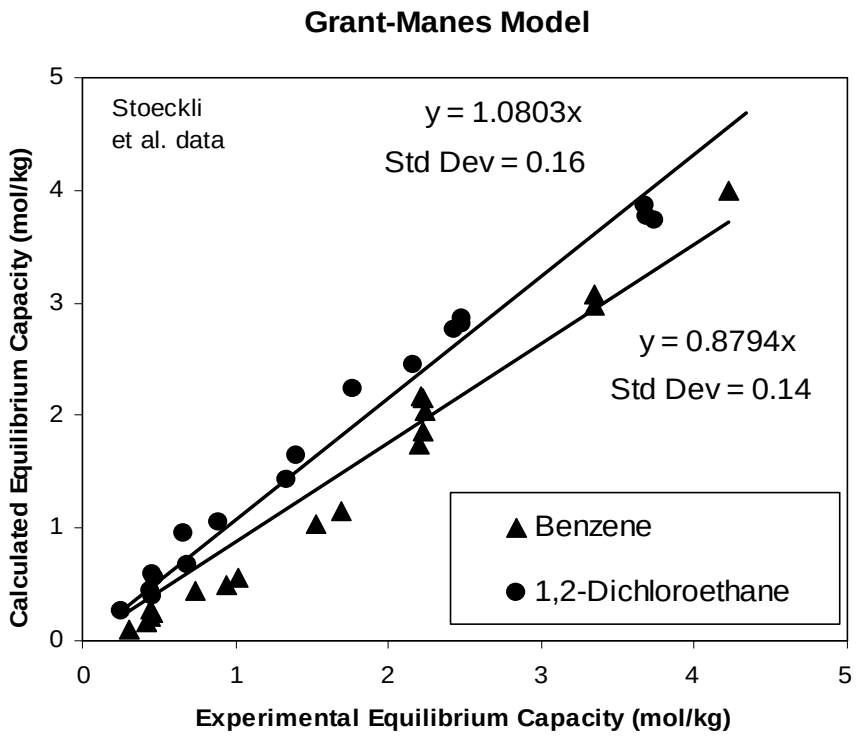

Figure 56. Results of applying the Grant-Manes Model to equilibrium capacity data for mixtures of benzene and 1,2-dichloroethane [100].

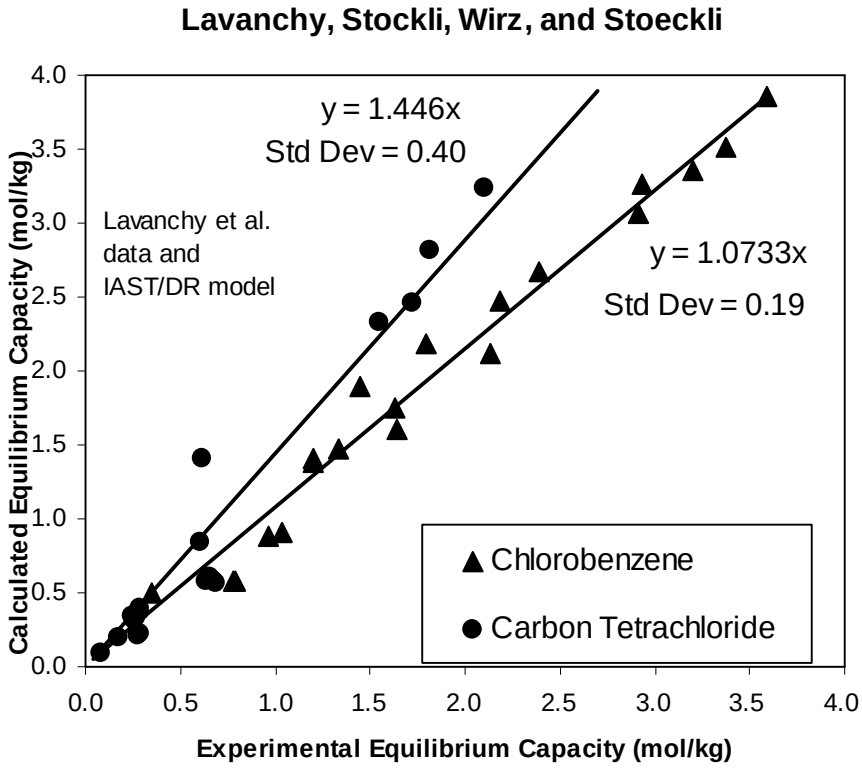

Figure 57. Results of applying the IAST/DR Model to equilibrium capacity data for mixtures of chlorobenzene and carbon tetrachloride [39].

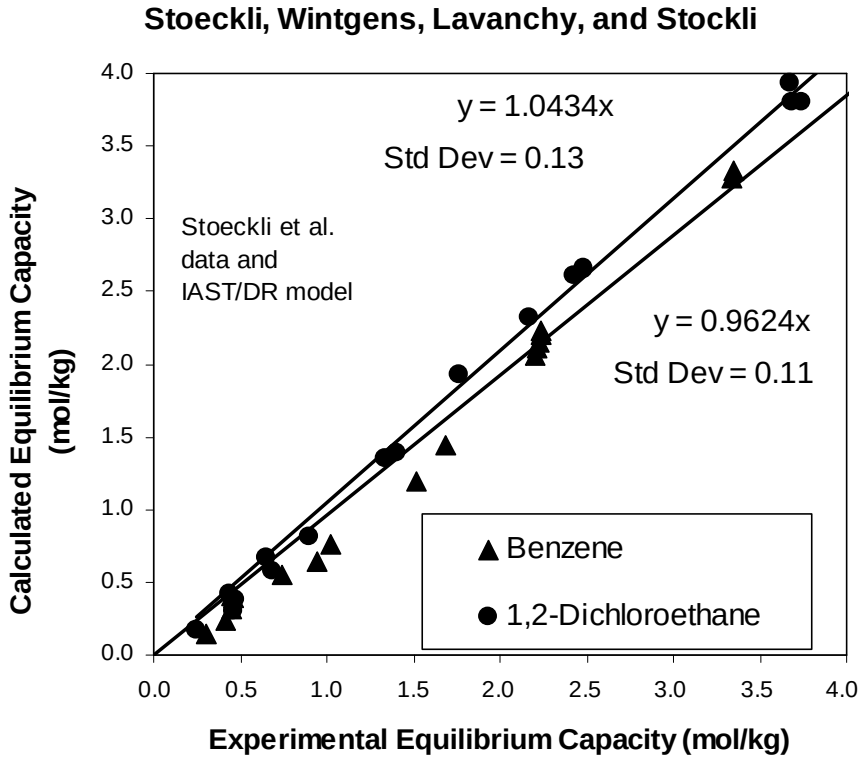

Figure 58. Results of applying the IAST/DR Model to equilibrium capacity data for mixtures of benzene and 1,2-dichloroethane [100].

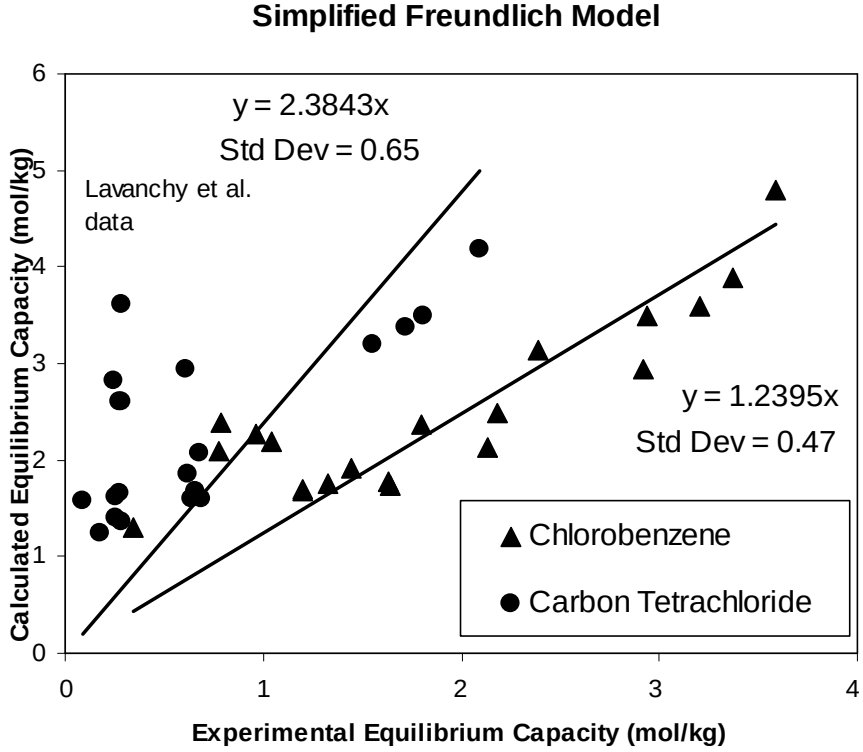

Figure 59. Results of applying the Simplified Freundlich Model to equilibrium capacity data for mixtures of chlorobenzene and carbon tetrachloride [39].

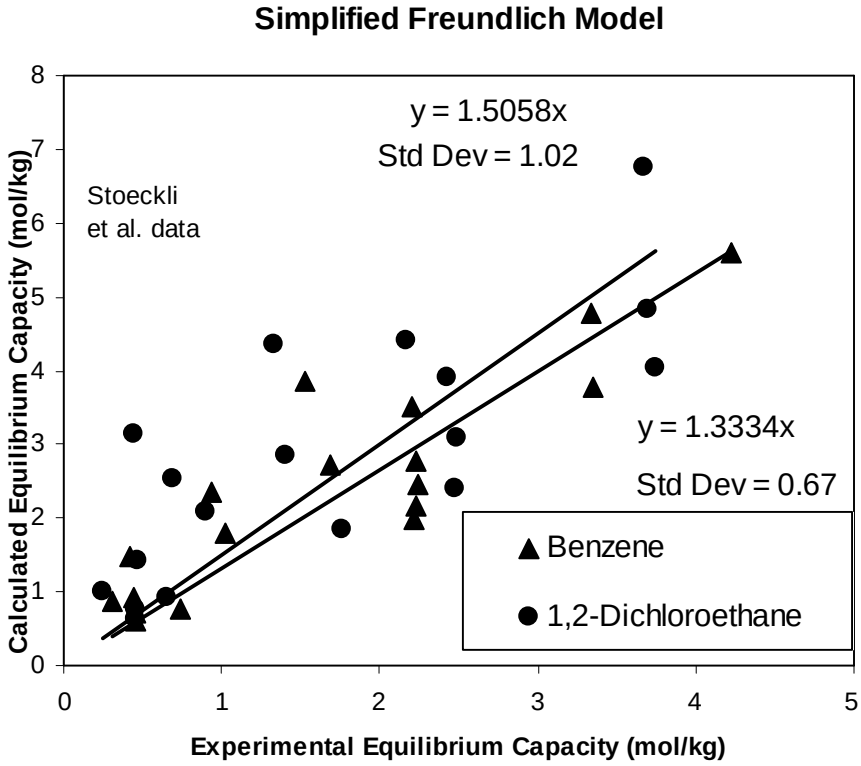

Figure 60. Results of applying the Simplified Freundlich Model to equilibrium capacity data for mixtures of benzene and 1,2-dichloroethane [100].

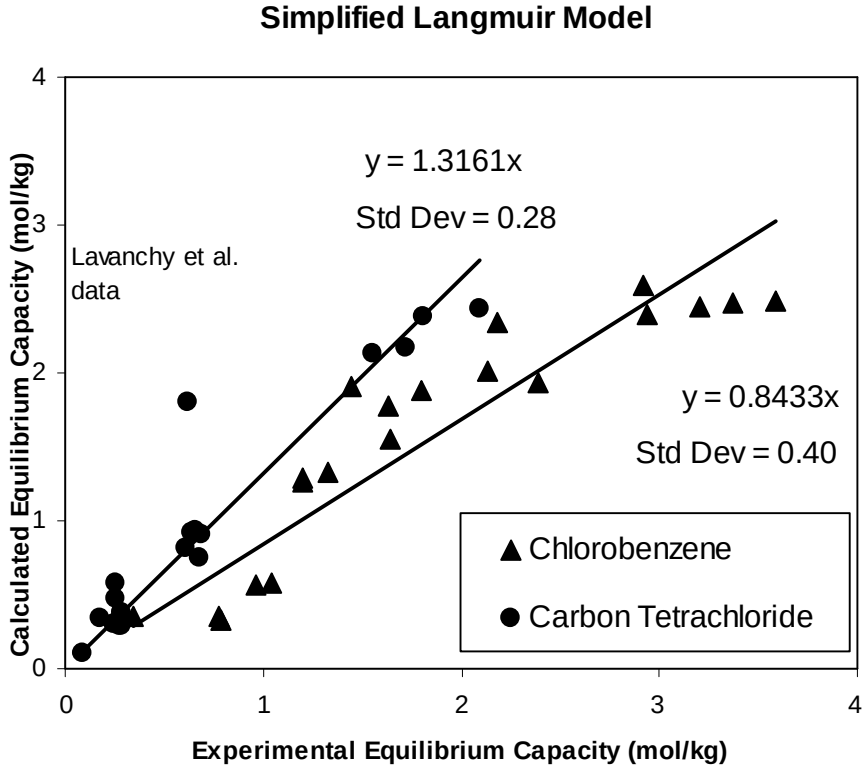

Figure 61. Results of applying the Simplified Langmuir Model to equilibrium capacity data for mixtures of chlorobenzene and carbon tetrachloride [39].

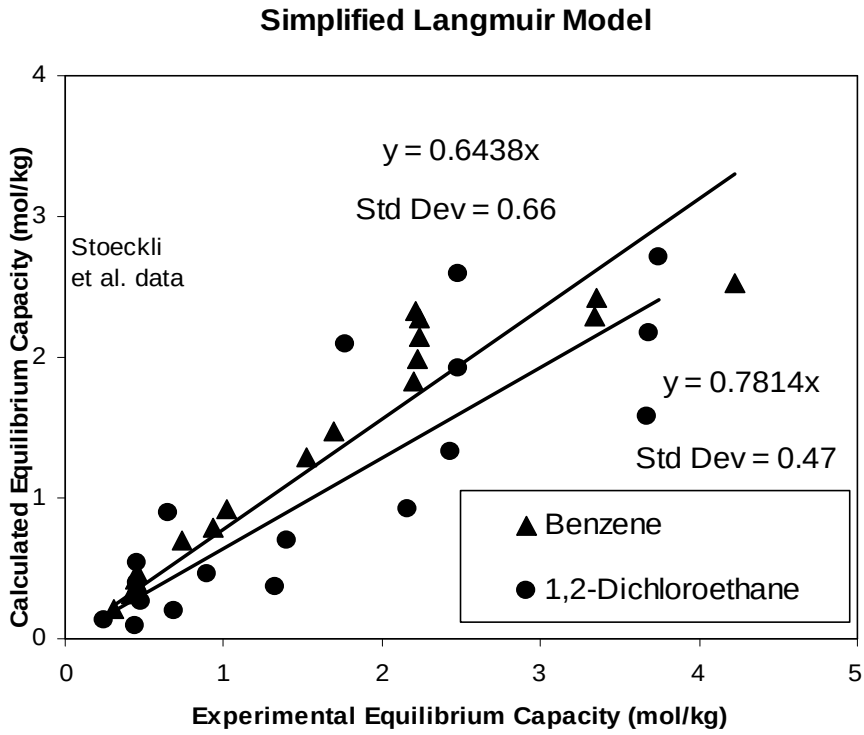

Figure 62. Results of applying the Simplified Langmuir Model to equilibrium capacity data for mixtures of benzene and 1,2-dichloroethane [100].

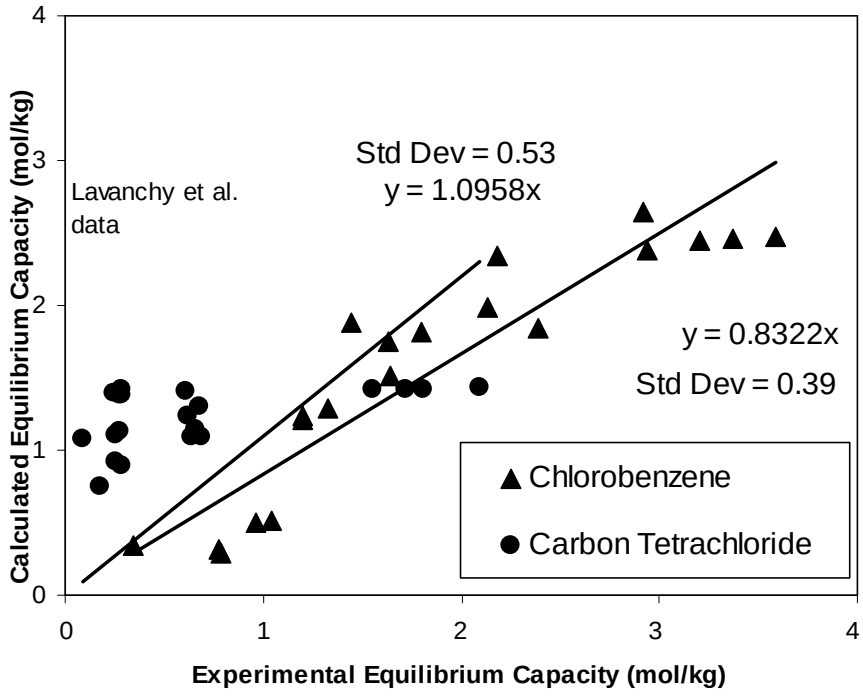

Figure 63. Results of applying the Kisarov Langmuir/Freundlich Model to equilibrium capacity data for mixtures of chlorobenzene and carbon tetrachloride [39].

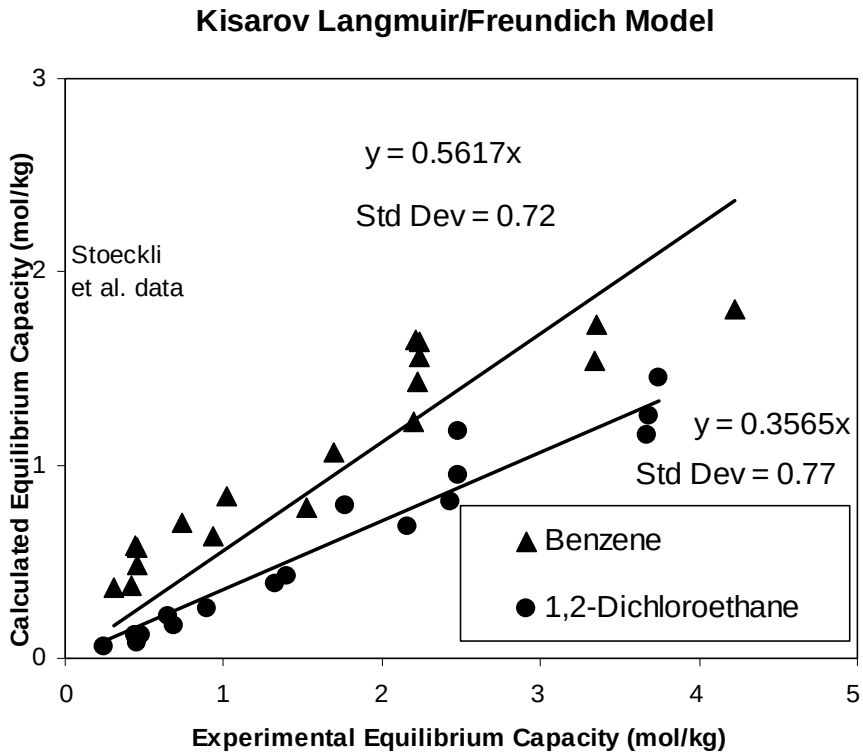

Figure 64. Results of applying the Kisarov Langmuir/Freundlich Model to equilibrium capacity data for mixtures of benzene and 1,2-dichloroethane [100].

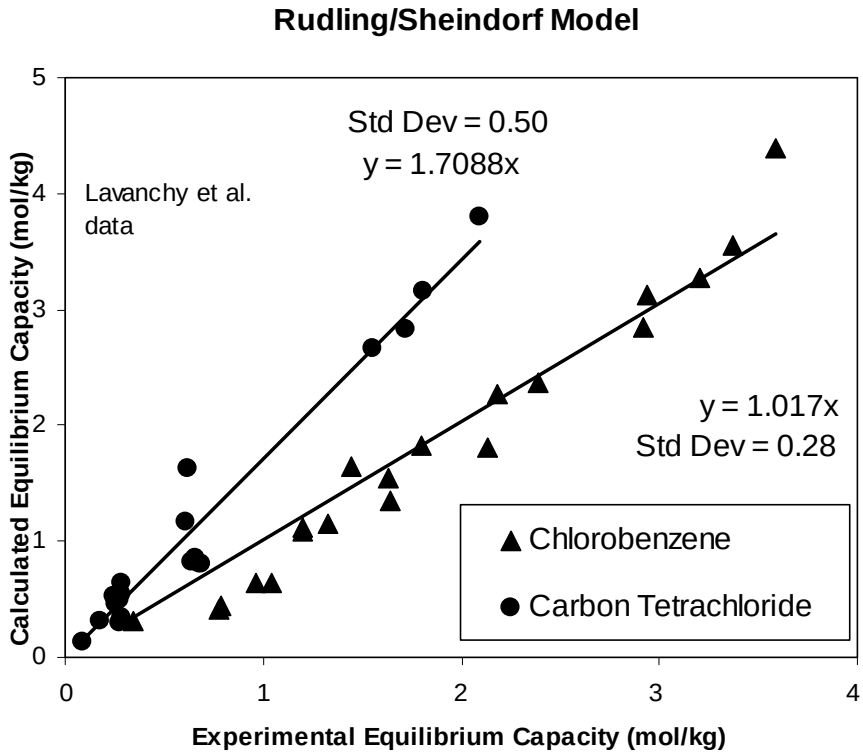

Figure 65. Results of applying the Rudling/Sheindorf Model to equilibrium capacity data for mixtures of chlorobenzene and carbon tetrachloride [39].

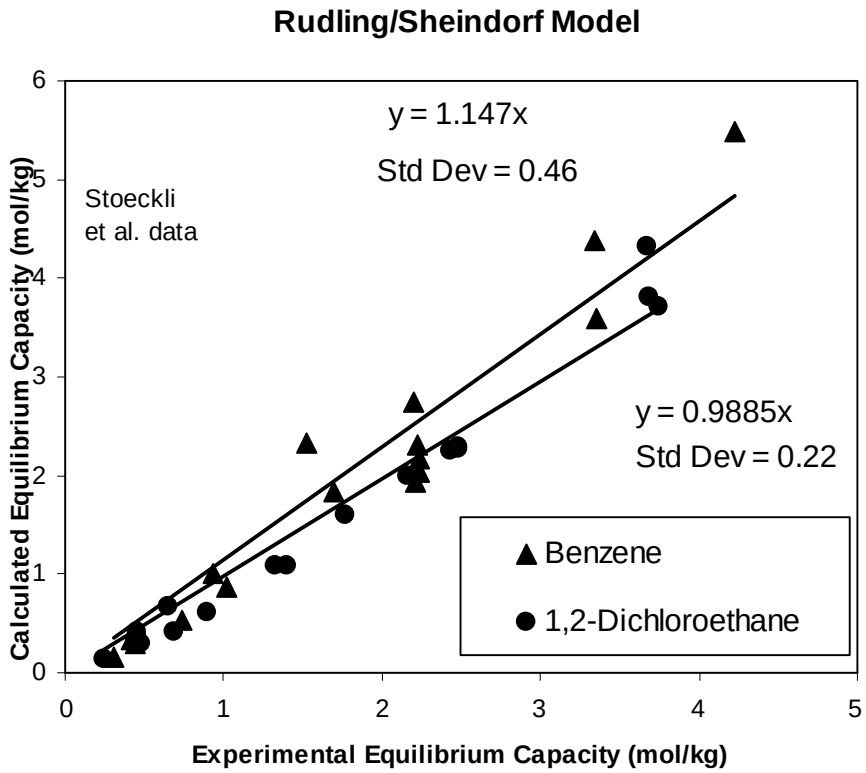

Figure 66. Results of applying the Rudling/Sheindorf Model to equilibrium capacity

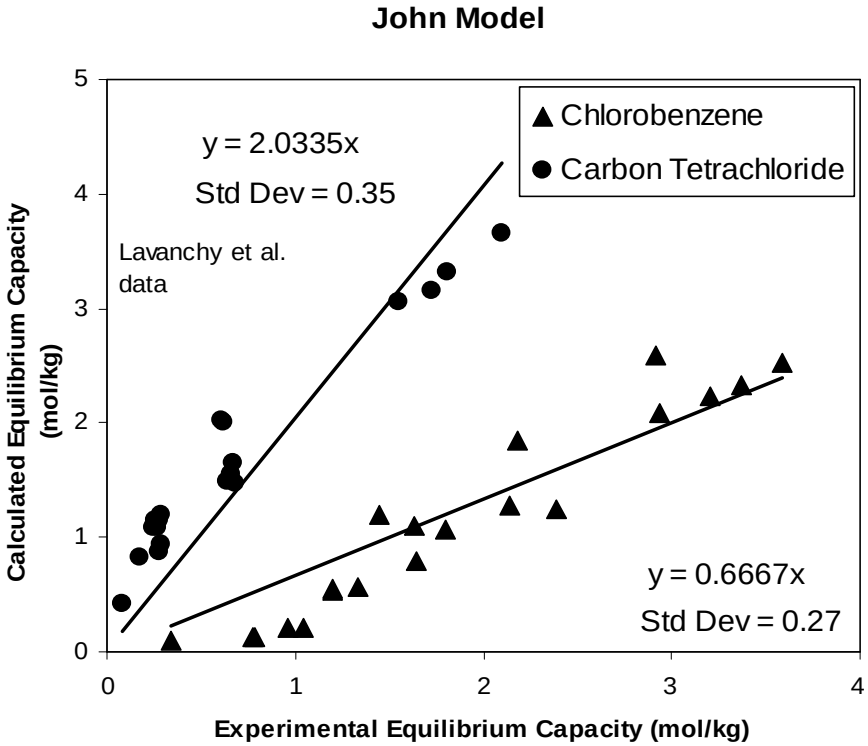

Figure 67. Results of applying the John Mixture Model to equilibrium capacity data for mixtures of chlorobenzene and carbon tetrachloride [39].

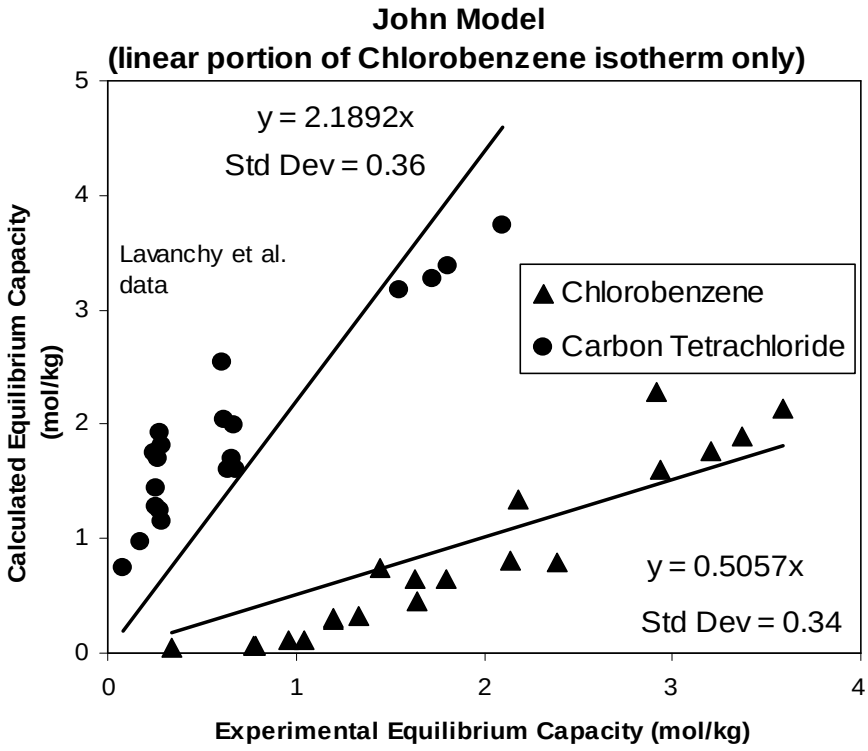

Figure 68. Results of applying the John Mixture Model to equilibrium capacity data for mixtures of chlorobenzene and carbon tetrachloride [39]. Only the linear portion of the chlorobenzene John isotherm was used.

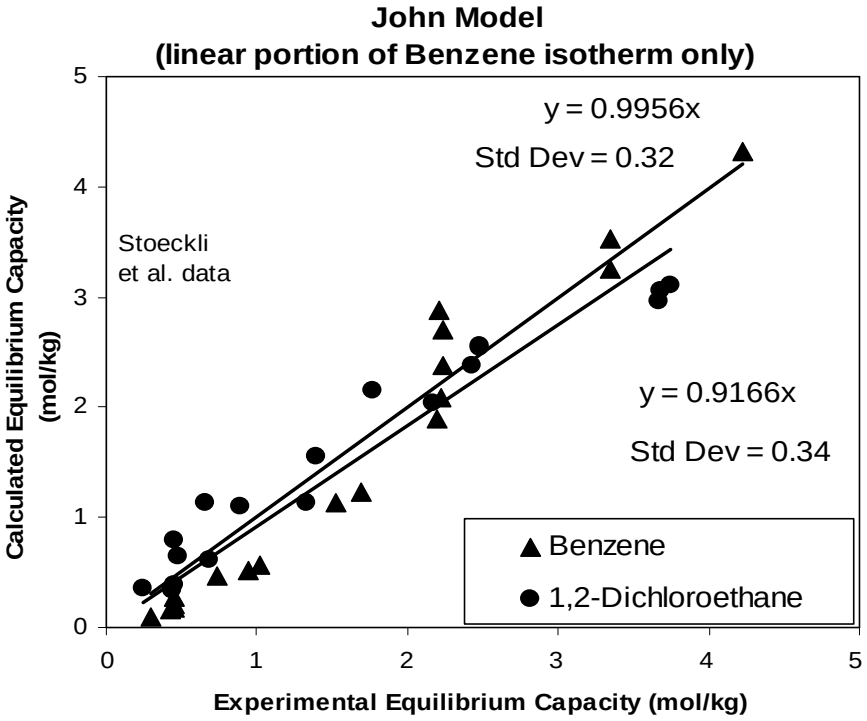

Figure 69. Results of applying the John Mixture Model to equilibrium capacity data for mixtures of benzene and 1,2-dichloroethane [100]. Only the linear portion of the benzene John isotherm was used.

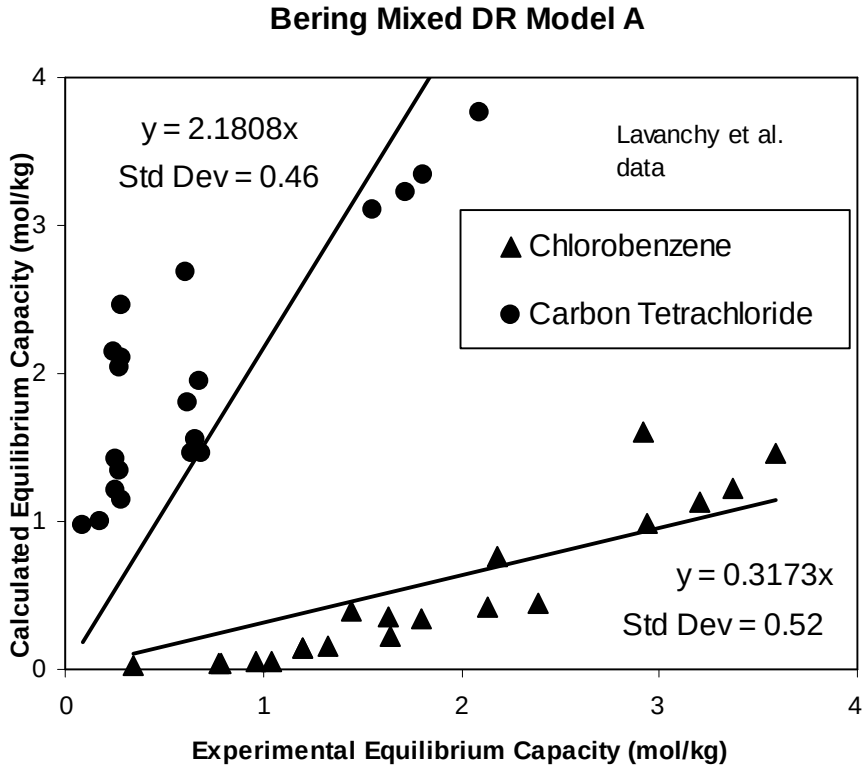

Figure 70. Results of applying a variant of the Mixed DR Model to equilibrium capacity data for mixtures of chlorobenzene and carbon tetrachloride [39].

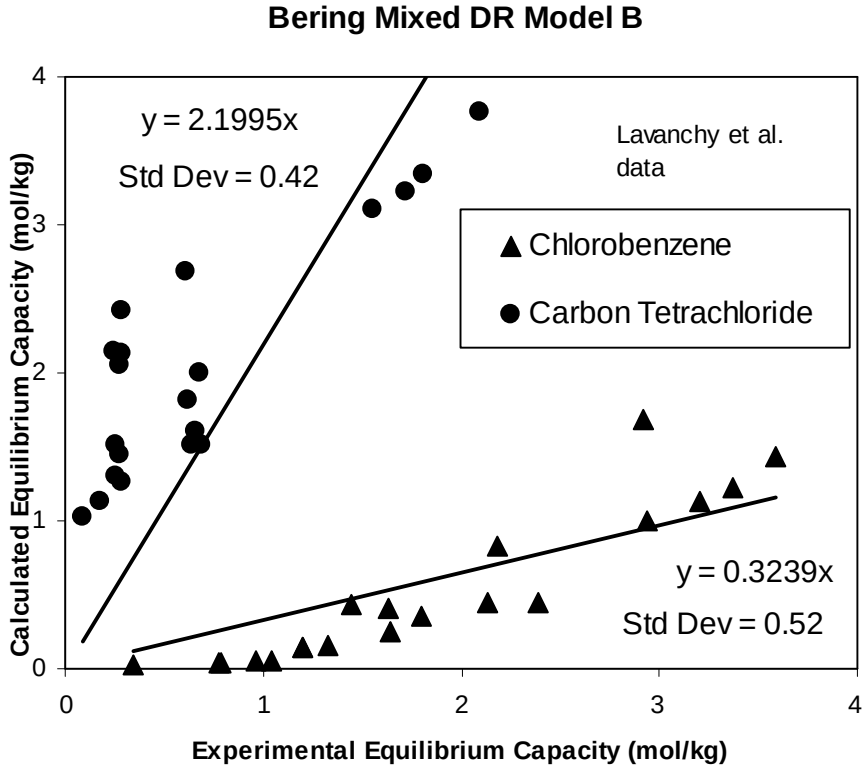

Figure 71. Results of applying a variant of the Mixed DR Model to equilibrium capacity data for mixtures of chlorobenzene and carbon tetrachloride [39].

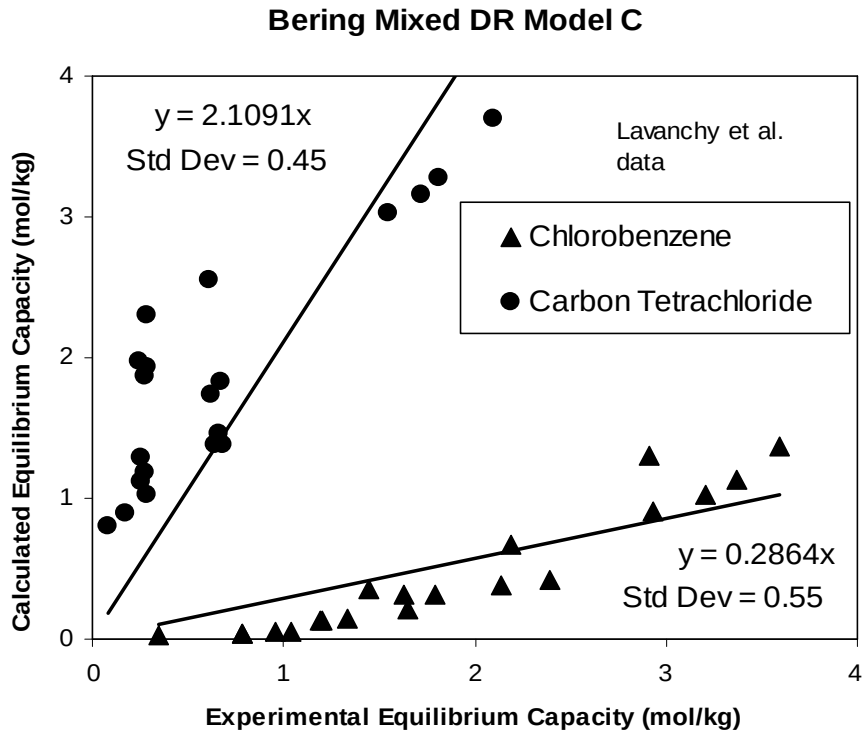

Figure 72. Results of applying a variant of the Mixed DR Model to equilibrium capacity data for mixtures of chlorobenzene and carbon tetrachloride [39].

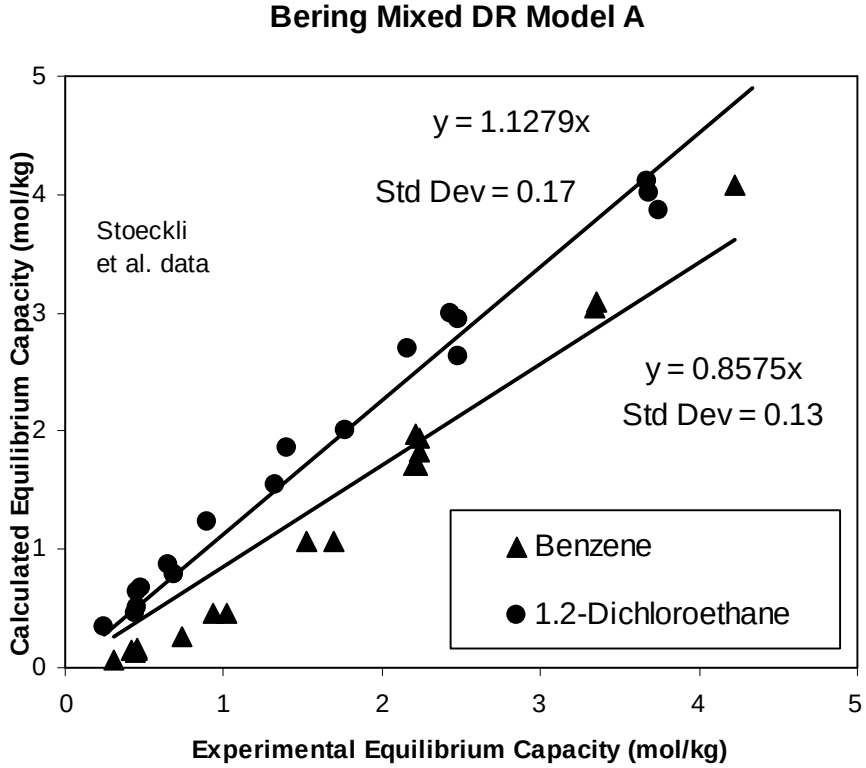

Figure 73. Results of applying a variant of the Mixed DR Model to equilibrium capacity data for mixtures of benzene and 1,2-dichloroethane [100].

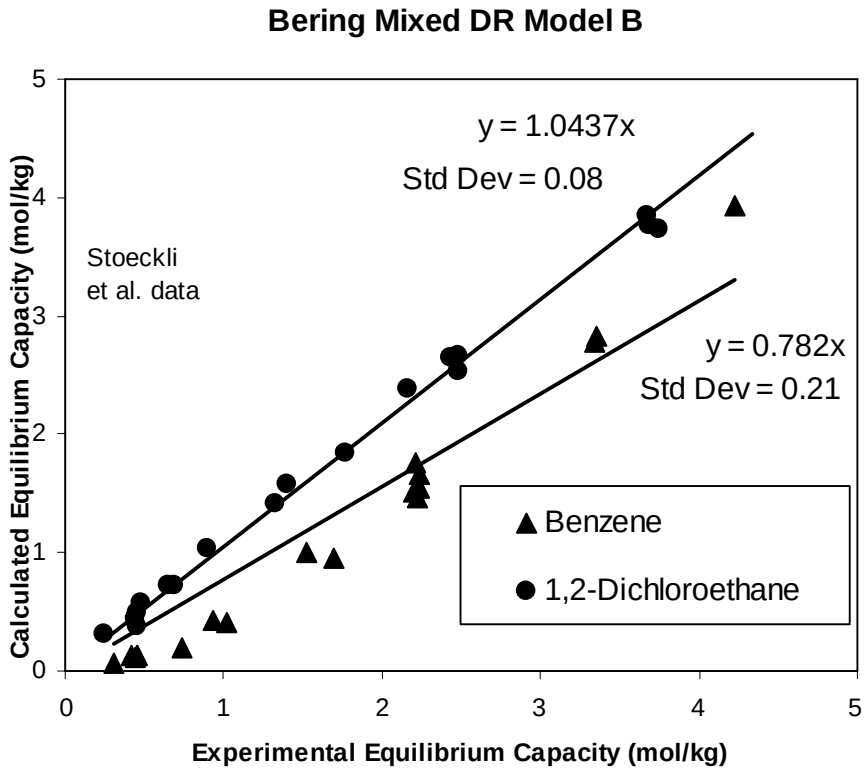

Figure 74. Results of applying a variant of the Mixed DR Model to equilibrium capacity data for mixtures of benzene and 1,2-dichloroethane [100].

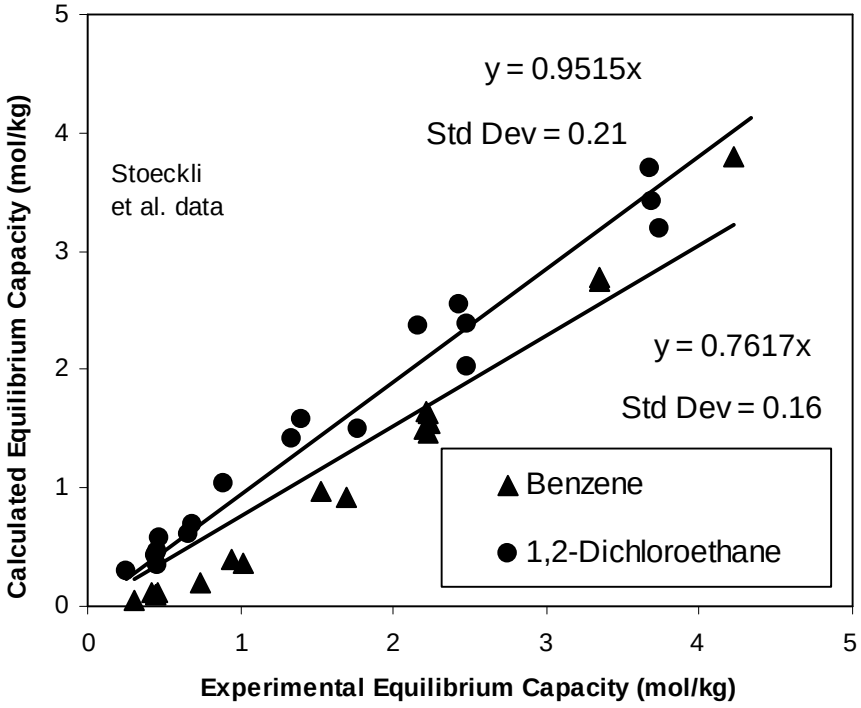

Figure 75. Results of applying a variant of the Mixed DR Model to equilibrium capacity data for mixtures of benzene and 1,2-dichloroethane [100].

E. Multicomponent Vapor Adsorption Kinetics

There are fewer theoretical models and experimental data concerning the kinetics (rates) of adsorption of mixtures of vapors onto sorbent beds from flowing air. Common observations include: a) The more weakly adsorbed vapor of a pair is the one whose ratio of capacity to concentration (in compatible units—molar, volumetric, or gravimetric) is the smallest. b) The more weakly adsorbed vapor 1 moves through the sorbent bed more rapidly than the more strongly adsorbed vapor 2. c) Vapor 2 displaces vapor 1 from the adsorbent to some extent, but not necessarily completely. c) This displacement can cause “rollover” or “overshoot”, in which concentration of vapor 1 downstream of the adsorption wavefront of vapor 2 can exceed the concentration of the vapor 1 entering the bed. d) The breakthrough curves of the individual mixture components have S- or sigmoidal-shapes similar to those observed for single vapors. e) Water vapor behaves differently than organic vapors on activated carbons.

Cooney and Strusi [106] defined five (distance into a sorbent bed) zones of vapor concentration in a sorbent bed with flowing binary mixture (Figure 76). Complete breakthrough curves for two components can also be defined by five (time) zones, since such curves are obtained from vapor concentration measurements at the bed exit as the adsorption pattern moves through the bed. These breakthrough curve zones are shown in Figure 77. The “rollover” effect ($C_1 > C_1^o$) due to displacement of vapor 1 by vapor 2 is seen in Zones II, III, and IV.

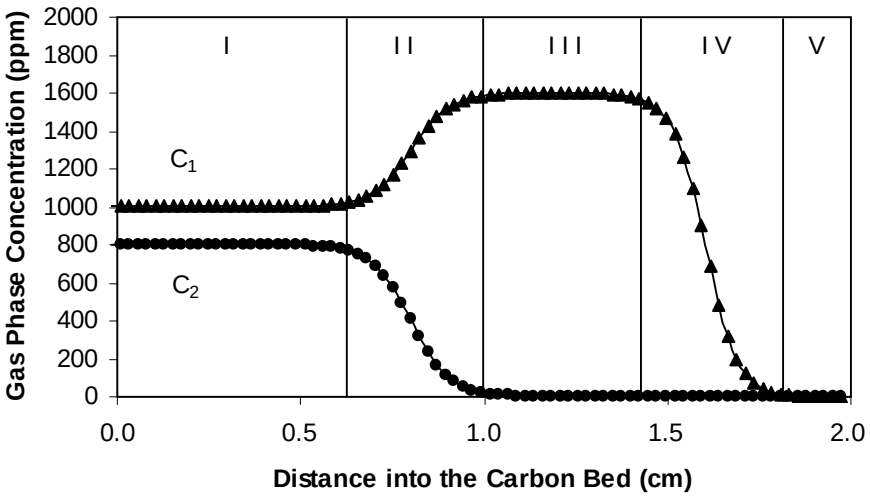

Figure 76. Zones of vapor concentrations C_1 and C_2 within a 2-cm deep carbon bed challenged with a mixture of two vapors. In Zone I the carbon is equilibrium saturated with both vapors. In Zone II Vapor 2 is adsorbing and displacing Vapor 1 from its saturated equilibrium. In Zone III Vapor 1 is at equilibrium at a higher (rollover) concentration than that entering the bed. In Zone IV Vapor 1 is adsorbing from this higher concentration without interference from Vapor 2.

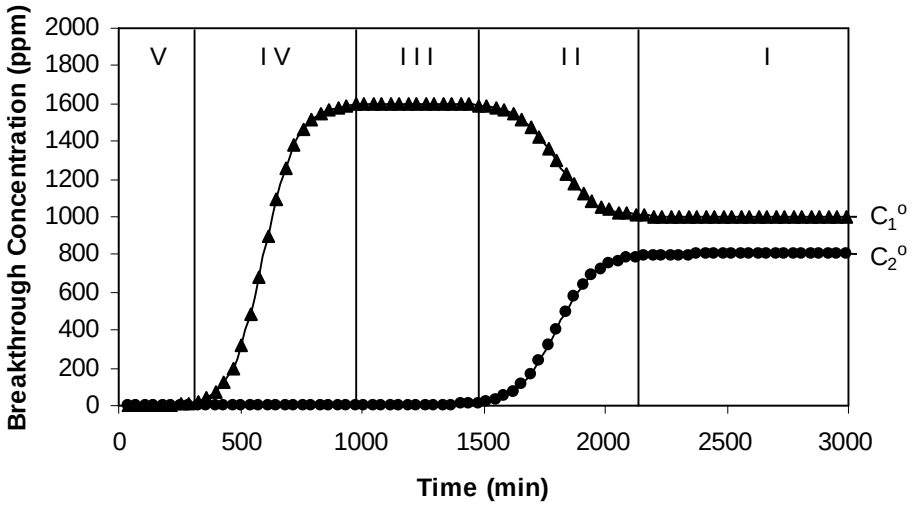

Figure 77. Zones of vapor concentrations in effluent (breakthrough curves) from a carbon bed challenged with a mixture of two vapors at concentrations C_1^o and C_2^o.

Yoon et al. [116-119] fit a Reaction Kinetic-type model to such multicomponent breakthrough curves for respirator cartridges:

$$\left(\frac{C}{C_o}\right)_i = \left[1 + \exp(k'_i\,(\tau_i - t)\right]^{-1} \qquad (91)$$

and extracted adsorption rate coefficients k'_i as well as breakthrough midpoints τ_i. The mixtures included acetone/m-xylene, acetone/cyclohexane/toluene, ethyl acetate/cyclohexane/toluene, cyclohexane/toluene/m-xylene, ethyl acetate/cyclohexane/toluene/m-xylene, and acetone/cyclohexane/toluene/m-xylene. For a binary mixture they concluded that the experimental adsorption rate coefficient of the more strongly adsorbed vapor, m-xylene, was unchanged by the presence of acetone. For acetone k'_1 was changed by m-xylene present, apparently due to displacement (affecting τ_1) and distortion (rollover) of the acetone breakthrough curve. However, when $k'_1\tau_1$ averages are compared (13.6 [Std Dev = 1.8] for the mixtures vs. 13.9 [Std Dev = 0.4] for the pure acetone data) there is no significant difference. For one ternary and one quaternary mixture the average $k'_1\tau_1$ for acetone was 14.9 $\pm$ 0.9, again not significantly different. Only in one case of overlapping acetone/m-xylene breakthrough curves was the $k'_1\tau_1$ for m-xylene reduced (13.9 vs 24.0 $\pm$ 2.2 for four other mixtures).

Jonas et al. [82] also saw no statistical differences between rate coefficients for components in mixtures and alone for carbon tetrachloride, chloroform, and benzene. Calculated k_i were referenced to carbon tetrachloride assuming inverse square dependence on molecular weight. Experimental rate coefficients were obtained from 1% breakthrough time vs. bed weight plots. Deviations of calculated values from experimental ones ranged from –30 to +27% with an average of +15%. Cohen et al. [85] reached the same conclusion that there was no significant difference, while acknowledging the inaccuracy of obtaining rate coefficients from breakthrough time plots. Thomas and Lombardi [107] in doing successful calculations for benzene/toluene mixtures assumed equivalent rate coefficients as for the pure vapors.

On the other hand, Zwiebel et al. [120] present good arguments why this assumption may not be valid. It assumes no component interactions and that the mechanism of adsorption is not affected by composition. Due to observed displacement, in some parts of the sorbent bed there is single-component adsorption, while in others there is simultaneous adsorption and desorption of different vapors. They showed experimentally with benzene/methylene chloride mixtures that the adsorption rate coefficients for the more weakly adsorbed methylene chloride in the mixture were close to those observed for methylene chloride alone. However, there was a big difference for benzene; k_2 was significantly smaller in the mixtures. From the graph shown for two carbons, it looks like the difference was not a consistent function of concentration, but averaged about 25 sec^{-1} (1500 min^{-1}).

Marutovsky and Bulow [121] pointed out that for *external* mass transfer, diffusion limiting cases, calculations show that diffusion interactions can be neglected. However, they did experimentally see interaction effects for pentane/heptane and hexane/ammonia gas mixtures on a zeolite. From this they concluded that the component whose relative adsorption proceeds faster retards the *internal* mass transfer of the other(s). This leads to the question of what is the mass transfer rate limiting step for an application of concern.

Robbins and Breysse [83] obtained results on the effects of second vapors (toluene, p-fluorotoluene, p-dichlorobenzene, or o-dichlorobenzene) on the measured adsorption rate coefficients for p-xylene or pyrrole. They reported some correlation of these effects with boiling point of the second vapor. This suggests that order of elution may have determined how (+ or – or not at all) rate coefficients were affected in the mixtures.

F. Models for Breakthrough Curves of Multicomponent Mixtures

Yoon, Lara et al. [116-119] produced a series of papers in which they show how to describe multicomponent breakthrough curves using capacity terms τ_i, rate coefficients k'_i, and

displacement parameters A_m. Displacement ratios and displacement fractions were also calculated. Since they obtained these parameters empirically from measured breakthrough curves, this was a descriptive (correlative) model, instead of a predictive one. With only a few parameters this model was able to well describe the breakthrough curves from which the values of these parameters were calculated.

A predictive multicomponent model would need to develop values for these parameters from independent sources, e.g., single and multiple component adsorption isotherms and rate coefficient models (discussed above).

Vahdat et al. [24] has taken just such an approach to transform the Yoon/Lara model into a predictive model. They used Langmuir single-component isotherm equations with the IAST mixture model. Rate coefficients were obtained from single-component breakthrough times at 0.001 and 0.999 breakthrough fractions, assuming a symmetric Wheeler/Reaction Kinetic model. We have transformed the steps they suggest for applying this model into a generic procedure in Table XIII.

Table XIII. A Generic Procedure for Predicting Breakthrough Curves and Times of Components of Binary Mixtures of Vapors from Vahdat et al. [24]

Step	Description	Comments
1	Choose an isotherm equation and obtain pure component parameters for it.	Vahdat et al. used the Langmuir equation
2	Use a multicomponent model to get capacities $W_{e\,i}$ for each component i at each concentration C_i.	Vahdat et al. used the Ideal Adsorbed Solution Theory Model with the easily integrated Langmuir isotherm equation.
3a	Obtain a rate coefficient k_{v2} for pure component 2 (the later eluting one).	Vahdat et al. obtained rate coefficients from breakthrough times at 0.001 and 0.999 breakthrough fractions. This assumes such times have been measured, that the breakthrough curve is symmetrical, and that the Reaction Kinetic form of the Wheeler equation applies.

3b	Calculate a breakthrough curve from k_{v2}, C_2, and W_{e2} and the selected breakthrough curve equation.	This assumes that W_{e2} is reduced from the single component capacity W^o_{e2}, but the rate coefficient is not affected by the first vapor. This will give breakthrough times for selected breakthrough fractions or concentrations of 2.
4a	Calculate the single component capacity W^o_{e1} of component 1 at C_1.	Use the selected single-component adsorption isotherm equation and parameters.
4b	Estimate the rollover (overflow) concentration C_1^{max} of component 1.	See Equations (92) and (93) and accompanying discussions in the text.
5	Calculate the single component 1 capacity W_{e1}^{max} at C_1^{max}	Use the selected single-component adsorption isotherm equation and parameters
6a	Obtain a rate coefficient k_{v1} for pure component 1.	See 3a and 3b comments above.
6b	Calculate a breakthrough curve from k_{v1}, C_1^{max}, W_{e1}^{max}, and the selected breakthrough curve equation.	See 3a and 3b comments above. This will give breakthrough times for selected breakthrough fractions or concentrations of component 1.
7-8	Reiterate this process to get a consistent value of C_1^{max}.	This is probably only necessary to get full breakthrough curves, but not if only breakthrough times at low breakthrough fractions are desired.

Vahdat et al. [24] also presented an equation for estimating C_1^{max}, the maximum rollover concentration of the first eluting component due to displacement by the second:

$$C_1^{max} = C_1 + \left(\frac{W_{e1}^{o} - W_{e1}}{W_{e2}} \right) C_2 \qquad (92)$$

This equation assumes displacement of one condensed volume by another (Volume Exclusion Model) and applies if the concentrations C_i and capacities W_{ei} are in gravimetric units (e.g., g/cm^3 and g/g, respectively). For C_i in molar or volumetric units (e.g., mol/L or ppm) this equation must include molecular weights M_{wi} :

$$C_1^{max} = C_1 + \left(\frac{W_{e1}^{o} - W_{e1}}{W_{e2}} \right) \left(\frac{M_{w2}}{M_{w1}} \right) C_2 \qquad (93)$$

Another type of model for breakthrough curve generation is numerical integration of equations including mass conservation, adsorption isotherms, and rate expressions. This is

beyond the scope of this report, but holds more promise for the future as desktop and portable computing power increases. An example of this approach is the work of Lavanchy and Stoeckli [88].

G. Discussion

1. Ease of Application of Capacity Models for Vapor Mixtures

Our experience with applying adsorption capacity models to data has led to some conclusions that may be relevant to their usefulness for estimating breakthrough times of components of vapor mixtures in air flowing through a packed carbon bed (e.g., a respirator cartridge). An order of increasing complexity and difficulty of application is given in Table XIV along with some comments.

Table XIV. Order of Increasing Difficulty of Application of Mixture Models

Difficult Category	Capacity Model	Comments
Direct Calculation	Molar Proportionality	
	Volume Exclusion	Requires liquid densities
	Ideal Lewis	Raoult's Law assumed
	Multicomponent Langmuir	Simplified version
	Multicomponent Freundlich	Simplified version
	Multicomponent John	
Iterative	Multicomponent DR	Combined with Lewis Eq.
	Greenbank-Manes	Inverse isotherm equation
	Grant-Manes	
Characteristic Curve Needed	Grant-Manes	Polanyi type
	Kisarov Combined L/F	
Second Isotherm Equation	Rudling/Sheindorf	Freundlich and Langmuir
Isotherm Integration	Ideal Adsorbed Solution Theory	May be circumvented by using an isotherm equation that can be integrated analytically
	Vacancy Solution Method	No such circumvention has been proposed due to complexity and empirical nature of isotherms

2. Second Equation Recommendation

Mixture capacity models based on single-component adsorption isotherms often require a second equation to solve for individual capacities. The two most popular are Raoult's Law, Equation (65), and the Lewis Equation (72). Comparisons of Reucroft et al. [84] showed molar proportionality gave best results 3.5 times more often than Lewis' equation (Table X). In the model comparisons in Table XIII the ideal Lewis Equation Method gave worse predictions than the Molar Proportionality Method for benzene, chlorobenzene, and 1,2-dichloroethane and only slightly better for carbon tetrachloride. Except for the original experiments and conditions, we have found no cases in which the Lewis equation consistently produced significantly better results than Raoult's Law. Until such is produced the former should be abandoned as a second equation in favor of the latter.

3. Mixture Capacity Model Results Compared

The best agreements of model predictions with experimental data are shown in Table XIII in bold print. The numbers in italics are within $\pm$ 10 % accuracy or $\leq$ 0.20 mol/kg Standard Deviation.

The model which had the most such "bests" (3) was the IAST/DR Model developed by the Swiss group [39, 100]. As shown in Tables X – XII, others have also found good precision with this model. The Grant-Manes Model also did consistently well (both accurate and precise) for chlorobenzene, benzene, and 1,2-dichloroethane. The Multicomponent DR models showed some success with benzene and 1,2-dichloroethane, but not with chlorobenzene or carbon tetrachloride. Doong and Yang [87] also found similar accuracies and precisions for the IAST and Grant-Manes Models (Table XII); but, Valenzuela and Myers [115] did not (Table XI).

None of the models did consistently well for carbon tetrachloride; the best precision was 0.28 mol/kg Standard Deviation with the Simplified Langmuir Model, which is surprising (and,

perhaps, coincidental) considering how poorly the data fit the Langmuir isotherm equation (Figure 42). Carbon tetrachloride has the largest molecular weight, greatest liquid density, and highest volatility of the four compounds studied; one or more of these parameters may be more important than the models account for.

4. OSHA Guidance for Mixtures

The Occupational Safety & Health Administration (OSHA) has provided guidance on factors that can reduce cartridge service life [122, 123]. The two guidance statements on accounting for multiple contaminants can be considered a "Rule-of-Thumb" model. Therefore, we have analyzed this guidance in light of the reviews of models and data given earlier in this report:

> "Where the individual compounds in the mixture have similar breakthrough times (i.e., within one order of magnitude), service life of the cartridge should be established assuming the mixture stream behaves as a pure system of the most rapidly migrating component or compound with the shortest breakthrough time (i.e., sum up the concentration of the components)." [122]

Comments on this statement:

1) This assumes complete displacement of one compound by another, which is not likely in most cases, but is a conservative assumption. However, displacement is not limited to vapors of similar volatilities ("i.e., within one order of magnitude"), so this direction could be misleading, particularly combined with the following statement (see below).

2) Adding the concentration of the displacing compound to that of the displaced one can be inaccurate if the wrong concentration units are used. Adding ppm, as specified in [123] implies mole-for-mole displacement. Since activated carbon is a volumetric adsorbent (Theory of Micropore Volume Filling), the displacement is more accurately condensed volume-for-condensed volume.

The ppm concentrations should be multiplied by their respective liquid molar volumes before adding them together; then the sum should be converted back to ppm by dividing by the molar volume of the displaced vapor.

3) It would be even more in error to add concentrations in g/m^3, since that implies gram-for-gram displacement. This has no physical or thermodynamic validity.

> "Where the individual compounds in the mixture vary by 2 orders of magnitude or greater, the service life may be based on the contaminant with the shortest breakthrough time." [122]

Comments on this statement:

1) Just because a second vapor is less volatile and has a much longer ("by 2 orders of magnitude or greater") breakthrough time does not mean it will not displace a much more volatile one. In fact, it is more likely to do so.
2) Ignoring the second vapor would be anti-conservative and overestimate the breakthrough time of the more volatile compound.

Perhaps this rule assumes the concentration of the much less volatile compound would be negligibly small; however, this assumption is not necessary.

IV. Models for Adsorption of Mixtures of Water and Organic Vapors (Humidity Effects)

A. Fundamentals

As with models for single vapors and mixtures of multiple organic vapors, models for adsorption of mixtures of organic vapors with water vapor (humidity) must include capacity and kinetic contribution parameters. No models have been found for directly calculating breakthrough times (service lives) of packed carbon beds through which organic vapors and high concentrations of water vapor are flowed (breathed). A few relative humidity "correction factors" for dry condition breakthrough times have been published, but these have very limited applicability. Therefore, to set the stage for developing good models for predicting breakthrough times at high humidities models of the effects on capacity and adsorption rate coefficients will be considered separately.

There are two situations that can be considered in developing humidity effect models from experimental data: 1) The cartridge or test carbon has been equilibrated (preconditioned, prehumidified, pre-equilibrated) with air at the humidity of the test. Or, 2) it is in its natural or prepared state equilibrated at a different humidity than the test. The first situation represents a worst-case application where the cartridge has been exposed (e.g., unsealed) to the use atmosphere before being used on a respirator. It is easier to handle theoretically, since presumably little or no water is added to or removed from the carbon during a test (or use). There is no temperature change due to water condensation or evaporation. However, the second situation is more realistic. In a properly controlled respirator program, it is likely that cartridges would be stored sealed from atmospheric humidity and used immediately upon unsealing. Testing or use without preconditioning at the test or use humidity can introduce complications, such as temperature changes or water loadings changing with time of use. These make modeling

more difficult.

Most studies of humidity effects (presence of water vapor) on adsorption capacities have been reported for equilibrium situations. Some have been tested against theoretical and correlation models. There are fewer studies of humidity effects on adsorption rates from flowing air and on breakthrough times.

B. Empirical and Correlation Models for High Humidity Capacities

The simplest model for the effect of relative humidity on adsorption capacity of an organic vapor is an empirical one proposed by Chou and Chiou [124]. Dry isotherms of cyclohexane and n-hexane were fit to Langmuir isotherm equations. At higher humidities these capacities were reduced according to the equation (in terms used previously in this report):

$$\frac{W_{e\,(RH)}}{W_{e\,(0\%RH)}} = 1 - k\,(RH)^{1/n} \qquad (94)$$

Empirical parameters k and n, tabulated for the two compounds at temperatures 33.6 – 76.4 ^{o}C, were functions of temperature and chemical. Fitting of published data for trichloroethylene, toluene, and benzene showed that these parameters are also functions of organic vapor concentrations. The value of n approached 0.5 at 30 ^{o}C. A difficulty with this equation is that such ratios can become negative at high humidities.

A second empirical model is that of Wood. [125,126] He developed and tested a model for relative humidity effects and vapor concentration effects on adsorption capacities of charcoal beds for vapors. It is a Langmuir/Freundlich-like equation with an empirical power function of relative humidity. It predicts that ratios of organic vapor capacities or breakthrough times at different humidities have the form:

$$\frac{t_{b\,(50\%RH)}}{t_{b\,(RH)}} = \frac{W_{e\,(50\%RH)}}{W_{e\,(RH)}} = 1 + k\,(RH)^{n} \qquad (95)$$

In this case n (experimental values 3.6 – 8.4) is interpreted as the average number of water molecules clustered in the adsorbed phase. He applied it to both preconditioned bed data (including Jonas et al. [127]) and dry bed data (including Werner [128] and Nelson et al. [69]) to yield linear plots of relative breakthrough times or inverse capacities. Slopes are functions of the adsorbate, as shown in Figure 78 for data of Nelson for four chemicals.

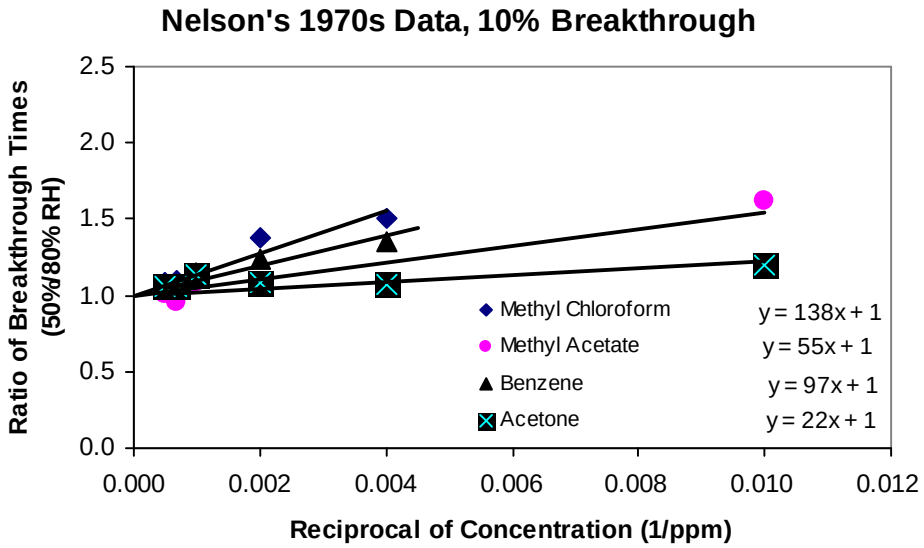

Figure 78. Ratios of 10% breakthrough times at two humidities as a reciprocal function of concentration.

Figure 79 shows that these ratios are not functions of breakthrough fractions, at least for 10 – 50% breakthrough. Since these slopes have not been related to independently obtainable properties, this is only a correlation method, not a predictive model. It can be used to interpolate or extrapolate capacity data at different relative humidities. Breakthrough time correction factors calculated from data fits and Equation (95) should also be functions of concentration and chemical vapor.

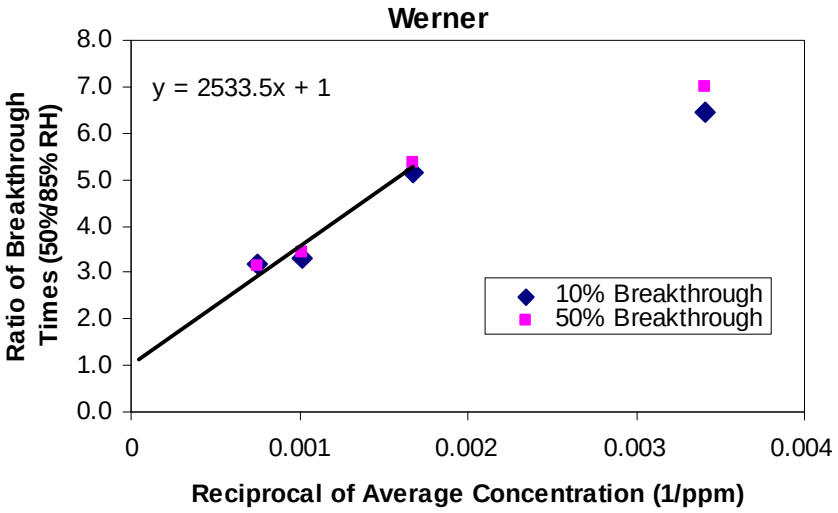

Figure 79. Ratios of breakthrough times at two humidities and two breakthrough percents as a reciprocal function of concentration.

Cohen et al. [129] applied this method of Wood to data from respirator cartridges and respirator carbon tubes (RCTs) containing the same carbon. Inverse relative (to 50% RH) breakthrough times for both coincided on the same straight line with n = 3.8 as the power of RH. In this case Cohen et al. used the method to demonstrate equivalent humidity effects for the RCTs and the cartridges.

Underhill [130] used the Polanyi concept of adsorption potential to correct the adsorption potential of a water-immiscible organic vapor for the presence of water vapor in air and condensed water in micropores. Complete equilibrium and a linear interpolation between dry and 100% RH conditions were assumed. The method gets values of two empirical parameters from iterative fits of data. When this corrected adsorption potential was put into the DR equation, he could reproduce the adsorption capacities of trichloroethylene measured by Werner [128]. This worked even though the Werner experiments likely were not at water equilibrium. Kawar and Underhill [131] extended this approach to water-miscible organic compounds in water-saturated air (100 % RH). The inclusion of activity coefficients “often available” adds complexity and

limits general applicability of the model for predictive purposes.

Yoon and Nelson [17] derived equations for describing asymmetrical organic vapor breakthrough curves that are often observed at high humidities. They took the organic vapor saturation capacity to be increasing linearly with time of exposure of an initially dry carbon bed to humid flowing air:

$$W_e = W_b\, t + W_{ab} \qquad (96)$$

where W_{ab} is the initial capacity. The breakthrough curve equation as a function of time t was:

$$Co/C = 1 - \exp[A - k'' \ln(W_a + t)] \qquad (97)$$

where the empirical constant $W_a < t$; A and k" are also fit parameters. Since no physical meanings can be assigned to these parameters, no correlations with vapor or carbon properties can be made. This model is correlative, but cannot be use predictively. In a later paper Yoon and Nelson [132] applied the Reaction Kinetic-type equation they had used earlier for 50% RH breakthrough curves to those at dry, 24%, 50%, and 80% RH. Curve midpoints (capacities) for 250 – 2000 ppm benzene and methyl chloroform were fit to the Freundlich isotherm equation. Up to and including 50% RH the two Freundlich parameters for each vapor were consistent; at 80% RH they were both significantly reduced.

Jonas [127] and Hall [133, 134] have reported no significant effects at all of high humidities (13-95% RH and 0-90% RH, respectively) on capacities and breakthrough times of dry carbon beds. These observations are due to the high concentrations of organic vapors they used: 22500 ppm chloroform by Jonas and 14600 ppm carbon tetrachloride, 6300 ppm 1,1,1-trichloroethane, 7800 ppm trichloroethylene, and 7600 ppm propanol by Hall. At such high concentrations the adsorption potential of the organic vapor so greatly exceeds that of water, that adsorbed water vapor is displaced or never adsorbed. These concentrations are much higher than would be encountered in air-purifying respirator applications.

C. Predictive Models for High Humidity Capacities

Okazaki et al [135] developed a capacity prediction model that sums up the amounts of organic vapor in three proposed phases:

$$W_e = W_{e(\text{dry surfaces})} + W_{e(\text{dissolved})} + W_{e(\text{wet surfaces})} \qquad (98)$$

They used Freundlich isotherm equations for dry (0% RH) and humid (59 – 90% RH) capacity correlations. The major disadvantage of this method is that it requires a great deal of thermodynamic and physical information for input, including: 1) single component vapor/solid isotherms; 2) single component liquid (aqueous) phase/solid isotherms; 3) vapor/liquid equilibrium data; and 4) pore volume and surface area distributions of the carbon.

Lodewyckx and Vansant [136] developed a semi empirical model based on extensive measurements of water adsorption and partial breakthrough curves with seven vapors on four activated carbons. It assumes that the effect of adsorbed water is to reduce the capacity for organic vapors (Volume Exclusion Model). However, water vapor can be added or taken off the adsorbent from flowing air. The organic vapor can also displace water vapor. The reduced micropore volume is:

$$W_o' = W_o - W_{(\text{preequilibrated})} - \Delta W_{(\text{adsorbed})} + \Delta W_{(\text{displaced})} \qquad (99)$$

Water adsorbed from air of a different humidity than that of preequilibration is calculated by integrating an empirical correlation up to the breakthrough time t_b:

$$\Delta W_{(\text{adsorbed})} = \int_0^{t_b} \frac{\Delta A_{tot}}{t_b}\left(1 - \exp\left[-\frac{0.00005\, T\, v_L\, t}{z\sqrt{|\Delta A_{tot}|}}\right]\right) dt \qquad (100)$$

where ΔA_{tot} (g/g) is the difference (+ or -) between two water capacities at different RH obtained from a water isotherm plot or equation. Temperature T is in ^oC, linear velocity v_L is in cm/s, bed depth z is in cm, and time is in min. For equilibrium or same humidity applications this

term is zero. Another empirical relationship was found for calculating the amount of adsorbed water displaced by an organic vapor:

$$\Delta W_{(displaced)} = (W_{(preequilibrated)} + \Delta W_{(adsorbed)})[1 - \log_{10}\left(\frac{C_{H20} + C}{C}\right)\log_{10}\left(\frac{p_{sat} + p_{satH20}}{p_{satH20}}\right)] \qquad (101)$$
$$= 0 \quad \text{if negative.}$$

where C is concentration in ppm and p_{sat} is saturation vapor pressure of the organic vapor. The reduced micropore volume calculated by Equations (99)-(101) can be put into an isotherm equation, such as the DR, and used to calculated a reduced capacity in the presence of water vapor. This reduced capacity and a reduced rate coefficient (see later discussion) can be put into a breakthrough curve equation, such as the Reaction Kinetic form of the Wheeler, to calculate a reduced breakthrough time.

The IAST Model of Myers and Prausnitz [92] has been discussed in the section on organic vapor mixtures. It equates spreading pressures of the mixture components. Since water and organic vapor isotherms are so different, it may not be possible to use the analytical solution developed by Lavanchy et al. [39] to avoid integrations from zero pressure. Also, since it was developed for ideal solutions (miscible components), how well would it do for immiscible or partly miscible components?

The Polanyi Adsorption Potential Model further developed by Grant and Manes [90] for mixtures of organic vapors (see previous discussion) has also been applied for immiscible mixtures containing water vapor [137, 138]. Grant et al. [138] applied a 0.4 multiplier to the molar volume of water to coalesce its Polanyi plot with organic vapors. Affinity coefficients for water and organic vapors (see previous tabulations and correlations) may accomplish the same. A difficulty with this method is that it requires an iterative solution that may not easily or always

converge [139].

Doong and Yang [139] published a potential theory-based method for water/organic vapor mixtures. It is a Volume Exclusion Model (fixed total pore volume) with a DR equation containing an additional hysteresis term $(\ln h_0)^2$ attributed to transitional pores. Water, benzene, acetone, toluene, and methanol adsorption capacity data of Okazaki et al. [135] were fit to this isotherm equation to obtain single component hysteresis terms and affinity coefficients. For two different carbons and water vapor the hysteresis terms were zero and the affinity coefficients were 0.063 and 0.059. They took activity coefficients for the organic vapors and for water at RH > 60% to be unity. The mixture data of Okazaki et al. covered the range 59 – 90% RH. An equation was given (but apparently not used) to calculate water activity coefficients below 60% RH, but this is the region of lesser interest for RH effects. With activity coefficients set to unity Doong and Yang's equations for adsorbed volumes of components 1 and 2 become:

$$W_1 = (W_o - W_2)\exp\left\{-\left(\frac{R\,T}{\beta_1 E_o}\right)^2\left[\left(\ln\frac{p_{sat1}}{p_1}\right)^2 - \left(\frac{\ln h_{01}}{1-\frac{p_2^{\,o}}{p_{sat2}}}\right)^2\right]\right\} \quad (102)$$

$$W_2 = (W_o - W_1)\exp\left\{-\left(\frac{R\,T}{\beta_2 E_o}\right)^2\left[\left(\ln\frac{p_{sat2}}{p2}\right)^2 - \left(\frac{\ln h_{02}}{1-\frac{p_1^{\,o}}{p_{sat1}}}\right)^2\right]\right\} \quad (103)$$

where $p_2^{\,o}$ is the pressure calculated from the pure component 2 isotherm for volume adsorbed v_2; $p_1^{\,o}$ is obtained similarly. These equations are nonlinear and coupled; Doong and Yang solved them by an iterative procedure. Huggahali and Fair [140] decoupled these equations, but this did not eliminate the need for iteration. These equations "blow up" for some values of $p_i^{\,o}/p_{sati}$

approaching unity. This model adds another empirical parameter to the isotherm equations; however, we noticed that using the affinity coefficients and nonzero values of $(\ln h_0)^2$ for organic vapors listed by Doong and Yang: $\ln h_0 = (1.735 \pm 0.010)\,\beta$. (104)

D. Predictive Models for High Humidity Rate Coefficients

Lodewyckx et al. [141] also examined the influence of humidity on the overall mass transfer coefficient. Organic vapor concentrations were kept at 5 g/m^3. The Reaction Kinetic form [Equation (1)] of the Wheeler-Jonas Equation (5), was applied to measured 0.1% and 1% breakthrough times to calculate capacities W_e and rate coefficients k_v. Unlike capacities, they found very little influence of the nature of the organic vapor on the decrease of k_v with increasing relative humidity. The ratio of the amount of water present in the carbon pore system A_{tot} to the total pore volume, TPV, was the important parameter in determining the corrected adsorption rate coefficent, k_v' :

$$k_v' = k_v (1 - A_{tot} / TPV) \quad (105)$$

The TPV is the sum of the micropore, mesopore, and smaller macropore volumes; it can be determined by the total volume of liquid nitrogen adsorption. The A_{tot} is the sum of preadsorbed water (determined from the isotherm) plus water adsorbed from (or minus that desorbed into) the flowing air stream (determined by Equation (100) above). The effects of both carbon pre-humidification and air humidity are taken into account by this model. While the model did not predict measured rate coefficients exactly, it did account for observed trends. Uncertainties in experimental breakthrough times are amplified in calculations of experimental rate coefficients.

These humidity and preadsorbed water effects on rate coefficients can be applied as corrections to rate coefficients measured or calculated at dry (up to 50 % RH) conditions. The corrected values would then be used in a breakthrough equation, such as Equation (1). A requirement (disadvantage) of the Lodewyckx model is the need to have an adsorption isotherm

for water on the carbon of interest. This isotherm can, itself, be changing with time [142].

The only other quantitative model found for humidity effects on adsorption rate coefficients was from the work of Hall et al. [133, 134]. Rate coefficients calculated from partial breakthrough curves (0.5 to 4 breakthrough %) and the Wheeler Equation (5) were plotted against RH. Test humidities were kept the same as preequilibration humidities. The conclusions were 1) no effect of RH on k_v below 50% RH; 2) apparent linear decrease in k_v with RH above 50%RH; and 3) different rates of decrease for different compounds. These results can be expressed as an equation:

$$k_v\ (min^{-1}) = a - b\ (\%RH-50) \quad \text{for RH} \geq 50\% \qquad (106)$$

Parameter values from Hall's dissertation [134] are listed in Table XV. Propanol, the only water-soluble compound of the four, had a much lower rate of decrease (b/a) with increasing RH.

Table XV. Empirical Parameters for RH Effects on Adsorption Rate Coefficients [134].

Compound	Conc (ppm)	a	b	b/a
Carbon Tetrachloride	14600	6530	64	0.0098
1,1,1-Trichloroethane	6300	7930	63	0.0079
Trichloroethylene	7800	8090	74	0.0091
Propanol	7600	3700	7	0.0019

E. Candidate Databases for Model Comparisons

The most cited study of relative humidity effects on organic vapor respirator service lives is that of Nelson et al. [69]. Seven vapors were studied at 20 – 90% relative humidity (RH), 1000 ppm challenge concentration, and 53.3 L/min flow through either of two commercial cartridges. Both preconditioning humidity and test air humidity were varied. From their results the authors prepared a "Breakthrough Time Correction Factor" table, normalized to 50% preconditioning and use humidity. That table is reproduced here as Table XVI.

Table XVI. Breakthrough Time Correction Factors of Nelson et al. [69]

At various humidities and 1000 ppm, 53.3 liters/min, and 22 ^{o} for a pair of cartridges containing coconut or petroleum base carbon. The data was normalized to the 50% preconditioning and test relative humidity. The footnotes indicate the test vapor employed and the carbon type. The number in parentheses is the standard deviation.

TEST RELATIVE HUMIDITY	BREAKTHROUGH TIME MULTIPLIER PRECONDITIONING RELATIVE HUMIDITY (%)					
(%)	0	20	50	65	80	90
0	0.94 (0.08)[a,b]	0.95 (0.04)[a-c]	0.99 (0.07)[a-c]	0.97 (estimated)	0.95 (0.07)[a-c]	0.95 (-----)[a]
20	1.02 (0.06)[a,b]	1.02 (0.03)[a,b,d-g]	1.03 (0.04)[a,b,d-g]	1.04 (0.03)[d-g]	1.01 (0.05)[a,b,d-g]	1.00 (0.05)[a,d-g]
50	0.98 (0.07)[a-c]	0.99 (0.03)[a,d,b-g]	1.00 (0.05)[a-g]	0.99 (0.04)[d-g]	0.95 (0.08)[a-g]	0.77 (0.20)[a,c-g]
65	0.97 (0.04)[a,b]	0.98 (0.04)[a,b,d-g]	0.99 (0.05)[a,b,d-g]	0.94 (0.04)[d-g]	0.84 (0.10)[a,b,d-g]	0.66 (0.25)[a,d-g]
80	0.87 (0.06)[a-c,e]	0.91 (0.05)[a,b,d-g]	0.88 (0.04)[a-g]	0.83 (0.09)[d-g]	0.72 (0.16)[a-g]	0.50 (0.27)[a,c-g]
90	0.84 (0.03)[a,b,c]	0.85 (0.04)[a,b,d-g]	0.83 (0.06)[a,b,d-g]	0.78 (0.09)[d-g]	0.67 (0.13)[a,b,d-g]	0.48 (0.20)[a,d-g]

[a] Isopropanol, coconut base.
[b] Hexane, coconut base.
[c] Benzene, petroleum base.
[d] Acetone, petroleum base.
[e] Carbon tetrachloride, coconut base.
[f] 1-Chlorobutane, coconut base.
[g] Ethyl acetate, petroleum base.

Four conclusions were presented, based on these results:

1. Both the preconditioning and use humidity alter the cartridge service life.
2. The use humidity has a greater effect than the preconditioning humidity.
3. Service life is approximately the same between 0 and 50% humidity.
4. Humidity has a greater effect on cartridge performance at lower concentrations.

While this table does not provide an equation model, in the absence of other options these factors have been used for applications. Unfortunately, the vapor concentration effect (conclusion 4) is often ignored.

Another set of relative humidity effect data often cited is the work of Werner [128] with trichloroethylene on dry carbon test beds. Both concentration (300 – 1300 ppm) and relative humidity (5 – 85%) were varied. Table XVII lists 10% breakthrough times relative to 50% RH

we have calculated from this data for 4 vapor concentrations. Reduction of breakthrough time was greatest at the highest humidity and the lowest vapor concentration. Unlike Nelson et al. [69], Werner observed relative humidity effects even below 50% RH; however, this can be attributed to his using very dry carbon, reactivated before use. In actual cartridge applications the carbon would have some water content (e.g., corresponding to 20% RH equilibration).

Table XVII. Relative Breakthrough Times of Trichloroethylene at Various Humidities and Vapor Concentrations Calculated from Werner's [128] Results.

TCE Influent Conc. (mg/m^3)	Relative Humidity 5	25	50	65	85
	Relative Breakthrough Times				
300	1.72	1.16	1.00	0.55	0.16
600	1.30	1.06	1.00	0.49	0.19
1000	1.25	1.16	1.00	0.60	0.30
1300	1.20	1.05	1.00	0.61	0.33

The set of data selected for testing water vapor effects on adsorption capacities was that of Okazaki et al. [135] previously mentioned. They give single vapor isotherm (30 ^oC) data for four organic compounds and water. Plus they give individual experimental component capacities and pressures for mixtures of each organic vapor with water vapor. The experimental data covers useful ranges of relative humidity (59 – 90% RH) and organic vapor pressures (49 - 44447 ppm). Doong and Yang [139], as already mentioned, fit the isotherm data to an extended DR equation and listed the appropriate parameter values. The only value they did not give was the carbon structural constant B. We have calculated from Okazaki's pure benzene data an average value for $B = 0.0119/R^2T^2$ $(= 1/E_o^2)$. This dataset includes two water-miscible compounds (methanol and acetone) and two water-immiscible compounds (benzene and toluene).

F. Comparisons of Selected Humidity Effect Models

Okazaki et al. [135] applied their model to predict the four organic vapor and water equilibrium capacities they measured experimentally for high humidity adsorption on two activated carbons. Doong and Yang [139] used the same pure component organic vapor and water isotherm data fit to an extended DR equation to predict these capacities using: a) their (Doong-Yang) model, b) the IAST model, and c) the Grant-Manes adsorption potential model. We have applied the same isotherm data and equations using the Lodewyckx-Vansant and Chou-Chiou capacity models for mixtures including water.

Model predicted capacities of the organic vapors applying these six models are plotted against experimental capacities in Figures 80 - 107. For the second carbon (HGI-780) only the Okazaki and Doong-Yang models were used for acetone and methanol (only). In these figures and in Table IXX we list average accuracies and precisions of the model predictions. Accuracies are the zero-intercept trend lines (minimized least squares deviations of calculated values from experimental ones). The precision (scatter around the trend lines) is calculated as the standard deviation of the deviations of the experimental values from the calculated ones.

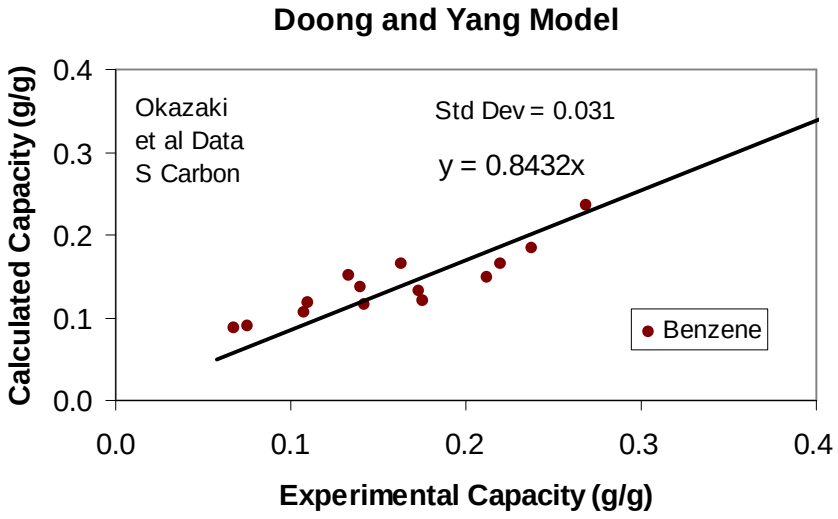

Figure 80. Comparison of Doong-Yang Model calculations for water covapor effects on benzene capacity with experimental data [135].

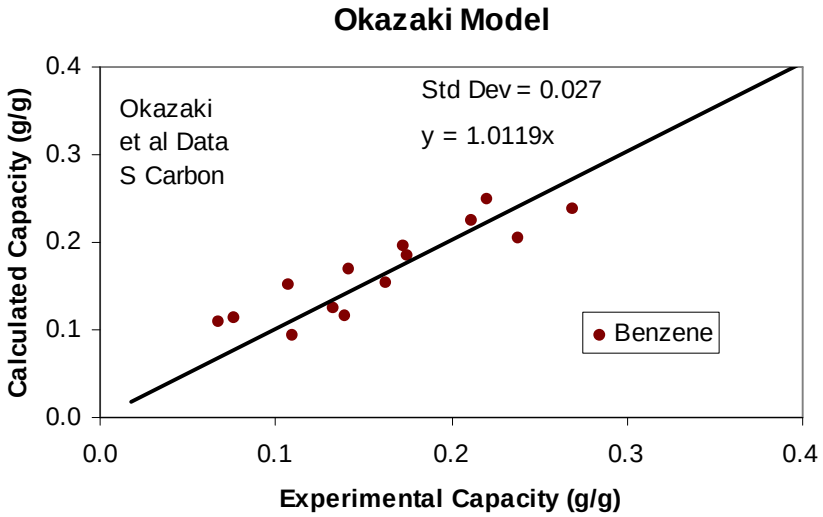

Figure 81. Comparison of Okazaki Model calculations for water covapor effects on benzene capacity with experimental data [135].

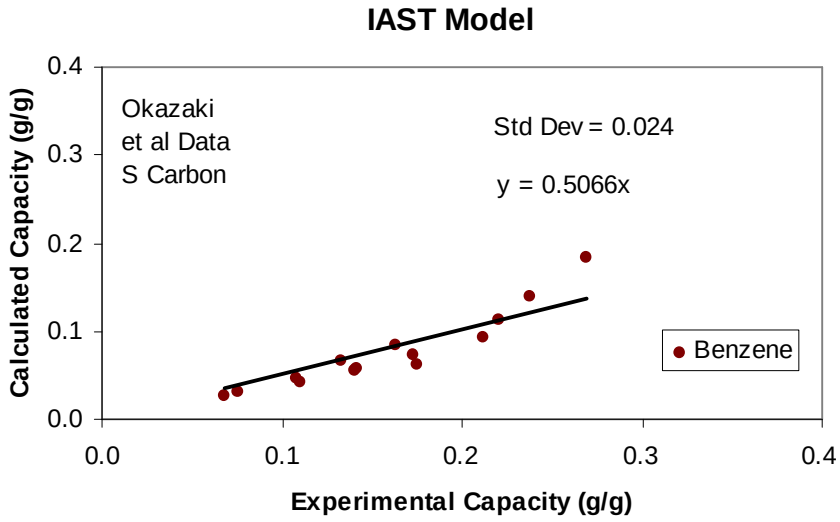

Figure 82. Comparison of Ideal Adsorbed Solution Theory Model calculations for water covapor effects on benzene capacity with experimental data [135].

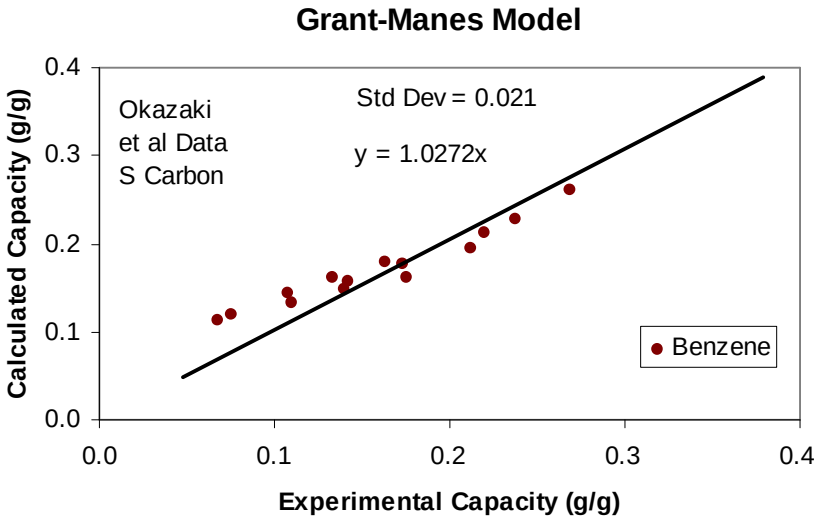

Figure 83. Comparison of Grant-Manes Model calculations for water covapor effects on benzene capacity with experimental data [135].

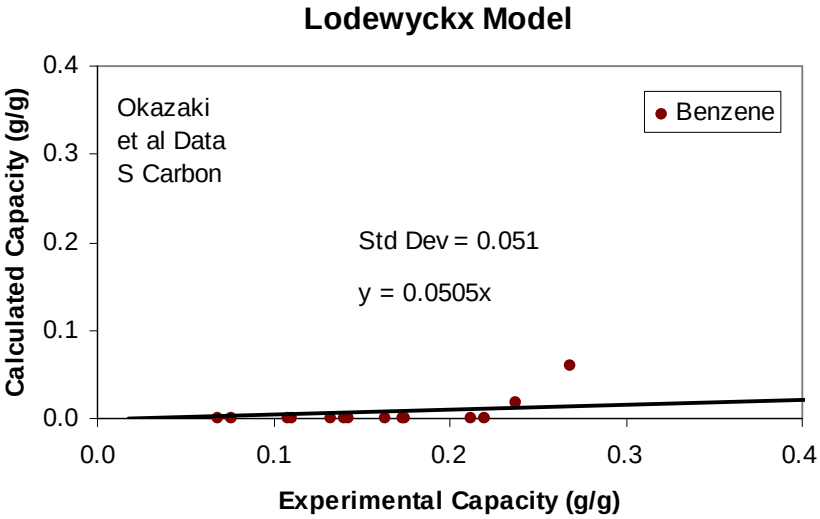

Figure 84. Comparison of Lodewyckx Model calculations for water covapor effects on benzene capacity with experimental data [135].

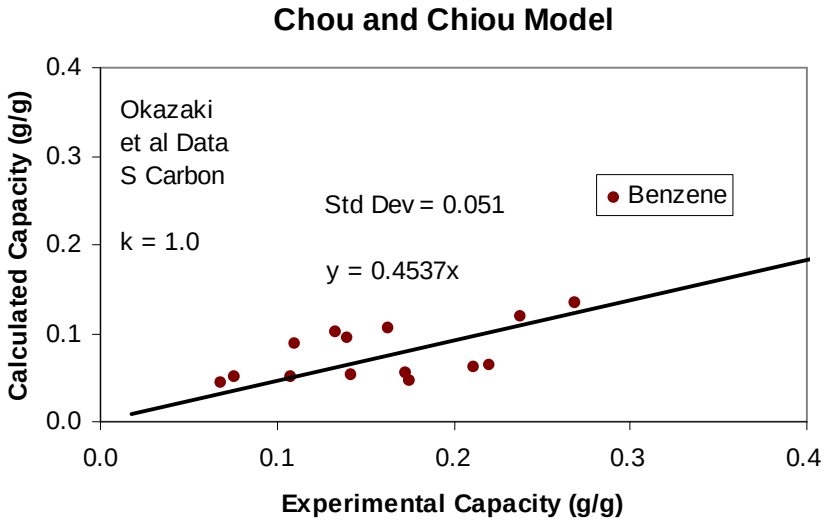

Figure 85. Comparison of Chou and Chiou Model calculations for water covapor effects on benzene capacity with experimental data [135].

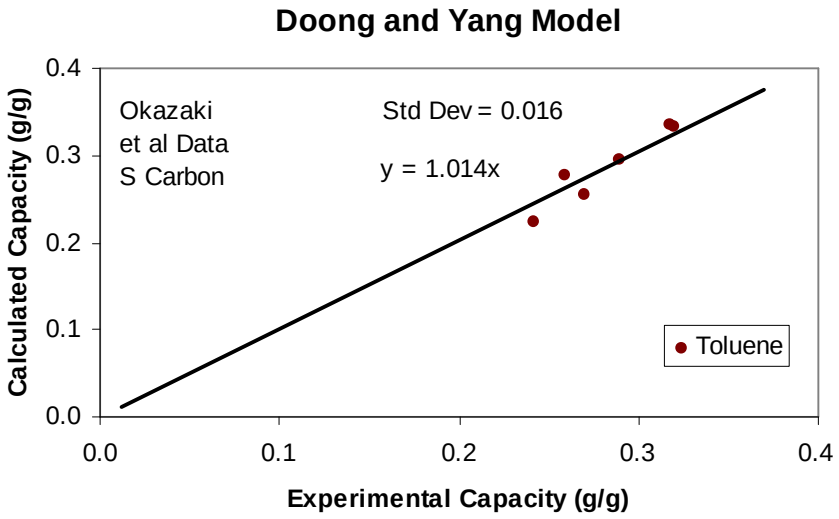

Figure 86. Comparison of Doong-Yang Model calculations for water covapor effects on toluene capacity with experimental data [135].

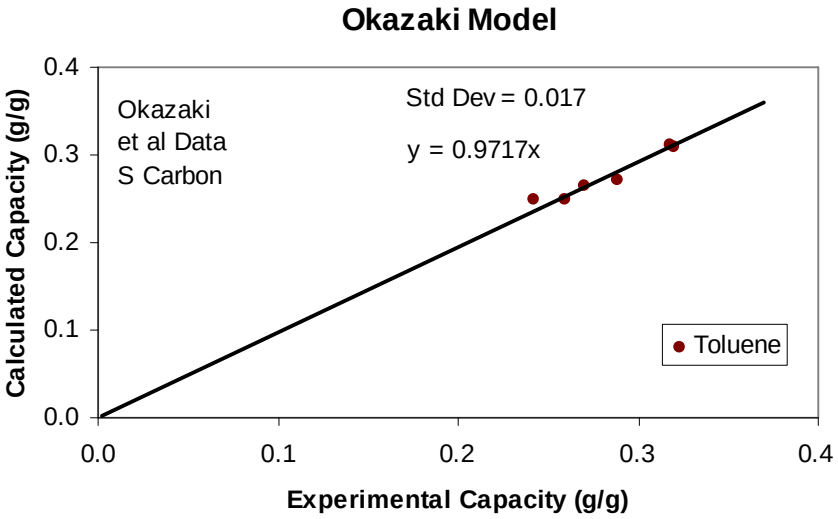

Figure 87. Comparison of Okazaki Model calculations for water covapor effects on toluene capacity with experimental data [135].

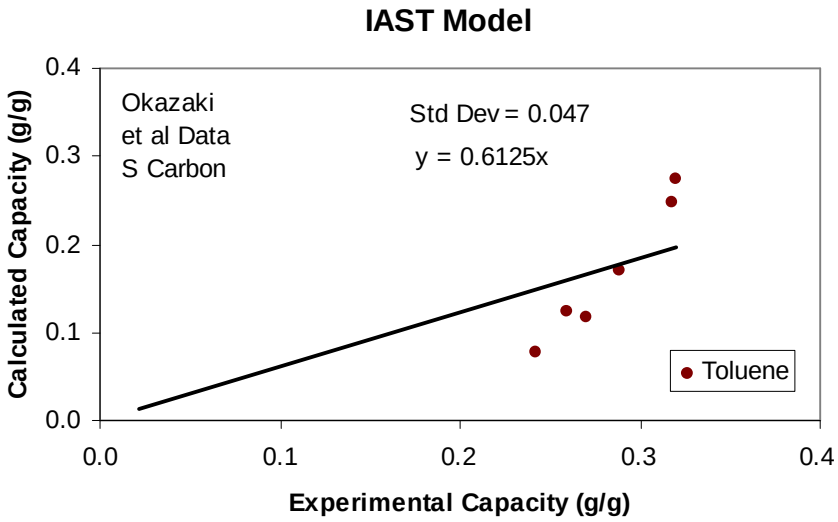

Figure 88. Comparison of Ideal Adsorbed Solution Theory Model calculations for water covapor effects on toluene capacity with experimental data [135].

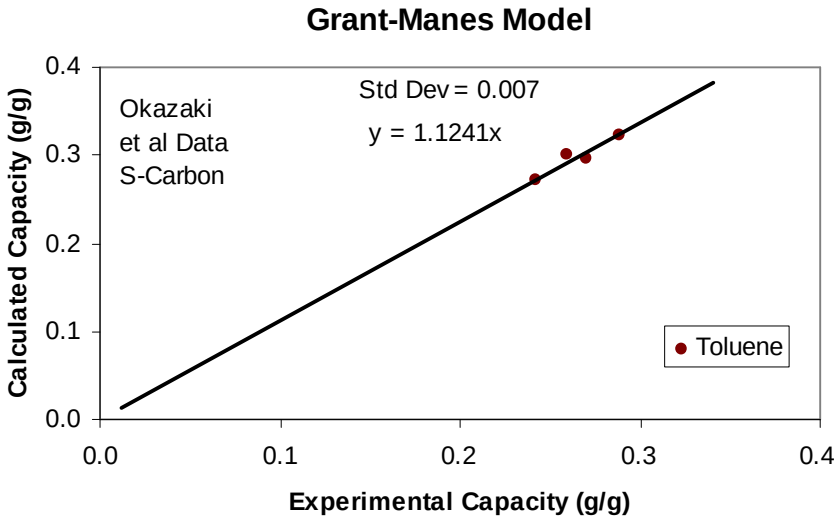

Figure 89. Comparison of Grant-Manes Model calculations for water covapor effects on toluene capacity with experimental data [135].

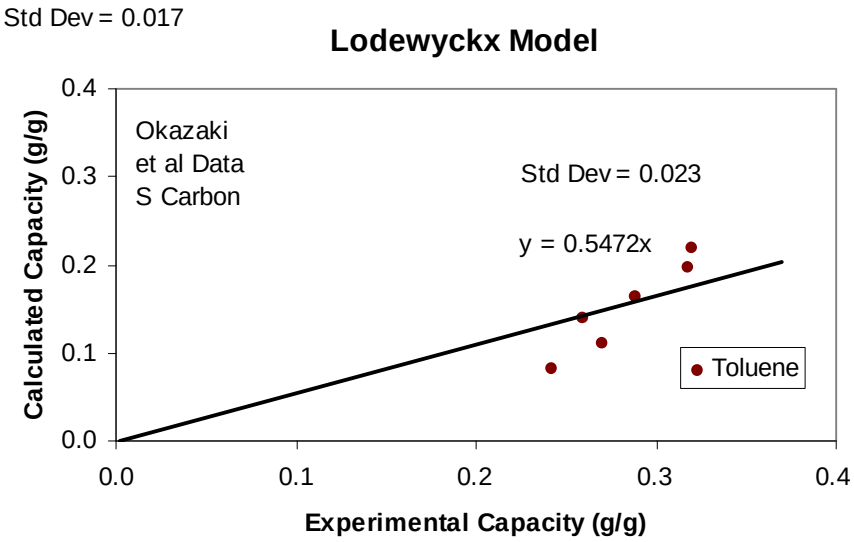

Figure 90. Comparison of Lodewyckx Model calculations for water covapor effects on toluene capacity with experimental data [135].

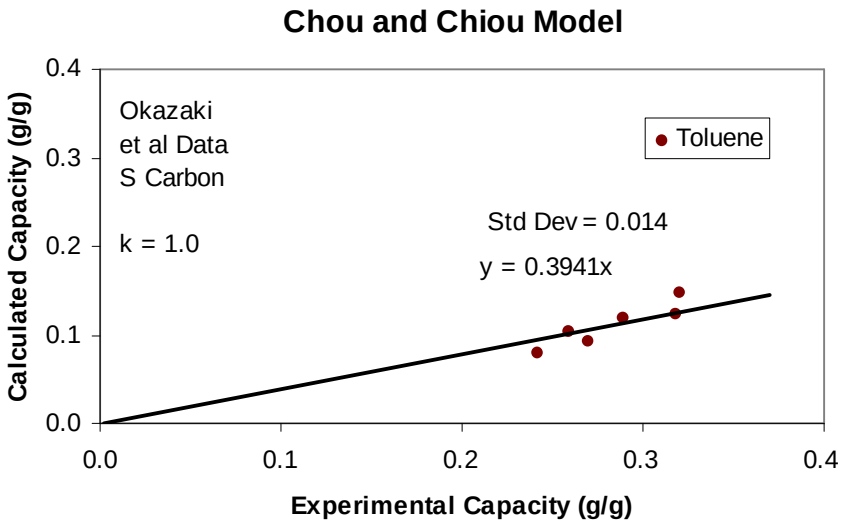

Figure 91. Comparison of Chou and Chiou Model calculations for water covapor effects on toluene capacity with experimental data [135].

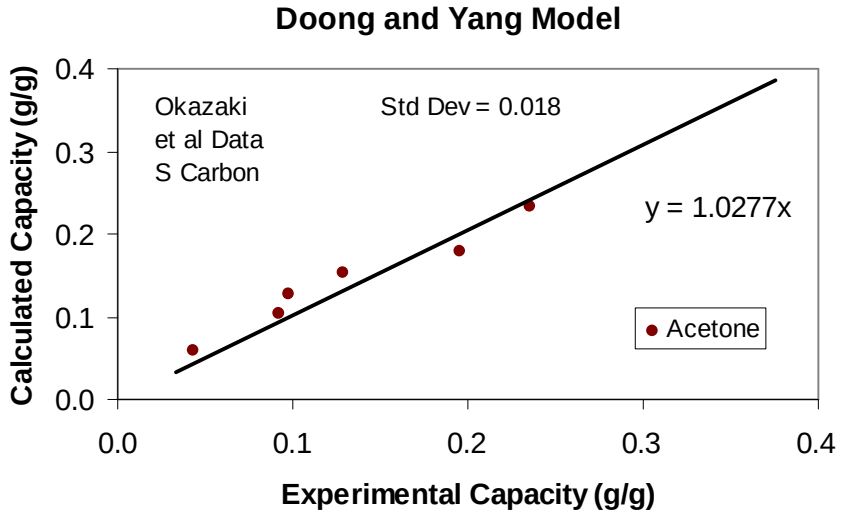

Figure 92. Comparison of Doong-Yang Model calculations for water covapor effects on acetone capacity with experimental data [135].

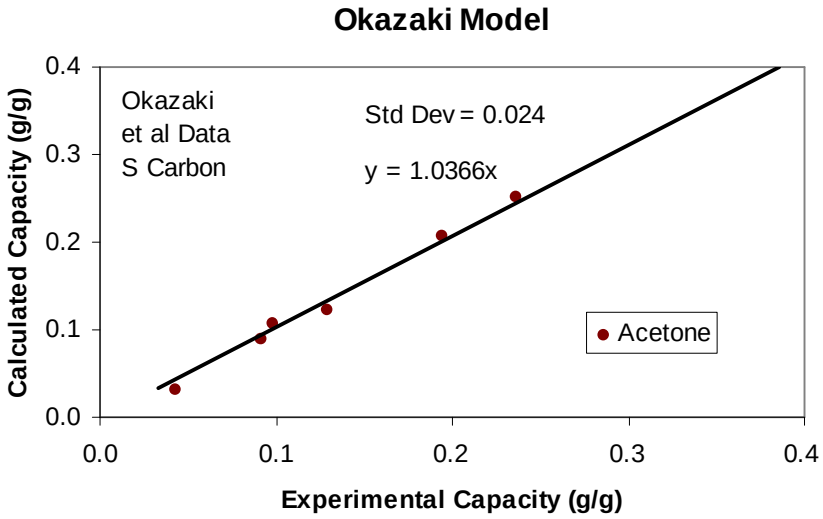

Figure 93. Comparison of Okazaki Model calculations for water covapor effects on acetone capacity with experimental data [135].

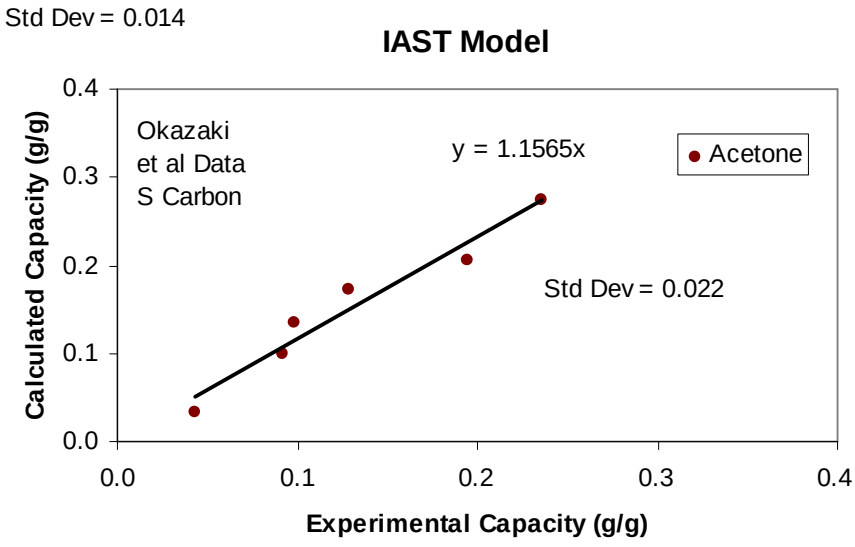

Figure 94. Comparison of Ideal Adsorbed Solution Theory Model calculations for water covapor effects on acetone capacity with experimental data [135].

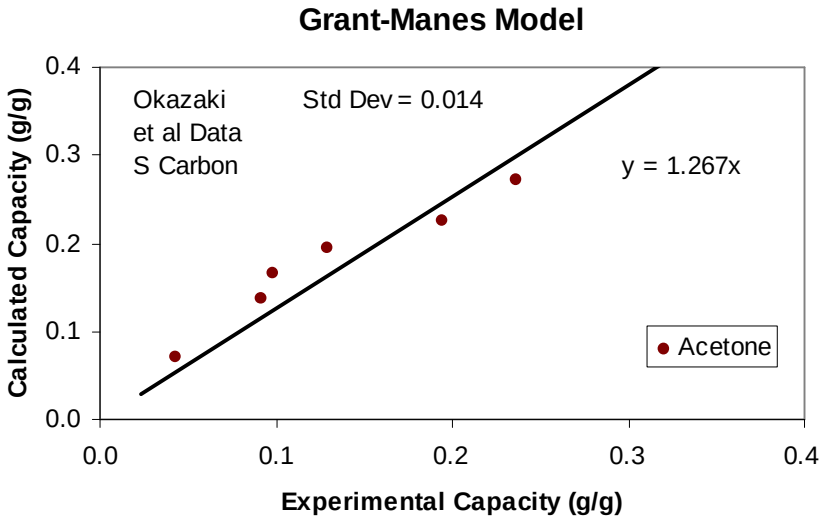

Figure 95. Comparison of Grant-Manes Model calculations for water covapor effects on acetone capacity with experimental data [135].

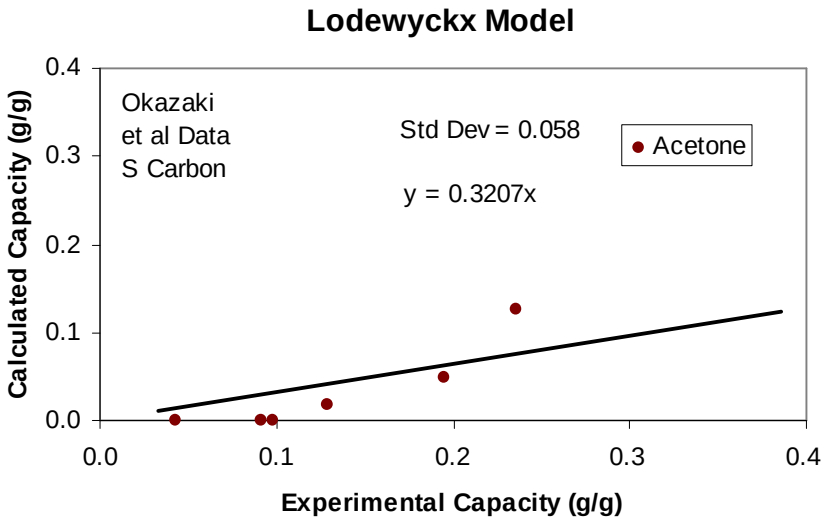

Figure 96. Comparison of Lodewyckx Model calculations for water covapor effects on acetone capacity with experimental data [135].

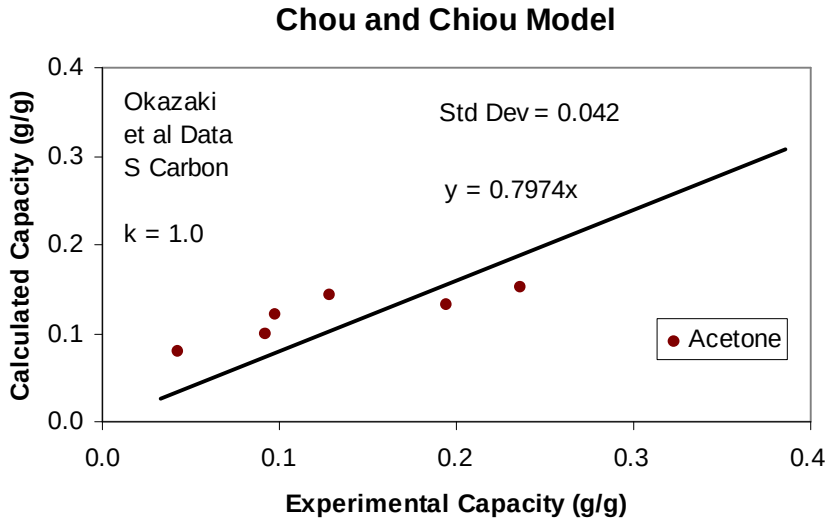

Figure 97. Comparison of Chou and Chiou Model calculations for water covapor effects on acetone capacity with experimental data [135].

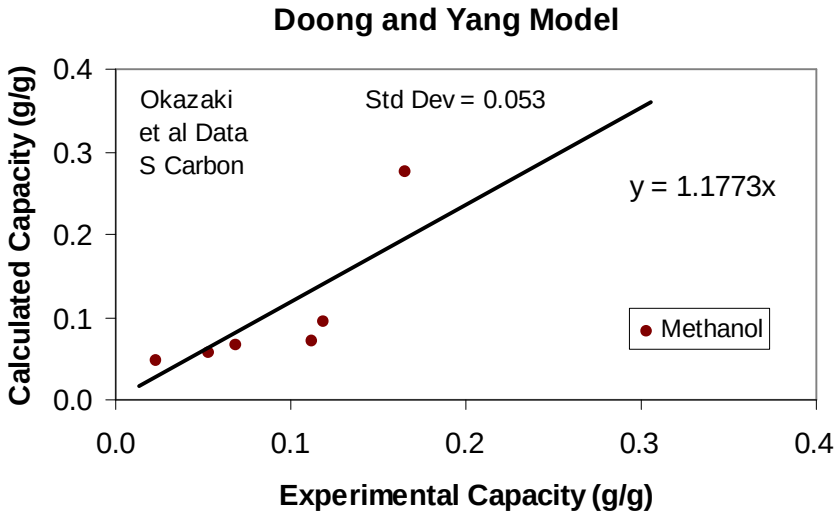

Figure 98. Comparison of Doong-Yang Model calculations for water covapor effects on methanol capacity with experimental data [135].

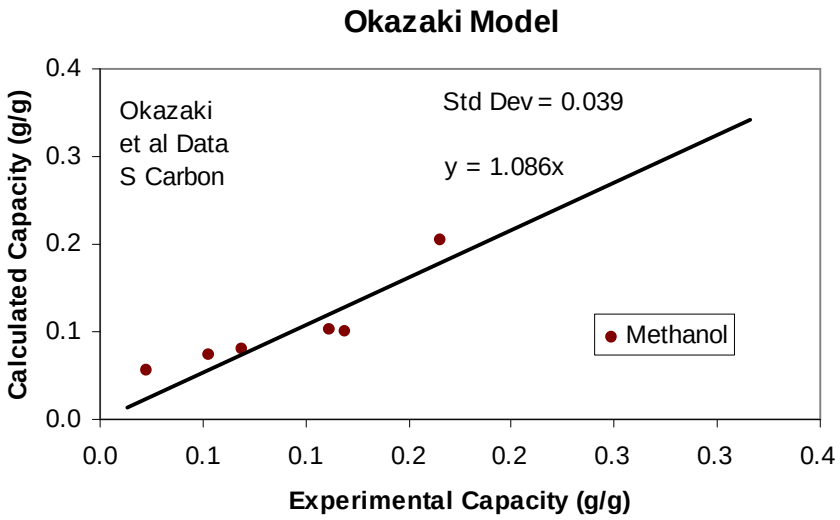

Figure 99. Comparison of Okazaki Model calculations for water covapor effects on methanol capacity with experimental data [135].

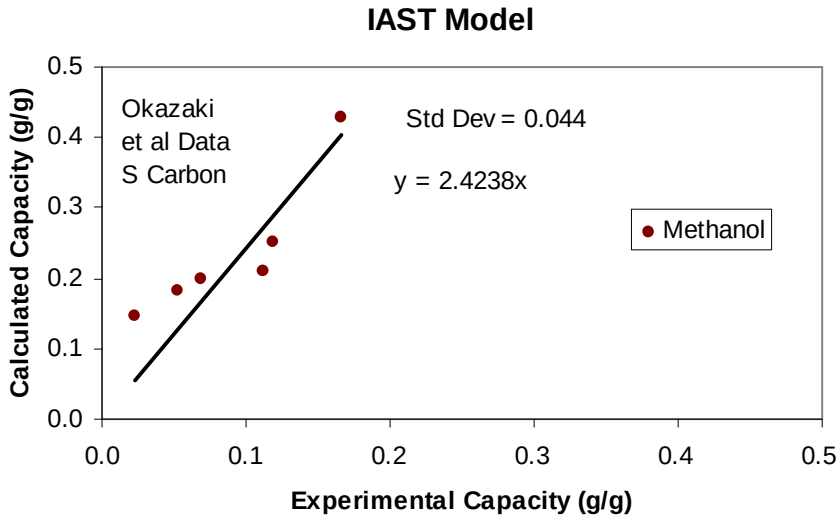

Figure 100. Comparison of Ideal Adsorbed Solution Theory Model calculations for water covapor effects on methanol capacity with experimental data [135].

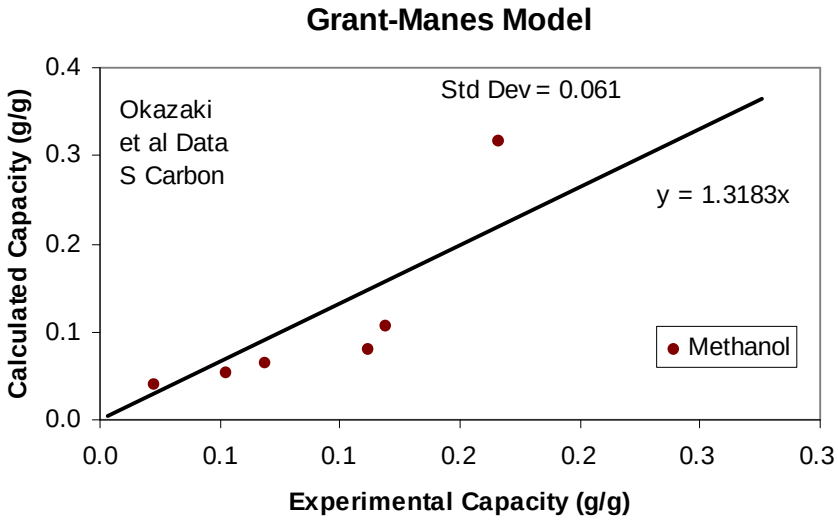

Figure 101. Comparison of Grant-Manes Model calculations for water covapor effects on methanol capacity with experimental data [135].

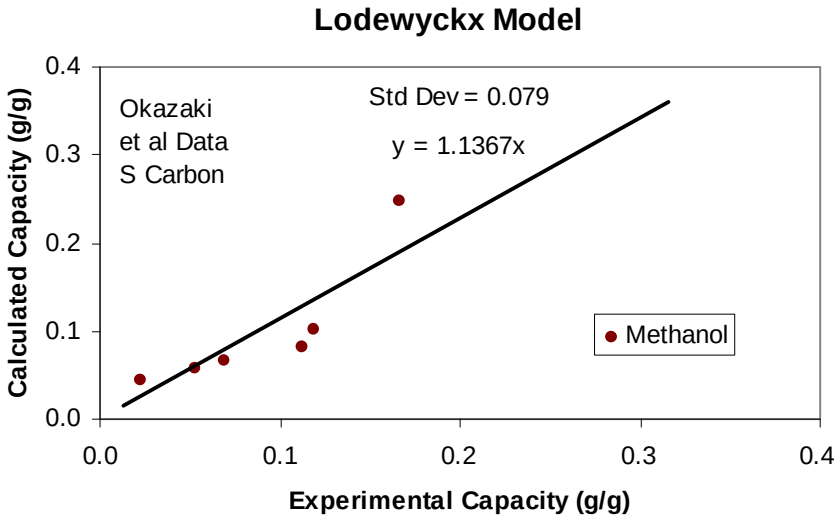

Figure 102. Comparison of Lodewyckx Model calculations for water covapor effects on methanol capacity with experimental data [135].

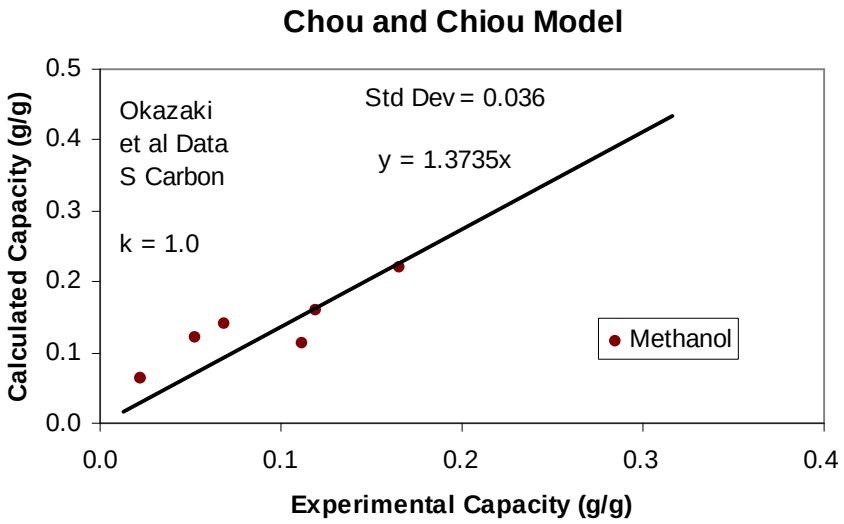

Figure 103. Comparison of Chou and Chiou Model calculations for water covapor effects on methanol capacity with experimental data [135].

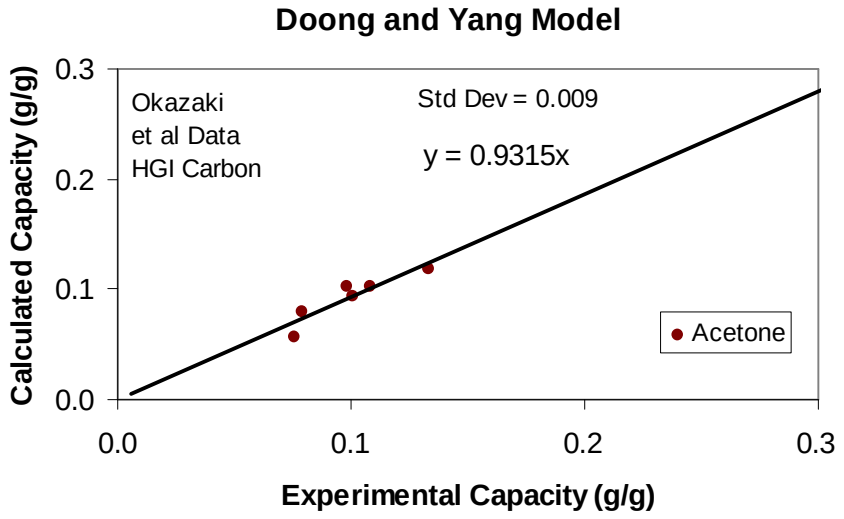

Figure 104. Comparison of Doong-Yang Model calculations for water covapor effects on acetone capacity with experimental data for HGI carbon [135].

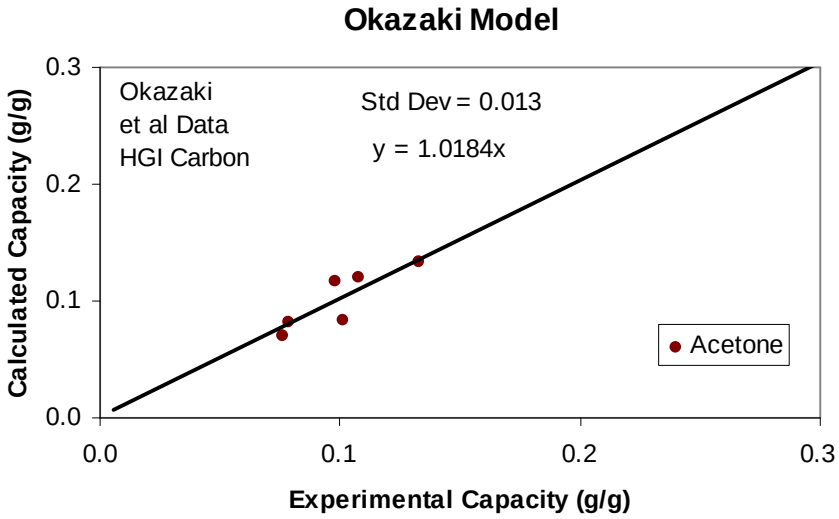

Figure 105. Comparison of Okazaki Model calculations for water covapor effects on acetone capacity with experimental data for HGI carbon [135].

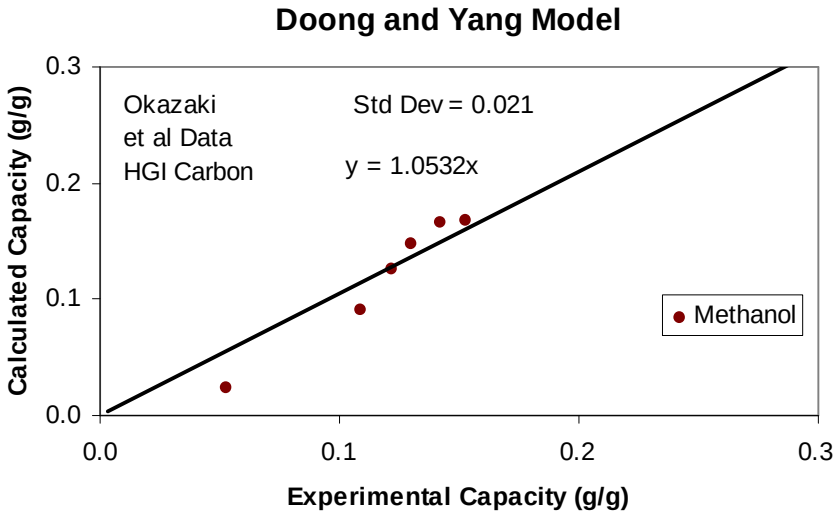

Figure 106. Comparison of Doong-Yang Model calculations for water covapor effects on methanol capacity with experimental data for HGI carbon [135].

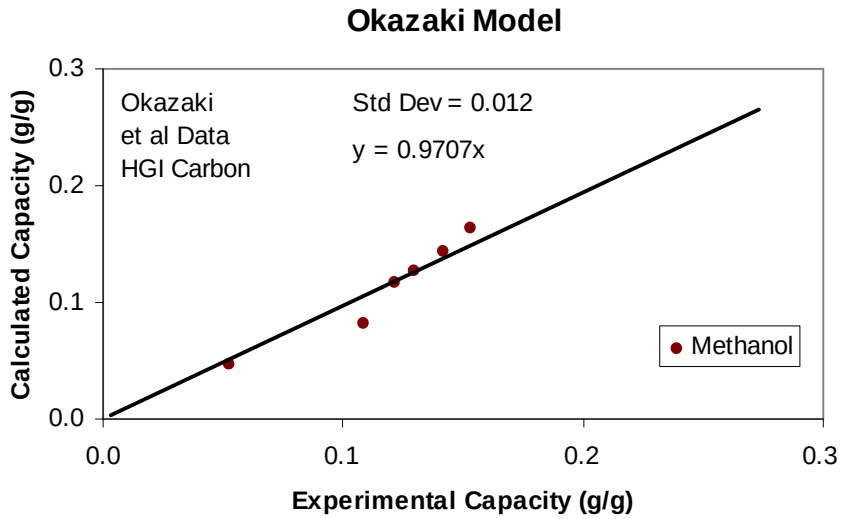

Figure 107. Comparison of Okazaki Model calculations for water covapor effects on methanol capacity with experimental data for HGI carbon [135].

The graphs give visualizations of the qualities of predictions, but these may be better compared in Table XVIII. The bolded numbers in this table represent (with one exception—see table footnote) the "best" accuracies (nearest to 1.00) and precisions (nearest to zero) for each carbon/organic vapor combination. The Okazaki model had 5 out of 12 such "bests"; the Doong-Yang 3 out of 12; the Chou-Chiou 2 out of 8 (both precisions); the Grant-Manes 2 out of 8 (both precisions); the Lodewyckx 0 out of 8; and the IAST 0 out of 8. From these results alone it seems that the Okazaki and Doong-Yang models are the best performers for this data set. However, some caveats should be considered.

The Okazaki Model predictions seem to be independent of the mixture data they attempted to reproduce; i.e., they did not seem to have been developed from the same data they predict. However, the general application of this model is limited by the availability of the equilibrium isotherm and solubility data required (see above discussion). How many chemicals do we have aqueous solution/activated carbon equilibrium data for?

Table XVIII. Accuracies and Precisions of Models for Adsorption Capacities of Activated Carbons for Organic Vapor and Water Vapor Mixtures using the Data of Okazaki et al. [135]

Organic Vapor	Carbon	Mixture Model	Average Accuracy (Calc/Exp)	Average Precision as Std Dev (g/g)
Benzene	Shirasagi S	Doong-Yang	0.84	0.031
	Shirasagi S	Okazaki	**1.01**	0.027
	Shirasagi S	IAST	0.51	0.024
	Shirasagi S	Grant-Manes	1.03	**0.021**
	Shirasagi S	Lodewyckx	0.05	0.051
	Shirasagi S	Chou-Chiou	0.45	0.051
Toluene	Shirasagi S	Doong-Yang	**1.01**	0.016
	Shirasagi S	Okazaki	0.97	0.017
	Shirasagi S	IAST	0.61	0.047
	Shirasagi S	Grant-Manes *	1.12	0.007
	Shirasagi S	Lodewyckx	0.55	0.023
	Shirasagi S	Chou-Chiou	0.39	**0.014**
Acetone	Shirasagi S	Doong-Yang	**1.03**	0.018
	Shirasagi S	Okazaki	1.04	0.024
	Shirasagi S	IAST	1.16	0.022
	Shirasagi S	Grant-Manes	1.27	**0.014**
	Shirasagi S	Lodewyckx	0.32	0.058
	Shirasagi S	Chou-Chiou	0.80	0.042
Methanol	Shirasagi S	Doong-Yang	1.18	0.053
	Shirasagi S	Okazaki	**1.09**	0.039
	Shirasagi S	IAST	2.42	0.044
	Shirasagi S	Grant-Manes	1.32	0.061
	Shirasagi S	Lodewyckx	1.14	0.079
	Shirasagi S	Chou-Chiou	1.37	**0.036**
Acetone	HGI-780	Doong-Yang	0.93	**0.009**
	HGI-780	Okazaki	**1.02**	0.013
Methanol	HGI-780	Doong-Yang	1.05	0.021
	HGI-780	Okazaki	**0.97**	**0.012**

***** Two of six iterative calculations did not converge, so this was not counted as "best" precision. Otherwise, numbers in bold are "bests" for each vapor and carbon.

The Doong-Yang Model, as presented, has the disadvantages of requiring iteration for solution and of adding another fit parameter to the isotherm equation. However, these shortcomings have been reduced by subsequent work (see above discussion).

The Grant-Manes adsorption potential model did not match the accuracies of the Okazaki or Doong-Yang. Also, convergence of its iterative solution is not easy and not always possible

[139].

The Chou-Chiou model was applied with an extrapolated (to 30 ^{o}C) exponent of 1/n = 2 and an arbitrarily chosen k = 1 in Equation (94). Since k and n vary with chemical, vapor concentration and temperature, it would have been surprising to have good results applying it to the Okazaki et al. data.

It was surprising that the IAST Model did not produce better predictions, especially for organic vapors miscible with water. This lack of accuracy may be due to using water molar volume as the adsorption potential divisor in equating spreading pressures. Using adjusted water molar volume as Grant et al [138] did or using affinity coefficients (experimental for water) should produce better results for this model.

The Lodewyckx Model of water exclusion and displacement was also surprisingly unsuccessful. However, it was developed from breakthrough curve (nonequilibrium) studies and may not apply to the equilibrium case, even though the equations allow it to.

V. Summary Conclusions and Recommendations

A. Current Models – Recommendations and Reasons

1. Single Vapors

The **Dubinin/Radushkevich Adsorption Isotherm** Equation (21) seems to be the most versatile, proven, and usable model for predicting adsorption capacities of organic vapors on ordinary commercial activated carbons. For specialized carbons the more general Dubinin/Astakhov Equation (23) with an additional parameter can be used. These have the advantages of including: a) carbon property parameters, b) vapor property parameters, and c) temperature. Only the Kisarov Equation (14) can also claim this, but it has been less proven and less successful in the analyses of this report. Other isotherm equations, particularly the Freundlich Equation (9), are useful for correlating experimental capacities and breakthrough time, but have little value for accurately predicting capacities for unmeasured vapors. The D/R equation has also been found to be useful for mixture and high humidity models.

Affinity Coefficient correlations using molar polarization, molecular parachor, and molar volume can all be used. This work has produced improved correlations (Table VIII) that give more options for this D/R, D/A, Kisarov and Polanyi theory parameter. We prefer to use molar polarizability, since it also includes inorganic gases and can be obtained several ways, experimentally and theoretically. The optimum molar polarizability correlation, $\beta = 0.0862\ P_e^{0.75}$ is nearly as good as the optimum molecular parachor correlation, $\beta = 0.00827\ \Omega^{0.9}$.

The **Lodewyckx** and **Wood-Stampfer Adsorption Rate Coefficient Models** are the only ones found to predict the trend of experimental rate coefficients with vapor type. They both include vapor parameters (molar polarizability and affinity coefficients, respectively) and air flow velocity parameter. The Lodewyckx Equation (57) also includes carbon granule diameter as

a parameter, but was developed only for 0.1% breakthrough. The Wood Equations (55-56) do not include granule diameter, but take into account observed breakthrough curve asymmetry (skew) to allow estimating rate coefficients at a range of breakthrough fractions. Our recommendation is that the these models be combined by adding skew parameters to the Lodewyckx equation and fitting the result to more data.

The **Reaction Kinetic** Equation (1) with a ln[(Co-C)/C] term is to be preferred over the (unnecessary) ln[Co/C] approximation often made, but justified by restricting it to low breakthrough fractions. For asymmetric breakthrough curves often observed, a skew term needs to be included. Equation (7) currently offers the best semi-empirical framework for describing and, perhaps eventually, predicting breakthrough curve skew. Incorporating skew into breakthrough curve equations should improve service life predictions, particularly at low breakthrough fractions.

Of the **complete breakthrough models** (Table I) currently available and tested the **Wood Model** was the most successful (Figure 3), in that it gave reasonably accurate predictions of measured breakthrough times without large overestimates. The other models had problems with overestimating breakthrough times (service lives), particularly at low vapor concentrations. Nevertheless, the Wood Model can be improved by the discoveries and recommendations made in this report.

2. Mixtures of Vapors

The **Grant-Manes (Polanyi Adsorption Theory) Model**, Equation (77), showed much promise for predicting capacities of mixtures of organic vapors on activated carbon (Tables X – XII), particularly when combined with the D/R equation. It is simple to apply and does not require isotherm data and integration at low loadings. The **IAST/DR Model**, Equation (78) is another alternative. Means of avoiding isotherm integration with the IAST/DR Model have been

reported, but applied only to mixtures of miscible components.

Volume Exclusion is to be preferred over Molar Proportionality in estimating capacities for mixture components, since activated carbon is a volumetric sorbent (fixed micropore volume), not a molar sorbent (fixed number of adsorption sites). Molar proportionality has seemed to describe data because the mixture components had similar molar volumes. Volume proportionality and exclusion would better incorporate vapors of differing molar volumes.

The evidence is mixed regarding the effects, if any, of one vapor on the adsorption rate of another. Until more data show otherwise, we recommend using **Single Vapor Adsorption Rate Coefficients** for mixture components. Skew may also need to be incorporated (see above).

For **complete breakthrough models of mixtures**, rollover is an established phenomenon. Volume, not molar, displacement should be used to predict rollover concentrations. Models should concentrate on accurately predicting initial (< 10% of challenge) breakthrough times, rather than accurately predicting complete breakthrough curves (Figure 77). The former are of practical interest (service lives), the latter of more theoretical interest.

3. High Humidity Cases

We prefer the **Doong-Yang Model,** Equations (102-103), over the **Okazaki Model,** Equation (98), since the former is simpler to use, is based on D/R single vapor isotherms, requires less equilibrium data input than the latter, and was nearly as accurate and precise in predictions (Table XVIII). There is still an iteration difficulty with the Doong-Yang model; however, we have found a correlation for its hysteresis term [Equation (104)].

However, the limitations of equilibrium models must be recognized. Water vapor does not adsorb as rapidly as organic vapors on activated carbons. Therefore, equilibrium may not be reached during the service life of the cartridge or other bed. **Lodewyckx and Vansant** [136] have reported Equations (99-101), which allow calculation of the extent of water capacity

reached as a function of exposure time. It requires knowing the water adsorption isotherm.

The **Lodewyckx Model,** Equation (105) gives effects of water loading on the **rate coefficient** of organic vapor adsorption. Total carbon pore volume and fraction filled with water need to be known. The **Hall** empirical Equation (106) can correlate data for water equilibrium, but this is not usually the case for using fresh cartridges.

In the absence of sufficient quantitative data on the effects of water on organic vapor breakthrough curve shapes, we recommend using single vapor **Reaction Kinetic** equations with **skew** incorporated (see above for single vapors).

B. Identified Model Gaps

1. A single-vapor adsorption rate coefficient model that incorporates all the important parameters, including flow velocity, granule size, vapor properties, and breakthrough fraction (skew) does not exist.

2. Quantification of breakthrough curve skew and identification of parameters affecting it are lacking.

3. More evidence regarding the effect of one vapor (including water vapor) on the adsorption rate of another in a mixture is needed.

4. Although the component models exist for an overall breakthrough model for mixtures of organic vapors in air, they have not been put together to form a complete predictive service live model.

5. Although the component models exist for an overall breakthrough model for organic vapors in high humidity air, they have not been put together to form a complete predictive service life model. The large body of existing data has not been completely and systematically analyzed.

C. Future Work for Improved Predictive Models

1. Mixtures Model

Develop multicomponent breakthrough curve equations based on:

a) D/R single component vapor isotherms

b) Known affinity coefficient correlations

c) Known carbon structural constant correlations

d) Grant-Manes mixture equations

e) Volume exclusion

f) Single vapor adsorption rate coefficients

If this combination proves to be inadequate, try:

a) IAST/DR as an alternative to Grant-Manes

b) Find a better correlation of the carbon structural constant

c) Try to take into account covapor effects on adsorption rates

d) Apply mixing volume corrections.

2. Humidity Model

Develop breakthrough curve equations incorporating water vapor effects based on:

a) Single vapor D/R isotherms, affinity coefficients, and carbon constants

b) Doong-Yang volume exclusion and mixing model

c) Lodewyckx water loading rate equations

d) Single vapor adsorption rate coefficients

e) Lodewyckx's reduction of rate coefficients equation

If this combination proves to be inadequate, try:

a) Grant-Manes Model or some kind of simplified Okazaki Model

b) Add empirical skew factors due to water loading

3. Combine Mixtures and High Humidity Models

4. Develop Computer Simulations of the Breakthrough Process

References

1. G. O. Nelson and A. N. Correia, "Respirator Cartridge Efficiency Studies: VIII. Summary and Conclusions," *Amer. Ind. Hyg. Assoc. J.* **37**, 514-525 (1976).
2. D. M. Smoot, "Development of Improved Respirator Cartridge and Canister Test Methods," *U.S. Department of Health, Education, and Welfare, Contract NAS 10-8842* (1977).
3. E. S. Moyer, "Review of Influential Factors Affecting the Performance of Organic Vapor Air-Purifying Respirator Cartridges," *Am. Ind. Hyg. Assoc. J.* **44**, 46-51 (1983).
4. M. D. Werner and N. L. Winters, "A Review of Models Developed To Predict Gaseous Phase Activated Carbon Adsorption of Organic Compounds," *CRC Critical Reviews in Environmental Control.* **16**, 327-356 (1988).
5. G. S. Bohart and E. Q. Adams, "Some Aspects of the Behavior of Charcoal With Respect To Chlorine," *J. Amer. Chem. Soc.* **42**, 523-544 (1920).
6. C. J. Danby, J. G. Davoud, D. H. Everett, C. N. Hinshelwood, and R. M. Lodge, "The Kinetics of Adsorption of Gases from Air Stream by Granular Reagents," *J. Chem. Soc.* **1946**, 918-934.
7. Y. H. Yoon and J. H. Nelson, "Application of Gas Adsorption Kinetics I. A Theoretical Model for Respirator Cartridge Service Life," *Am. Ind. Hyg. Assoc. J.* **45**, 509-516 (1984).
8. T. Vermeulen, M. D. LeVan, N. K. Hiester, and G. Klein, "Adsorption and Ion Exchange," in Perry's Chemical Engineers Handbook, 6th Edition, R. H. Perry, et al., eds, Section 16, 1-48, McGraw-Hill, New York (1984)..
9. W. Mecklenburg, "Uber Schichtenfiltration, Ein Beitrag zur Theorie der Gasmaske," *Z.*

Electrochem. **31**, 488-495 (1925) and Part II, *Kolloid. Zh.* **52**, 88-103 (1930).

10. M. Klotz, "The Adsorption Wave," *Chem. Rev.* **39**, 241-268 (1946).
11. B. W. Gamson, G. Thodos, and O. A. Hougen, "Heat, Mass and Momentum Transfer In the Flow of Gases Through Granular Solids," *Trans. Am. Inst. Chem. Engrs.* **39**,1-35 (1943).
12. Wheeler and A. J. Robell, "Performance of Fixed-Bed Catalytic Reactors with Poison in the Feed," *J. Catalysis.* ***13***, 299-305 (1969).
13. L. A. Jonas and J. k Rehrmann, "The Kinetics of Adsorption of Organo-Phosphorus Vapors From Air Mixtures by Activated Carbons," *Carbon.* **10**, 657-663 (1972).
14. G. O. Wood and E. S. Moyer, "A Review of the Wheeler Equation and Comparison of Its Applications to Organic Vapor Respirator Cartridge Breakthrough Data," *Am. Ind. Hyg. Assoc. J.* **50**, 400-407 (1989).
15. Grubner and W. A. Burgess, "Calculation of Adsorption Breakthrough Curves in Air Cleaning and Sampling Devices," *Environ. Sci. Tech.* **15**, 1346-1351 (1981).
16. G. O. Wood, "Organic Vapor Respirator Cartridge Breakthrough Curve Analysis," *J. Int. Soc. Resp. Prot.* **10**(4), 5-17 (1993).
17. Y. H. Yoon and J. H. Nelson, "A Theoretical Study of the Effect of Humidity on Respirator Cartridge Service Life," *Am. Ind. Hyg. Assoc. J.* **49**, 325-33, (1988).
18. Y. H. Yoon and J. H. Nelson, "Application of Gas Adsorption Kinetics II. A Theoretical Model for Respirator Cartridge Service Life and Its Practical. Applications," *Am. Ind. Hyg. Assoc. J.* **45**, 517-524 (1984).
19. S. Brunauer, L. S. Deming, W. E. Deming, and E. J. Teller, "On a Theory of the van der Waals Adsorption of Gases," *J. Am. Chem. Soc.* **62**, 1723-1732 (1940).
20. G. O. Wood and E. S. Moyer, "A Review and Comparison of Adsorption Isotherm

Equations Used To Correlate and Predict Organic Vapor Cartridge Capacities," *Am. Ind. Hyg. Assoc. J.* **52**, 235-242 (1991).

21. G. O. Nelson and C. A. Harder, "Respirator Cartridge Efficiency Studies: VI. Effect of Concentration," *Am. Ind. Hyg. Assoc. J.* **37**, 205-216 (1976).

22. G. O. Nelson, G. J. Carlson, and J. S. Johnson, "Service life of Respirator Cartridges at Various Concentrations of Common Organic Solvents," Lawrence Livermore Laboratory. Report. UCRL-52982. **1980**.

23. I. Langmuir, "The Adsorption of Gases on Plane Surfaces of Glass, Mica, and Platinum," *J. Am. Chem. Soc.* **40**, 1361-1402 (1918).

24. N. Vahdat, "Theoretical Study of the Performance of Activated Carbon In the Presence of Binary Vapor Mixtures," *Carbon.* **35**, 1545-1557 (1997).

25. V. M. Kisarov, "A New Equation for the Adsorption Isotherm," *Russ. J. Phys. Chem.* **43**(4), 580-581 (1969) translated from *Zh. F. Kh.* **43**, 1037 (1969).

26. L. B. Begun, V. M. Kisarov, A. I. Subbotin, and V. I. Trachenko, "Adsorption of Aromatic Hydrocarbons and Lower Aliphatic Alcohols on AR-3 Activated Charcoal," *Sov. Chem. Ind.* **5**(3), 162-164 (1973).

27. A. C. Rasmuson, "Adsorption Equilibria on Activated Carbon of Mixtures of Solvent Vapours," 451-460 in Fundamentals of Adsorption, A. L. Myers and G. Belfort, eds., Engineering Foundation, New York (1984).

28. J. J. Hacskaylo and M. D. LeVan, "Correlation of Adsorption Equilibrium Data Using a Modified Antoine Equation: A New Approach for Pore-Filling Models," *Langmuir.* **1**, 97-100 (1985).

29. M. Polanyi, "Adsorption from the Point of View of the Third Law of Thermodynamics," *Verh. Deut. Phys. Ges*. **16**, 1012-1016 (1914).

30. B. P. Bering, M. M. Dubinin, and V. V. Serpinsky, “Theory of Volume Filling for Vapor Adsorption,” *J. Colloid Interface Sci*. **21**, 378-393 (1966).

31. L. G. Gurvitsch, “Physicochemical Attractive Force,” *J. Russ. Phys. Chem. Soc*. (*Zh. Russ. Fiz. Khim*) **47**, 805-827 (1915).

32. M. Polanyi, “Causes of Forces of Adsorption,” *Z. Elektrochem*. **26**, 370-374 (1920). And “Theories of Adsorption of Gases. General Survey and Some Additional Remarks,” *Trans. Farad. Soc*. **28**, 316-333 (1932).

33. G. O. Nelson and C. A. Harder, “Respirator Cartridge Efficiency Studies: V. Effect of Solvent Vapor,” *Am. Ind. Hyg. Assoc.* J. **July**, 391-410.

34. G. O. Nelson and G. J. Carlson, "Prediction of Service Life of Organic Vapor Respirator Cartridges,” Lawrence Livermore Laboratory. Report. UCRL-35005. **1980**.

35. M. M. Dubinin, E. D. Zaverina, and L. V. Radushkevich, “Sorption and Structure of Active Carbons. I. Adsorption of Organic Vapors,” *Zh. Fiz. Khim*. **21**, 1351-1362 (1947).

36. M. M. Dubinin and V. A. Astakhov, “Development of the Concepts of Volume Filling of Micropores in the Adsorption of Gases and Vapors by Microporous Adsorbents,” *Izv. Akad. Nauk SSSR, Ser. Khim*. 5-11 (1971).

37. F. Stoeckli, “Dubinin’s Theory for the Volume Filling of Micropores: An Historical Approach,” *Adsorption, Sci. Technol.* **10**, 3-16 (1983)

38. F. Stoeckli, “Recent Developments in Dubinin’s Theory,” *Carbon* **36**, 363-368 (1998).

39. A. Lavanchy, M. Stockli, C. Wirz, and F. Stoeckli, “Binary Adsorption of Vapors in Active Carbons Described by the Dubinin Equation,” *Adsorption, Sci. Technol.* **13**, 537-545 (1996).

40. G. O. Wood, “Activated Carbon Adsorption Capacities for Vapors,” *Carbon*. **30**, 593-599 (1992).

41. D. R. Lide, ed., CRC Handbook of Chemistry and Physics, 75th Edition, CRC Press, Inc., Boca Raton, FL (1994).

42. R. R. Dreisbach, Physical Properties of Chemical Compounds, Advances in Chemistry Series #15 (1995), Vol. II, #22 (1959), Vol. III, # 29 (1961), American Chemical Society Washington, D.C.

43. L. Berenyi, "Examination of the Polanyi Theory of Adsorption," *Z. Physik. Chem*. **94**, 628-662 (1920).

44. M. Dubinin and E. Sawerina, "Charakter der Porositats- und Sorptionseigenschaften Aktiver Kohle," *Acta Physicochemica URSS*. **4**, 647-674 (1936).

45. M. M. Dubinin and D. P. Timofeyev, "Adsorption of Vapors on Active Carbons in Relation to the Properties of the Adsorbate," *Dokl. Akad. Nauk SSSR*. **54**, 701-704 (1946).

46. B.A. Vaskovsky, cited in M. M. Dubinin and E. D. Zaverina. Adsorption of Gases by Activated Carbons. *Dokl. Akad. Nauk SSSR*. **72**, 319 (1950).

47. O. R. Quayle, "The Parachors of Organic Compounds," *Chem. Rev*. **53**, 439-589, esp. Table 25 on p 484 (1953).

48. P. J. Reucroft, W. H. Simpson, and L. A. Jonas, "Sorption Properties of Activated Carbon," *J. Phys. Chem*. **75**, 3526-3531 (1971).

49. A. Golovoy and J. Braslaw, "Adsorption of Automobile Paint Solvents on Activated Carbon: I. Equilibrium Adsorption of Single Vapors," *J. A. P. C. A*. **31**, 861-865 (1981).

50. K. E. Noll, D. Wang, and T. Shen, "Comparison of Three Methods to Predict Adsorption Isotherms for Organic Vapors from Similar Polarity and Nonsimilar Polarity Reference Vapors," *Carbon*. **27**, 239-245 (1989).

51. A. E. Duisterwinkel, "Activated Carbon Adsorption Capacities for Vapors, an Alternative

Approach," *Carbon*. **31**, 1354-1357 (1993).

52. D. K. Friday, D. T. Croft, and L. C. Buettner, "Multi-Component Filter Breakthrough Experiments and Modeling," in Proceedings of the 1997 ERDEC Scientific Conference on Chemical and Biological Defense Research, Report ERDEC-SP-063, Edgewood Research, Development & Engineering Center, Aberdeen Proving Ground, MD (1998).

53. Y. C. Xiang, J. C. Zeng, and S. Q. Yan, "A Simplified Equation for Predicting Breakthrough Time of a Fixed Carbon Bed," *Carbon.* **36**, 1057-1060 (1998).

54. N. Wakao and T. Funazkri, "Effect of Fluid Dispersion Coefficients on Particle-To-Fluid Mass Transfer Coefficients in Packed Beds," *Chem. Eng. Sci.* **33**, 1375-1384 (1978).

55. A. Wheeler, "Reaction Rates and Selectivity in Catalyst Pores," in Catalysis, P. Emmett, ed., **Vol 2**, Chapter 2, 105-165, Reinhold, New York (1955).

56. O. A. Hougen and K. M. Watson, "Mass and Heat Transfer in Catalytic Beds," Chapter 20 in Chemical Process Principles, Part 3, Kinetics and Catalysis, 973-1008, New York, John Wiley & Sons, Inc., (1947).

57. L. A. Jonas and J. A. Rehrmann, "Predictive Equations In Gas Adsorption Kinetics," *Carbon*. **11**, 59-64 (1973).

58. L. A. Jonas and J. A. Rehrmann, "The Rate of Gas Adsorption by Activated Carbon," *Carbon.* **12**, 95-101 (1974).

59. J. A. Rehrmann and L. A. Jonas, "Dependence of Gas Adsorption Rates on Carbon Granule Size and Linear Flow Velocity," *Carbon.* **16**, 47-51 (1978).

60. L. A. Jonas, Y. B. Tewari, and E. B. Sansone, "Prediction of Adsorption Rate Constants of Activated Carbon for Various Vapors," *Carbon*. **17**, 345-349 (1979).

61. E. B. Sansone and L. A. Jonas, "Prediction of Activated Carbon Performance for

Carcinogenic Vapors," *Am. Ind. Hyg. Assoc. J*. **42**, 688-691 (1981).

62. G. O. Wood and J. F. Stampfer, "Adsorption Rate Coefficients for Gas and Vapors on Activated Carbons," *Carbon.* **31**, 195-200 (1993).

63. O. Grubner and D. W. Underhill, "Calculation of Adsorption Bed Capacity by the Theory of Statistical Moments," *Sep. Sci.* **5**, 555-582 (1970).

64. P. Lodewyckx and E. F. Vansant, "Estimating the Overall Mass Transfer Coefficient k_v of the Wheeler-Jonas Equation: A New and Simple Model," submitted for publication in the *Am. Ind. Hyg. Assoc. J*. (1999).

65. V. R- Deitz, C. H. Blachly, and L. A. Jonas, "Dependence of Gas Penetration of Charcoal Beds on Residence Time and Linear Velocity," *Nucl. Tech.* **37**, 59-64 (1978).

66. L. A. Jonas and W. J. Svirbely, "The Kinetics of Adsorption of Carbon Tetrachloride and Chloroform from Air Mixtures by Activated Carbon," *J Catalysis.* **24**, 446-459 (1972).

67. L. A. Jonas, J. C. Boardway, and E. L. Meseke, "Prediction of Adsorption Behavior of Activated Carbons," *J Colloid Interface Sci.* **50**, 538-544 (1975).

68. G. O. Nelson and G. J. Carlson, "Prediction of Service Life of Organic Vapor Respirator Cartridges," Lawrence Livermore Laboratory. Report. UCRL-35005. (1980).

69. G. O. Nelson, A. N. Correia, and C. A. Harder, "Respirator Cartridge Efficiency Studies: VII. Effect of Relative Humidity and Temperature," *Am. Ind. Hyg. Assoc. J*. **37**, 280-288. (1976).

70. D. M Smoot, "Organic Vapor Respirator Service Life Prediction," *National Institute for Occupational Safety and Health. Report PB82-189739* (1981).

71. G. O. Wood, "Estimating Service Lives of Organic Vapor Cartridges," *Am. Ind. Hyg. Assoc. J*. **55**, 11-15 (1994).

72. Y. H. Yoon and J. H. Nelson, "Breakthrough Time and Adsorption Capacity of

Respirator Cartridges," *Am. Ind. Hyg. Assoc. J.* **53**, 303-316 (1992).

73. E. Balieu and E. Bjarnov, "Activated Carbon Filters in Air Cleaning Processes-II. Prediction of Breakthrough Times and Capacities from Laboratory Studies of Model Filters," *Ann. Occup. Hyg.* **34**, 1-11 (1990).

74. M. W. Ackley, "Residence Time Model for Respirator Sorbent Beds," *Am. Ind., Hyg. Assoc. J.* **46**, 679-689 (1985).

75. H. J. Cohen and R. P. Garrison, "Development of a Field Method for Evaluating the Service Life of Organic Vapor Cartridges: Results of Laboratory Testing Using Carbon Tetrachloride," *Am. Ind. Hyg. Assoc. J.* **50**, 486-495 (1989).

76. Mine Safety Appliances Company, "MSA Respirator Test Data Index," published at the Internet site http://www.msanet.com/safetyproducts/resptest/dataindex.stm (1998).

77. S. J. Smith, "Replacement of Carbon Tetrachloride as an Organic Vapour Respirator Filter Test Agent," *J. Int. Soc. Resp. Prot.* **14**(2), 6-24 (1996).

78. S. Tanaka, S. Kido, Y. Seki, S. Imamiya, "Service Lives of Respirator Cartridges for 46 Organic Solvent Vapors," *Jpn. J. Ind. Health* **35**, 290-291 (1993).

79. R. W. Freedman, B. I. Ferber, and A. M. Hartstein, "Service Lives of Respirator Cartridges versus Serveral Classes of Organic Vapors," *Am. Ind. Hyg. Assoc. J.* **34**(2), 55-60 (1973).

80. A. J. Robell, C. R. Arnold, A. Wheeler, G. J. Kersels, and R. P. Merrill, "Trace Contaminant Adsorption and Sorbent Regeneration," Report NASA CR-1582, National Aeronautics and Space Administration (1970).

81. G. O. Wood, "Affinity Coefficients of the Polany/Dubinin Adsorption Isotherm Equations: A Review with Compilations and Correlations," Report LA-UR-00-59, Los Alamos National Laboratory, submitted for publication in *Carbon* (2000).

82. L. A. Jonas, E. B. Sansone, and T. S. Farris, “Prediction of Activated Carbon Performance for Binary Vapor Mixtures,” *Am. Ind. Hyg. Assoc. J.* **44**, 716-719 (1983).

83. C. A. Robbins and P. N. Breysse, “The Effect of Vapor Polarity and Boiling Point on Breakthrough for Binary Mixtures on Respirator Carbon,” *Am. Ind. Hyg. Assoc. J.* **57**, 717-723 (1996).

84. P. J. Reucroft, H. K. Patel, W. C. Russell, and W. M. Kim, “Modeling of Equilibrium Gas Adsorption for Multicomponent Vapor Mixtures Part II,” *Chemical Research, Development & Engineering Center. CRDEC-CR-87015.* **1986**.

85. H. J. Cohen, D. E. Briggs, and R. P. Garrison, “Development of a Field Method for Evaluating the Service Lives of Organic Vapor Cartridges-Part III: Results of Laboratory Testing Using Binary Organic Vapor Mixtures,” *Am. Ind. Hyg. Assoc. J.* **52**, 34-43 (1991).

86. L. A. Jonas and E. B. Sansone, “Prediction of Activated Carbon Performance for Sequential Adsorbates,” *Am. Ind. Hyg. Assoc. J.* **47**, 509-511 (1986).

87. S. J. Doong and R. T. Yang, “A simple Potential-Theory Model for Predicting Mixed-Gas Adsorption,” *Ind. Eng. Chem. Res.* **27**, 630-635 (1988).

88. A. Lavanchy and F. Stoeckli, “Dynamic Adsorption, in Active Carbon Beds, of Vapour Mixtures Corresponding to Miscible and Immiscible Liquids,” *Carbon*. **37**, 315-321 (1999).

89. W. K. Lewis, E. R. Gilliland, B. Chertow, and W. P. Cadogan, “Adsorption Equilibria Hydrocarbon Gas Mixtures,” *Ind. Eng. Chem.* **42**, 1319-1326 (1950).

90. R. J. Grant and M. Manes, “Adsorption of Binary Hydrocarbon Gas Mixtures on Activated Carbon,” *I & EC Fundamentals*. **5**, 490-498 (1966).

91. M. Greenbank and M. Manes, “Application of the Polanyl Adsorption Potential Theory

to Adsorption from Solution on Activated Carbon. 11. Adsorption of Organic Liquid Mixtures from Water Solution," *J. Phys. Chem.* **85**, 3050-3059 (1981).

92. A. L. Myers and J. M. Prausnitz, "Thermodynamics of Mixed-Gas Adsorption," *A. I. Ch. E. J.* **11**, 121-127 (1965).

93. A. J. Kidnay and A. L. Myers, "A Simplified Method for the Prediction of Multicomponent Adsorption Equilibria from Single Gas Isotherms," *A. I. Ch. E. J.* **12**, 981-986 (1966).

94. F.A. Digiano, G. Baldauf, B. Frick, and H. Sontheimer, "A Simple Competetitive Equilibrium Adsorption Model," *Chem. Eng. Sci.* **33**, 1667-1673 (1978).

95. B. K. Kaul, "Correlation and Prediction of Adsorption Isotherm Data for Pure and Mixed Gases," *Ind. Eng. Chem. Process Des. Dev.* **23**, 711-716 (1984).

96. D. P. Valenzuela and A. L. Myers, Adsorption Equilibrium Data Handbook. Prentice Hall, Englewood Cliffs, 1989.

97. T. L. Hill, P. H. Emmett, and L. G. Joyner, "Calculation of Thermodynamic Functions of Adsorbed Molecules from Adsorption Isotherm Measurements: Nitrogen on Graphon,"

98. N. Sundaram and R. T. Yang, "Incorporating Henry's Law in the Dubinin Isotherm,"

99. J. J. Mahle, "A Henry's Law Limit for the DR and DA Equations," *Carbon* **35**, 432-435 (1997).

100. F. Stoeckli, D. Wintgens, A. Lavanchy, and M. Stockli, "Binary Adsorption of Vapours in Active Carbons Described by the Combined Theories of Myers-Prausnitz and Dubinin (II)," *Adsorption, Science & Technology.* **15**, 677-683 (1997).

101. S. Suwanayuen and R. P. Danner, "A Gas Adsorption Isotherm Equation Based on Vacancy Solution Theory," *A. I. Ch. E. J.* **26**, 68-76 (1980).

102. S. Suwanayuen and R. P. Danner, "Vacancy Solution Theory of Adsorption From Gas

Mixtures," *A. I. Ch. E. J.* **26**, 76-83 (1980).

103. E. Costa, J. L. Sotelo, G. Calleja, and C. Marron, "Adsorption of Binary and Ternary Hydrocarbon Gas Mixtures on Activated Carbon: Experimental Determination and Theoretical Prediction of the Ternary Equilibrium Data," *A. I. Ch. E. J.* **27**, 5-12 (1981).

104. V. Gusev, J. A. O'Brien, C. R. C. Jensen, and N. A. Seaton, "Theory for Multicomponent Adsorption Equilibrium: Multispace Adsorption Model," *A. I. Ch. E. J.* **42**, 2773-2783 (1996).

105. E. Gluckauf, "Contributions to the Theory of Chromatography," *Proc. Roy. Soc., Ser. A* **186**, 35-57 (1946).

106. D. O. Cooney and F. P. Strusi, "Analytical Description of Fixed-Bed Sorption of Two Langmuir Solutes Under Nonequilibrium Conditions," *Ind. Eng. Chem. Fundam.* **11**, 123-126 (1972).

107. W. J. Thomas and J. L. Lombardi, "Binary Adsorption of Benzene-Toluene Mixtures," *Trans. Instn Chem. Engrs.* **49**, 240-250 (1971).

108. W. Fritz and E. U. Schluender, "Simultaneous Adsorption Equilibria of Organic Solutes in Dilute Aqueous Solutions on Activated Carbon," *Chem. Eng. Sci.* **29**, 1279-1282 (1974).

109. D. Basmadjian and P. Coroyannakis, "Equilibrium Theory Revisited. Isothermal Fixed-Bed Sorption of Binary Systems-I. Solutes Obeying the Binary Langmuir Isotherm," *Chem. Eng. Sci.* **42**, 1723-1735 (1987).

110. D. Basmadjian and P. Coroyannakis, "Equilibrium Theory Revisited. Isothermal Fixed-Bed Sorption of Binary Systems-II. Non-Langmuir Solutes with Type I Parent Isotherms: Azeotropic Systems," *Chem. Eng. Sci.* **42**, 1737-1752 (1987).

111. C. Sheindorf, M. Rebhun, and M. Sheintuch, "A Freundlich-Type Multicomponent

Isotherm," *J. Colloid Interface Sci.* **79**, 136-142 (1981).

112. J. Rudling, "Multicomponent Adsorption Isotherms for Determinate of Recoveries in Liquid Desorption of Mixtures of Polar Solvents Adsorbed on Activated Carbon," *Am. Ind. Hyg. Assoc. J.* **49**, 95-100 (1988).

113. P. T. John, "A Method to Determine the Total and Partial Adsorptions from a Binary Mixture When Component Gases Have Similar Adsorbabilities," *Carbon*. **22**, 559-562 (1984).

114. B. P. Bering, V. V. Serpinsky, and S.I. Surinova, "Adsorption of a Gas Mixture. Communication 7. Joint Adsorption of a Binary Mixture of Vapors on Activated Charcoal," a translation from *Izv. Akad. Nauk. SSSR, Ser. Khim.* **5**, 769-776 (1965).

115. D. Valenzuela and A.L. Myers, "Gas Adsorption Equilibria," *Sep. and Purif. Methods* **13(2)**, 153-183 (1984).

116. Y. H. Yoon, J. H. Nelson, J. Lara, C. Kamel, and D. Fregeau, "A Theoretical Interpretation of the Service Life of Respirator Cartridges for the Binary Acetone/m-Xylene System," *Am. Ind. Hyg. Assoc. J.* **52**, 65-74 (1991).

117. Y.H. Yoon, J.H. Nelson, J. Lara, C. Kamel, and D. Fregeau, "A Theoretical Model for Respirator Cartridge Service Life for Binary Systems: Application to Acetone/Styrene Mixtures," *Am. Ind. Hyg. Assoc. J.* **53(8)**, 493-502 (1992)

118. J. Lara, Y.H. Yoon, and J.H. Nelson, "The Service Life of Respirator Cartridges with Binary Mixtures of Organic Vapors," *J. Int. Soc. Resp. Prot.* **Spring 1995**, 7-26 (1995).

119. Y. H. Yoon, J. H. Nelson, and J. Lara, "Respirator Cartridge Service-Life: Exposure to Mixtures," *Am. Ind. Hyg. Assoc. J.* **57**, 809-819 (1996).

120. I. Zwiebel, F. R. Myers, and D. A. Neusch, "Multicomponent Mass Transfer In Fixed-Bed Carbon Adsorption Columns," *Carbon*. **25**, 85-95 (1987).

121. R. M. Marutovsky and M. Bulow, “Sorption Kinetics of Multi-Component Gaseous and Liquid Mixtures on Porous Sorbents,” *Gas Separation & Purification.* **1**, 66-76 (1987).

122. U.S. Department of Labor, Occupational Safety and Health Administration, OSHA Instruction, Directive Number CPL 2-0.120, “Inspection Procedures for the Respiratory Protection Standard,” Effective Date September 25, 1998.

123. U.S. Department of Labor, Occupational Safety and Health Administration, “Factors that can Reduce Cartridge Service Life,” available at internet web site: http://www.osha-slc.gov/STLC/respiratory_advisor/factors/factors.html (1999).

124. M-S. Chou and J-H Chiou, “Modeling Effects of Moisture on Adsorption Capacity of Activated Carbon for VOCs,” *J. Env. Eng.* **123(5)**, 437-443 (1997).

125. G.O. Wood, “A Model for Adsorption Capacities of Charcoal Beds I. Relative Humidity Effects,” *Am. Ind. Hyg. Assoc. J.* **48(7)**, 622-625 (1987).

126. G.O. Wood, “A Model for Adsorption Capacities of Charcoal Beds II. Challenge Concentration Effects,” *Am. Ind. Hyg. Assoc. J.* **48(8)**, 703-709 (1987).

127. L.A. Jonas, E.B. Sansone, and T.S. Farris, “The Effect of Moisture on the Adsorption of Chloroform by Activated Carbon,” *Am. Ind. Hyg. Assoc. J.* **46(1)**, 20-23 (1985).

128. M.D. Werner, “The Effects of Relative Humidity on the Vapor Phase Adsorption of Trichloroethylene by Activated Carbon,” *Am. Ind. Hyg. Assoc. J.* **46(10)**, 585-590 (1985).

129. H.J. Cohen, E.T. Zellers, and R.P. Garrison, “Development of a Field Method for Evaluating the Service Lives of Organic Vapor Cartridges: Results of Laboratory Testing Using Carbon Tetrachloride. Part II: Humidity Effects,” *Am. Ind. Hyg. Assoc. J.* **51(11)**, 575-580 (1990).

130. D.W. Underhill, “Calculation of the Performance of Activated Carbon at High Relative Humidities,” *Am. Ind. Hyg. Assoc. J.* **48(11)**, 909-913 (1987).

131. K.H. Kawar and D.W. Underhill, “Effect of Relative Humidity on the Adsorption of Selected Water-Miscible Organic Vapors by Activated Carbon,” *Am. Ind. Hyg. Assoc. J.* **60,** 730-736 (1999).

132. Y.H. Yoon and J.H. Nelson, “Effects of Humidity and Contaminant Concentration on Respirator Cartridge Breakthrough,” *Am. Ind. Hyg. Assoc. J.* **51(4)**, 202-209 (1990).

133. T. Hall, P. Breysse, M. Corn, and L.A. Jonas, “Effects of Adsorbed Water Vapor on the Adsorption Rate Constant and Kinetic Adsorption Capacity of the Wheeler Kinetic Model,” *Am. Ind. Hyg. Assoc. J.* **49(9)**, 461-465 (1988).

134. T.A. Hall, Effects of Adsorbed Water Vapor on the Wheeler Kinetic Rate Constant and Kinetic Adsorption Capacity for Activated Carbon Adsorbents, Ph.D. Dissertation, John Hopkins University, Baltimore, MD (1992).

135. M. Okazaki, H. Tamon, and R. Toei, “Prediction of Binary Adsorption Equilibria of Solvent and Water Vapor on Activated Carbon,” *J. Chem. Eng. Japan* **11**, 209-215 (1978).

136. P. Lodewyckx and E.F. Vansant, “Influence of Humidity on Adsorption Capacity from the Wheeler-Jonas Model for Prediction of Breakthrough Times of Water Immiscible Organic Vapors on Activated Carbon Beds,” *Am. Ind. Hyg. Assoc. J.* **60**, 612-617 (1999).

137. M. Manes, “Estimation of the Effects of Humidity on the Adsorption onto Activated Carbon of the Vapors of Water-Immiscible Organic Liquids,” published in Fundamentals of Adsorption, A.L. Myers and G. Belfort, eds., Engineering Foundation, New York, 335 – 344 (1983).

138. R.J. Grant, R.S. Joyce, and J.E. Urbanic, “The Effect of Relative Humidity on the Adsorption of Water-Immiscible Organic Vapors on Activated Carbon,” published in Fundamentals of Adsorption, A.L. Myers and G. Belfort, eds., Engineering Foundation,

New York, 219-227 (1983).

139. S.J. Doong and R.T. Yang, "Adsorption of Mixtures of Water Vapor and Hydrocarbons by Activated Carbon Beds: Thermodynamic Model for Adsorption Equilibrium and Adsorber Dynamics," *AICHE Symposium Series* **83(259)**, 87-97 (1987).

140. M. Huggahalli and J.R. Fair, "Prediction of Equilibrium Adsorption of Water onto Activated Carbon," *Ind. Eng. Chem. Res.* **35**, 2071-2074 (1996).

141. P. Lodewyckx, The Influence of Water on Adsorption of Organic Vapours by Activated Carbon, Ph.D. Thesis, University of Antwerpen, Anthwerpen, Belgium (1998). Also submitted for publication in the *Am. Ind. Hyg. Assoc. J.* (1999).

142. P. Lodewyckx, E.F. Vansant, P.R. Norman, and L. Pears, "Influence of Adsorption on the Water Isotherm for Activated Carbon," in Carbon '97, Extended Abstracts and Program of the 23rd Biennial Conference on Carbon, Vol. I, 116-117, Penn State University, University Park, PA (1997).